PE-01

Quality improvement in HE staining of pathological sections by Plan-Do-Check-Act (PDCA) methods

Hsing-Cheng Tseng, Jia-Bin Liao, Jyh-Seng Wang, Herng-Sheng Lee
Department of Pathology and Laboratory Medicine, Kaohsiung Veterans General Hospital, Taiwan

Background:

There is a trend of increasing the number of gastric biopsy specimens year by year in our hospital (Table 1). Histological examination is usually considered to be the gold standard in the direct detection of *Helicobacter pylori (H. pylori)* infection. Hematoxylin and eosin (HE) stain is used in daily practice and is usually sufficient to identify *H. pylori* in routine clinical histological examination. However, several factors influence the diagnostic accuracy, such as biopsy site, size and number of biopsies, experience of the examining pathologist, and staining quality, especially when artifact occurs during staining procedure which may interfere *H. pylori* interpretation. In our daily practice, we found an artifact which severely interferes with the interpretation of *H. pylori* identification (Figure 1). How to enhance the effectiveness of the work and to improve the quality of the HE staining procedure is an important issue. The aim of our study was to improve the quality of HE stain by Plan-Do-Check-Act (PDCA) methods for biopsy specimen.

Methods and Results:

Plan: We focused on several factors, including slide baking, hematoxylin reagent, and xylene solution.

Do: We tested the temperature and duration of slide baking (Fig. 2), hematoxylin with or without filtration (Fig. 3), and the frequency of changing xylene (Fig. 4).

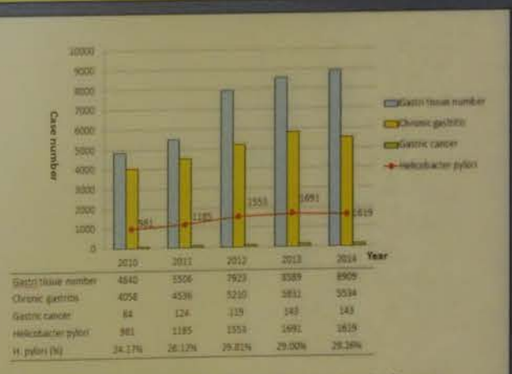

	2010	2011	2012	2013	2014
Gastric tissue number	4840	5506	7929	8589	8909
Chronic gastritis	4058	4536	5210	5832	5534
Gastric cancer	64	124	119	143	143
Helicobacter pylori	981	1185	1553	1691	1619
H. pylori (%)	24.17%	26.12%	29.81%	29.00%	28.36%

Table1. Statistical analysis of H. pylori in gastric diseases (exclude diagnosis of gastric erosion/ ulcer).

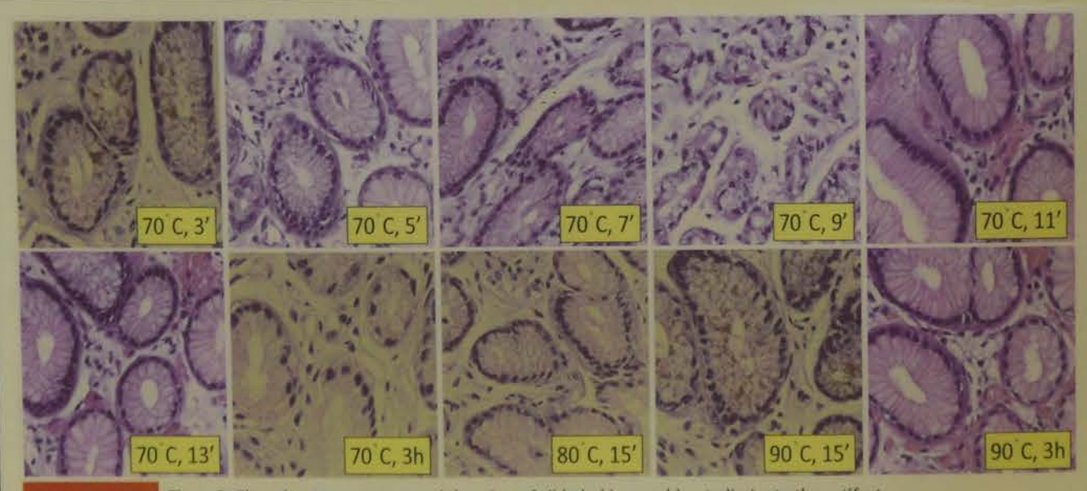

Check1 Figure2. Changing temperature and duration of slide baking could not eliminate the artifact.

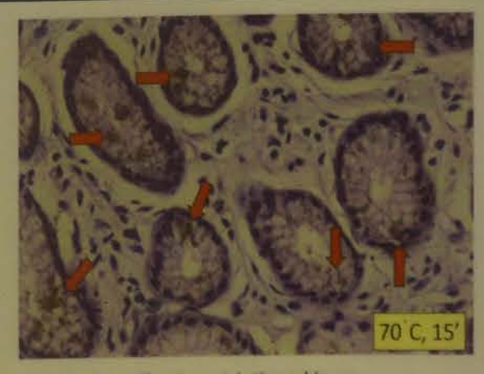

Figure1. An artifact in gastric tissue biopsy.

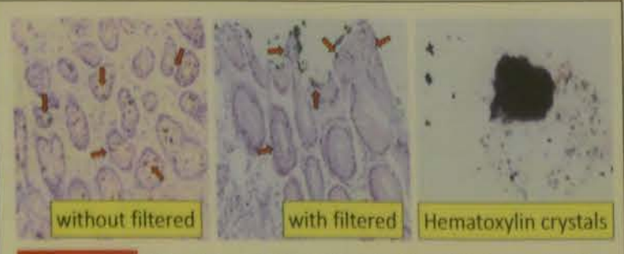

Check2 Figure3. Hematoxylin with and without filtration all had the same artifact.

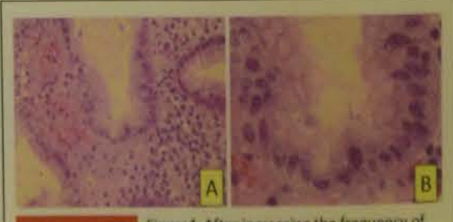

Check3 Figure4. After increasing the frequency of changing xylene, the tiny brown refractile granules disappeared (A) and with clearly visible *H. pylori* (B).

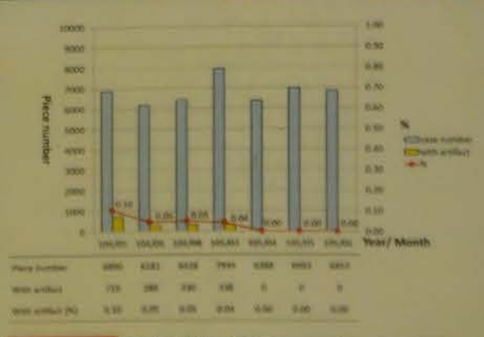

Action Table2. We kept the new procedure of changing xylene in HE staining, the artifact decreased dramatically.

Discussion:

After PDCA, we found that the artifact can be prevented by increase of the frequency of changing xylene (Figure 4). This artifact was not caused by high baking temperature or hematoxylin crystal and only increase of the frequency of changing xylene can prevent this artifact. The quality of staining was improved by changing xylene every two days in stead of every one week (Table 2). The artifact seems to result from inadequate dewax by xylene which results in formation of tiny brown refractile small paraffin granules. In conclusion, the quality of xylene used during HE staining may result in artifact which may interfere with the identification of the *H. pylori* gastric biopsy specimen.

References:

1. Fock KM. Review article: the epidemiology and prevention of gastric cancer. 2014; 40: 250-260
2. Wang YK et al . Diagnosis of H. pylori infection: Current options and developments. 2015; 21; 40: 11221-11235

PE-03

Clinico-pathological analysis of HER family expression in human colorectal cancer

Co-expression of HER family is clinico-pathological biomarker which relates to progression in human colorectal cancer

H Nozaka[1)2)], M Togashi[1)], S Kurosawa[1)], A Igarashi[1)], N Yamada[2)], Y Takahashi[2)], K Ishida[2)], T Sugai[2)]
1) Graduate school of health sciences, Hirosaki university 2) Iwate Medical University School of Medicine

Clinico-pathological analysis of HER family expression in human colorectal cancer
- Co-expression of HER family is clinico-pathological biomarker which relates to progression in human colorectal cancer -
H Nozaka[1,2)], M Togashi[1)], S Kurosawa[1)], A Igarashi[1)], N Yamada[2)], Y Takahashi[2)], K Ishida[2)], T Sugai[2)]
1) Graduate school of health sciences, Hirosaki university 2) Iwate Medical University School of Medicine

Background and Objectives

HER family is composed of four members, and Epidermal Growth Factor Receptor (EGFR) is a member of HER family. EGFR is expressed in the case of 60-80% of colorectal cancer, and it is reported that the expression of EGFR is strongly involved in the invasion and metastasis. Meanwhile, it is known that HER family member formed dimer structure with other HER family member, but a few reports shows co-expression of HER family and clinicopathological significance in human colorectal cancer. In this study, we examined co-expression of HER family mRNA and protein in human colorectal cancer, and evaluated significance as the clinicopathological biomarker.

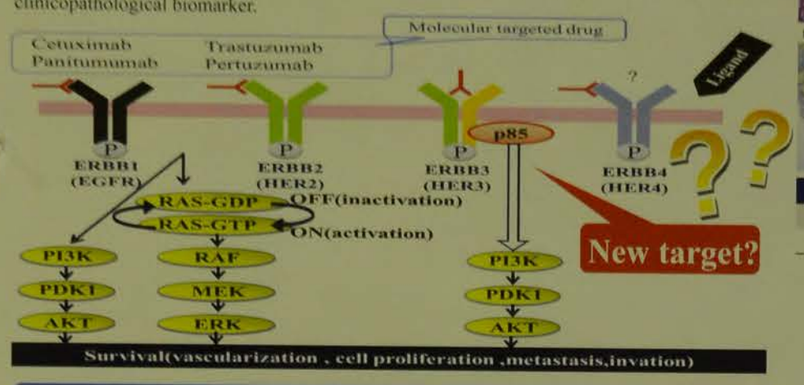

Materials

Tumors for this study were collected from 60 patients diagnosed with primary advanced colorectal cancer in Iwate Medical University between 2009 and 2015.

Clinical Features					
Gender	Male	41(68%)	Differentiation	Moderate	49(82%)
	Female	19(32%)		Well	9(15%)
Age	≦65	20(33%)		Other	2(3%)
	>65	40(67%)	Localization	Colon	35(58%)
	median	70year		Rectum	25(42%)
pTMN Stage	I	15(25%)	Invasion	m	3(5%)
	II	17(28%)		sm	4(7%)
	III	24(40%)		mp	8(13%)
	IV	4(7%)		ss	38(63%)
Tumor size	≦1000mm²	15(25%)		se	4(7%)
	>1000mm² ≦2000mm²	23(38%)		si	3(5%)
	>2000mm² ≦3000mm²	12(20%)			
	>3000mm²	10(17%)			
	median	1625mm²			

Methods

1. Immunohistochemistry

IHC staining was performed on formalin – fixed, paraffin-embedded (FFPE) tissue sections.

1st Antibody	Company	Clone No	Activation	Dilution
EGFR	Dako	DAK-H1-WT	HEAT (TE pH8.0)	×250
HER2	Dako	A0485	HEAT (TE pH8.0)	×250
HER3	CST	D22C5	HEAT (TE pH8.0)	×250

2. mRNA expression by qRT-PCR

Total RNA was extracted using the TRIzol reagent (Invitrogen). Total RNA was reverse transcribed by High Capacity cDNA Reverse Transcription Kit (Applied biosystems) and random hexamer. The quantitative evaluation of each gene expression (*EGFR, HER2, HER3*) was analyzed by qRT-PCR (TaqMan® Gene Expression Assays, Applied biosystems). The relative quantification value of mRNA expression compared with normal tissues was calculated (ΔΔCt). The relative values compared with normal tissues were calculated.

3. Clinicopathological analysis

Statistical analysis was carried out by SPSS 21 (IBM).

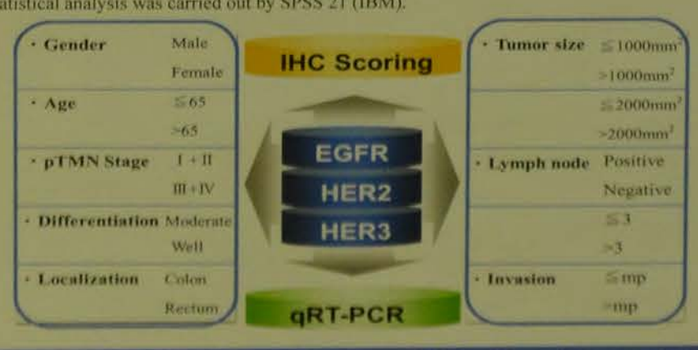

Results

1. Immunohistochemistry

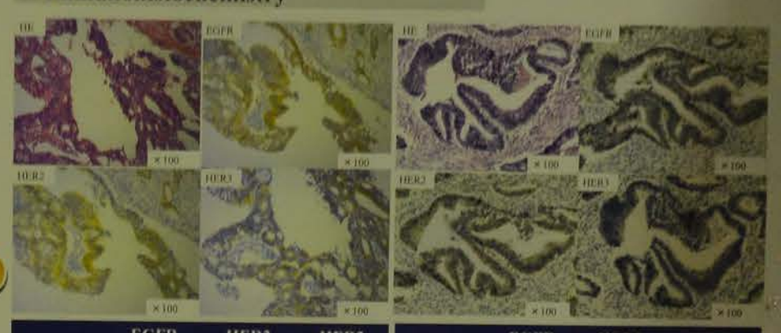

	EGFR	HER2	HER3
mRNA	−	+	−
IHC	+	1+	2+

	EGFR	HER2	HER3
mRNA	−	−	−
IHC	−	−	−

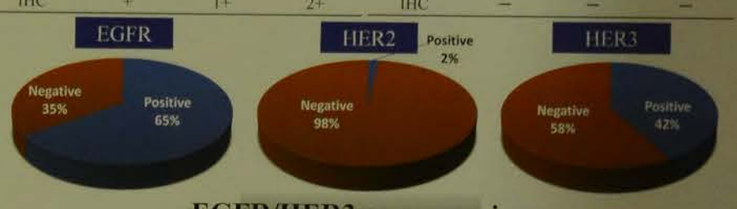

EGFR/HER3 co-expression

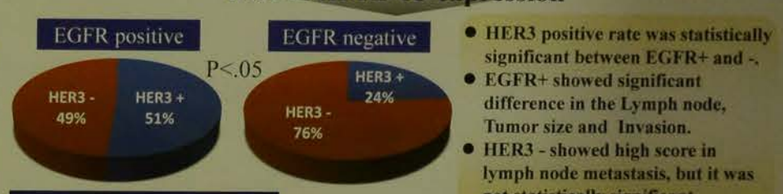

- **HER3 positive rate was statistically significant between EGFR+ and -.**
- **EGFR+ showed significant difference in the Lymph node, Tumor size and Invasion.**
- **HER3 - showed high score in lymph node metastasis, but it was not statistically significant.**

Clinicopathological analysis

EGFR			HER3		
Lymph node p<.05*			Lymph node N.S (p=.10)		
	(-)	(+)		(-)	(+)
≦3	20(33%)	29(48%)	≦3	26(43%)	23(38%)
>3	1(2%)	10(17%)	>3	9(15%)	2(3%)
Tumor size p<.05*			Tumor size N.S (p=.88)		
	(-)	(+)		(-)	(+)
≦1000mm²	9(15%)	6(10%)	≦1000mm²	9(15%)	6(10%)
>1000mm²	12(20%)	33(55%)	>1000mm²	26(43%)	19(32%)
Invasion p<.001**			Invasion N.S(p=.23)		
	(-)	(+)		(-)	(+)
≦mp	11(18%)	4(7%)	≦mp	11(18%)	4(7%)
>mp	10(17%)	35(58%)	>mp	24(40%)	21(35%)

EGFR (+) 38cases

HER3 (+)/(-)		
Lymph node N.S (p=.12)		
	(-)	(+)
≦3	12(32%)	17(45%)
>3	7(18%)	2(5%)
Tumor size N.S (p=.66)		
	(-)	(+)
≦1000mm²	2(5%)	4(11%)
>1000mm²	17(45%)	15(39%)
Invasion N.S(p=1.0)		
	(-)	(+)
≦mp	2(5%)	2(5%)
>mp	17(45%)	17(45%)

2. mRNA expression by qRT-PCR

HER2 or HER3

Clinicopathological analysis

HER2 mRNA		<2.0	≧2.0	p-value
Gender	Male	55%	13%	.066
	Female	19%	13%	
Age	≦65	25%	8%	.837
	>65	48%	19%	
pTMN Stage	I + II	40%	13%	.755
	III + IV	34%	13%	
Differentiation	Moderate	64%	23%	.114
	Well	10%	3%	
Tumor size	≦2000mm³	47%	17%	.738
	>2000mm³	26%	10%	
Localization	Colon	38%	20%	.114
	Rectum	35%	7%	
Invasion	≦mp	18%	7%	.736
	>mp	55%	20%	
Lymph node	≦3	66%	22%	.409
	>3	13%	5%	

HER3 mRNA		<2.0	≧2.0	p-value
Gender	Male	59%	9%	.953
	Female	27%	5%	
Age	≦65	29%	4%	.951
	>65	57%	10%	
pTMN Stage	I + II	48%	4%	.209
	III + IV	37%	11%	
Differentiation	Moderate	72%	15%	.540
	Well	13%	0%	
Tumor size	≦2000mm³	58%	4%	<.05*
	>2000mm³	27%	11%	
Localization	Colon	50%	7%	.956
	Rectum	36%	7%	
Invasion	≦mp	20%	2%	.172
	>mp	65%	13%	
Lymph node	≦3	33%	7%	<.05*
	>3	11%	7%	

HER3 mRNA status

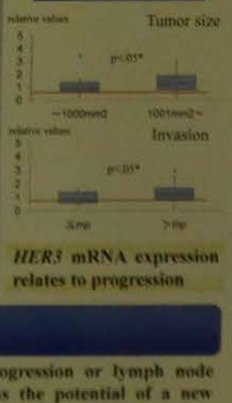

***HER3* mRNA expression relates to progression**

Conclusion

It was suggested that EGFR/HER3 associated with the progression or lymph node metastasis of the colorectal cancer. It seems that HER3 has the potential of a new molecular target in colorectal cancer therapy. However, this study does not disclose the relevance of KRAS or PI3K mutations. In our future work, we will study the relationship of cancer-related gene mutations or the prognosis.

Copyright © Hirosaki University Graduate School of Health Sciences, Japan

Our hand out Take Free
ご自由にお取りください

Acknowledgement and COI

Acknowledgement

This work was supported by JSPS KAKENHI Grant Number 25280103.

Conflict of interest

The authors have no conflict of interest (COI) directly relevant to the content of this article

PE-04

Producing an AFB Control Block

Chae Jong-hyuck, Ma Sang-chul, Kim Ki-hyun, Oh Jong-won,
Lee Moon-jung, Hong Sung-chul, Park Wook-jae

SAMSUNG Medical Center Pathology

Background

As one of the methods of measuring the accuracy of staining in special staining, there is a method of evaluating the accuracy of staining using positive control. The positive control is carried out in order to see the structure of a tissue and to check the microorganism infected functionally or externally, and in AFB staining, it is necessary to evaluate the accuracy of staining by staining a positive control group, together, in order to evaluate that.

The existing method used positive tissues into which tubercular bacilli invaded as a positive control, but it became more difficult to supply this, constantly, as the rate of the initial discovery of tuberculosis increased. So, in order to maintain quantitative, qualitative staining, the need for the production of a positive control block using an acid-fast stain was brought forward. Thus, if the control block is produced, integrated with an AFB stain by the process of producing a cell block used in a cellular pathology lab, the quantity or distribution of bacteria is constant in the section because of the characteristic of the cell block, so such a block was produced as it was expected that it could serve as an AFB positive control sufficiently.

Method

The types of the culturing medium include Ogawa medium, a solid medium and Middlebrook 7H9, a liquid medium. A control block was produced through the following procedures: First, scoop out the colony of bacteria cultured on the solid medium, Ogawa medium and mix physiological saline for vortex mix.

Put egg albumin in it like producing a cell block. Then, spin it in a centrifuge and process it with an automatic tissue processor. On the liquid medium, Middlebrook 7H9, it was produced in the same way. First, spin the cultured bacteria in a centrifuge. Put them in a cassette and process them with an automatic tissue processor.

▶ The type of culture medium ◀

Solid media	Liquid media
• Egg-based media	• Dubs oleic acid-albumin medium
a. Lowenstein-Jensen medium	• Middlebrook 7H9
b. Ogawa medium (2.3%)	• Middlebrook 7H12, 7H13 (BACTEC 12B & 13B)
• Agar media	
a. Middlebrook 7H10	
b. Middlebrook 7H11	

Visually observable	Visual observation required
Low detection rate	Convenience of the examination
The slow growth rate	High detection rate
Low contamination rate	The rapid growth
	High contamination rate

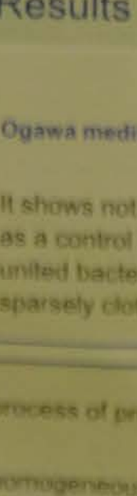

① Ogawa medium (2.3%)

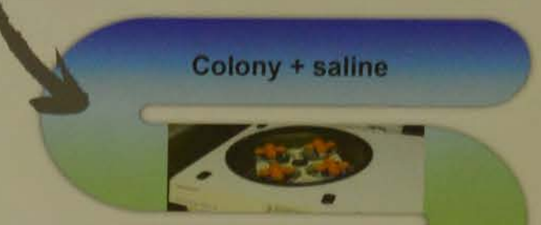

② Middlebrook 7H9

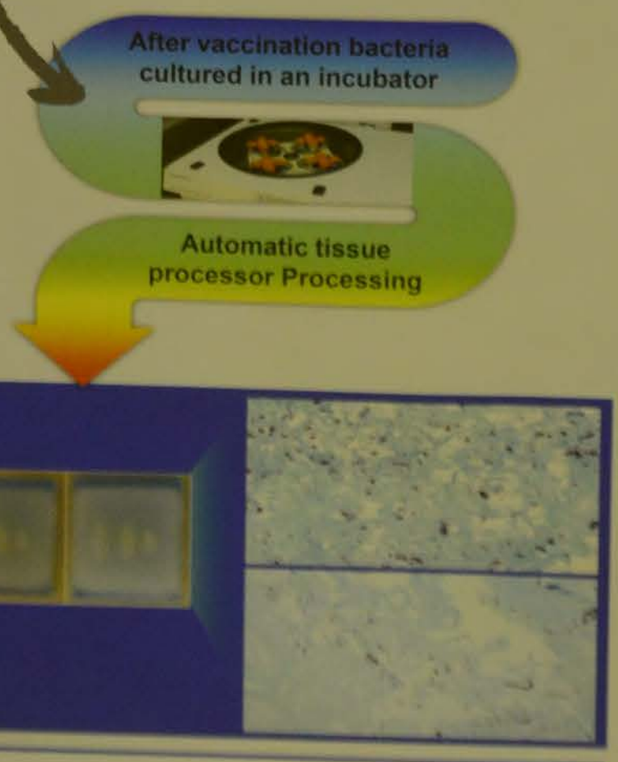

Results

① Ogawa medium (2.3%) culture	② Middlebrook 7H9 culture
It shows not suitable for use as a control block that has united bacteria grows sparsely clot	Showing fast growth these bacteria have been mass distributed on the slide is suitable as a control block

Discussion

1) Producing an AFB Control Block with the process of producing a cell block has a merit that it is easy to produce and supply it at any time.
2) There were more bacteria and they were homogeneous when the AFB control block was made by culturing on the liquid medium than on the solid medium, so it could maintain a better quality, and
3) It is concluded that using a harmless NTM stain allows the lab staff

D-3 D-3

Pathology
PE-05

FAST PML/RARA FISH
- at the suspicion of Acute Promyelocyte leukemia (APL)

BLS Vinni Bredahl, Denmark
Zealand University hospital, Department of surgical Pathology

Introduction
If a patient morphological or clinical features of acute promyelocyte leukemia (APL) and has a translocation of PML/RARa, t(15;17) the patient has APL and can start treatment right away. It is therefore essential for the diagnosis to perform a rapid FISH PML/RARa.

Materials and method
Blood- or bone marrow smears from 15 different patients, 5 suspected of APL and 10 controls, were analyzed for t(15;17) using the quick FISH and the FAST FISH method and the agreement between the two method were assessed.
The only difference in protocol are the hybridization time for the probe. The quick FISH hybridizes for 4 hours, with a conventional probe and the FAST FISH 1 hour, with the FAST PML/RARa Probe.

Results
There were bright and clear signals with both probes. In 13 cases, the results from the two FISH methods showed no translocation and in two cases, a translocation was detected. There were a complete agreement between the two methods.

Discussion and conclusion
There were no difference in the signals, whether it was blood- or bone marrow smears.
The FAST PML/RARa probe gives a valid result, equal to conventional PML/RARa probe. Cytocell has produced a probe, that is easy to work with and the signals obtained with the two probes are comparable.
We now routinely use the FAST PML/RARa probe.

REGION SJÆLLAND
ZEALAND UNIVERSITY HOSPITAL

Get the poster as PDF

A case of sicklecell disease with abnormally low level of HbA1c by the HPLC method

Prostate Cancer: A novel technique
om radical prostatectomy specimen

Conclusions

Results

Pathology

PE-06

Preperation of tissue section of nail specimen

SUNGEUI KIM, SUNGCHUL HONG, SEUNGWOO HAN

SMASUNG MEDICAI CENTER

Background

Quicker and more accurate diagnosis of nail disease is possible through histological examination, so it is most important to prepare and provide quality slides.

nail tissues in which 50% of the components are keratin component, it is difficult to cut them and prepare a quality slide, so it is a burden to a pathologist, and there is a difficulty in diagnosis, as well. In addition, even if they are cut uniformly, the impact of the reagent in the process of softening the tissues may be an inhibitory factor in special staining, so the process of softening nail specimens requires careful attention.

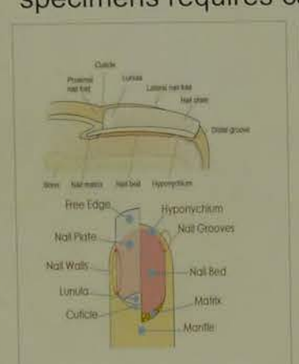

Nail structure

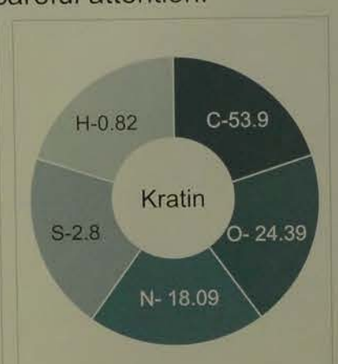

Nail components

Nail biopsy form

Nail gross

Method

In the generalized process of preparing nail specimens, it is common to soften tissues in 4% KOH solution and cut them into pieces sized 3 to 4 ㎛ but this study prepared tissue sections and carried out stain.

Staining by changing the process as follows :surface softening in 10% HCL solution for 30 min. and 1 micro microtome cutting.

	Pre-softening	Post-softening	Thickness
group1	NON	NON	1 ㎛
group 2	NON	4% KOH, 1 hour	1 ㎛
group 3	NON	10% HCL, 30 min	1 ㎛

Results I

In addition, in preparing sections, there were wide differences in the falling off of the tissues on the slide, according to their thickness, but surface softening in HCL solution, too, should be done in the shortest possible time for other types of staining.(H&E)

Group1

Group2

Group3

Results II

There was a falling off of the fungal colony on the slide in the existing process of softening using KOH solution; however, the fungal colony remained intact on the slide in the process of softening using HCL solution. (H&E)

	Group2(KOH)	Group3(HCL)
Colony		

Statistics				
	Total	Fungus +	Cancer	Abnomal %
2013	337	165	6	50.7 %
2014	344	190	6	55.2 %

Discussion

Thus, the production of tissue sections of nail specimens requires quite difficult conditions, unlike the existing softening processing does, so observations by histopathological examination are needed, but in reality, the credibility of the histological examination itself is not high.

Therefore, it is judged that it is important for a medical laboratory technologist to prepare good tissue sections by repeatedly improving research and experiment on it so as to have a good effect on diagnosis and treatment.

SAMSUNG MEDICAL CENTER

D-3

Pathology
PE-07

Biobanking of Prostate Cancer: A novel technique for harvesting of fresh tissue from radical prostatectomy specimens

Jóna Gudjonsdottir, Claes Lindh, Lars Egevad
Dept. of Oncology and Pathology, Karolinska Institutet, Stockholm, Sweden

Background

Harvesting of fresh tumor tissue for cancer research provides better access to genetic information than formalin fixed paraffin-embedded tissue. Biobanking of representative prostate cancer is particularly challenging because of difficulties in identifying tumor macroscopically. We developed a method that allows biobanking of fresh prostate tissue without hampering morphological assessment.

Conclusions

This novel method for biobanking of prostatectomy specimens provides high quality frozen tissue for research purposes while it also allows mapping of cancer distribution for accurate reporting. Cancer is harvested in most cases and the technique allows identification of tumor location in multifocal cancer. Disadvantages with this method is that it is labor intensive and requires considerable freezer space, but these problems can be minimized by cutting only blocks that are likely to contain tumor.

Method

From fresh prostate tissue to H&E stained section. Biobanking of prostate

Fresh prostate arrives to the lab

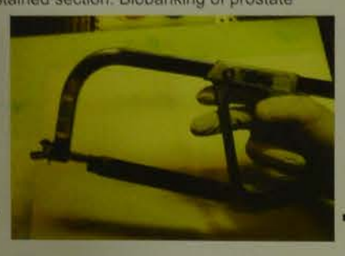

Custom-made double bladed knife for harvesting of whole sections

Section from the prostate being cut with double bladed knife for even section

Biobank material after dividing into 9 parts

Tissueblocks ready to be frozen in OCT gel at -80°C

Cryosectioning of a frozen block at -20°C

Frozen section before staining

Whole section stained in H&E

Design

A custom-made double-bladed knife was developed for harvesting of tissue from unfixed radical prostatectomy specimens. A 4 mm thick slice was cut by a horizontal section through the prostate and then split in smaller segments that were frozen in OCT gel at -80°C. The rest of the prostate was pinned to cork, formalin-fixed, sliced at 4 mm, paraffin-embedded and whole-mounted. This technique was used for biobanking of 20 prostatectomy specimens. Frozen sections were cut from all blocks and cutting time monitored. A pathologist marked out tumor areas, slides were scanned and the slice reconstructed.

Discussion

This unique method offers good quality material (average RIN 9) with possibilities to identify specific parts of the tumor (PIN, PNI and extraprostatic extension can be identified). Chances of finding the tumor are very high (85% of cases had tumor). The morphology of the tissue has very good quality.

Results

A total of 155 frozen blocks were cut (4-9 per case). Average cutting time per case was 162 minutes (range 79-253 minutes). Tumor was found in frozen sections of 85% (17/20) of cases and in 46% (72/155) of blocks. None of the radical prostatectomy specimens were over-sampled (pT0). Gleason scores were 6, 7 (3+4), 7 (4+3), 8 and 9 in 4, 7, 6, 2 and 1 of the cases, respectively.

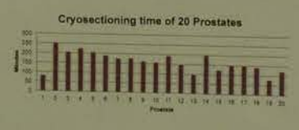

Jóna is working as a Biomedical Scientist at the Karolinska Institute. Mainly she works with prostate cancer, processing both fresh frozen and formalin fixed, paraffin embedded material.

Freeze artifacts in fresh frozen specimen, frozen without OCT gel.

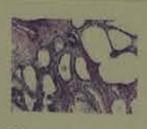

Morphology of large fresh frozen tissue, frozen with OCT gel.

Fresh frozen prostate tumor harvested with the new method.

Karolinska Institutet
Jóna Guðjónsdóttir
Biomedical Scientist
Dept. Of Oncology and Pathology
Cancer Centrum Karolinska
R8:04

KAROLINSKA INSTITUTET ANNO 1810

Karolinska Institutet

hology
E-09

Case Report: Empy
tenax in an Elderly

Hsin-Chieh Lu[1] | Hsiang-Lin Wan[2]
[1,2]Department of Laboratory Medicine, Taipei Tzu Chi H
[1]Department of Molecular Parasitology and Tropical Dis
*Correspondence

ntroduction

npyema is one of the potential complications of lo
fections of the pleural space are usually bacterial
npyema can be the result of microorganisms other tha
npyema caused by *Trichomonas canistomae* from dog

'atients & methods

case of an 83-year-old female patient with type II d
no complained of cough with sputum and dyspnea fo
lp in March 29, 2016. At ER, physical examinatio
eath sound, wheezing and lower leg pitting edema (
t show anemia (Hgb: 10.2g/dl); in contrast, the data
th left shift and impaired renal function (BUN/CRE:3
usion (Fig. 1) and chest CT showed RLL pulmonary
gtail insertation was done. The pleural fluid was exa
unt reached 83308/ul.

Results

wet mount of the pleural fluid showed many n
monstrating tumbling motility. A Liu's stains of a cy
monstrated small, pale staining, flagellated organism
ecies with size and morphology most consistent with
nfirmed as evidenced by presence of two bands of
tracted from empyema fluid by using PCR. (Fig 4)
fter sequencing of the PCR product of this organis
entified to be *T. canistomae* with 91% identity via BL
ig 3, 4)It is likely that the patient acquired *T. canistom*

g01.
ht pleural effusion

g03.
chomonas canistomae trophozoite (arrow)
h anterior flagellate (red arrow head) by Liu's
in at 1000 X magnification

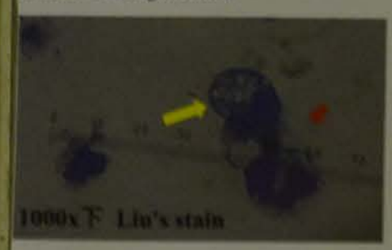

Discussion

e denied any history of smoking, alcohol, and betel nut
r further evaluation and management due to suspected
e bacterial staining of pleural fluid was identified
tibiotics of Cravit was given. On April 1, she was under
ht pleural by using thoracoscopic decortication of pleu
vity with purulent effusion. Simultaneously, one 32 Fr.
S and the other 32 Fr. curved tube was inserted via orig
single lumen, she was sent to MICU under stable co
adant fibrinopurulent exudate and fibrin with no ma
ient's condition has improved and discharged. Pulmon
derestimated because of diagnostic difficulties. The
ntification is underlined and the pathogenicity of *Trich*
gnored.

C-3 C-3

Pathology
PE-08

Th2-type cytokines and Treg upregulation in patients with immunoglobulin G4-related aortic aneurysm

Satomi Kasashima[1,2], Atsuhiro Kawashima[1,2], Satoru Ozaki[3], and You Zen[4]

[1] Department of Pathology,[2] Department of Clinical Laboratory, National Hospital Organization, Kanazawa Medical Center
[3] Department of Clinical Laboratory Science, Kanazawa University
[4] Department of Diagnostic Pathology, Kobe University Graduate School of Medicine

IgG4-related aortic aneurysm

IgG4-related aortic aneurysm (IgG4-AA) is one of the consequences of IgG4-related diseases (IgG4-RD), which is novel disease category. It is pathologically characterized by massive lymphoplasmacytic infiltration rich in IgG4+ plasma cells, storiform fibrosis, and obliterative phlebitis, which predominantly affects the adventitia and occasionally the media.

Soft tissue density surrounding aorta — Adventitial thickening seen in IgG4-AA — Numerous IgG4+ plasmacytes infiltration in the adventitia

Immune-reaction

Local immune-reaction is controlled by the valance of helper T cell subtypes, as T helper 1(Th1) and T helper 2(Th2). Regulatory T cells(Tregs) inhibits local active immune-reaction.

The pathogenesis of most allergic disease and autoimmune are concerned with unbalance of Th1/Th2. Each T cell subtypes is characterized by cytokine productions.

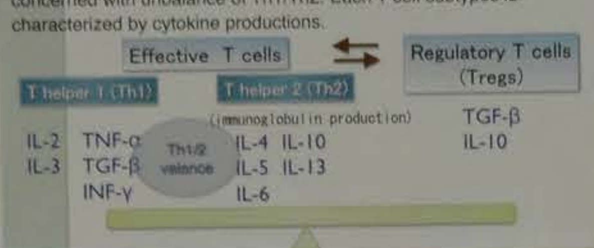

Pathogenesis of IgG4-RD

Cytokine imbalance contributes to the pathogenesis of IgG4-RD, particularly Th2 predominant. Tissue examination revealed an overproduction of Th2-type cytokines (e.g., IL-4, IL-5, and IL-13) in several affected organs of igG4-RD. Tregs, including IL-10 and TGF-β, were also overexpressed in the affected organs.

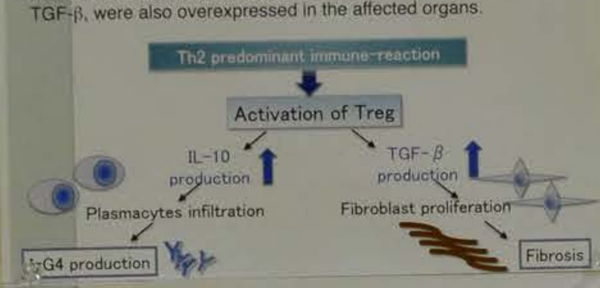

Aim of this study

Based on previous reports, we hypothesized that the Th1/Th2 cytokine balance plays an important role in the pathogenesis of IgG4-AA, similar to other organ's IgG4-RD.

We investigated the serum circulating level of key cytokines, and then extended to clarify the cytokine-producing cells in the local aortic tissue with both protein level (immuno-histochemistory) and mRNA level (In situ hybridization).

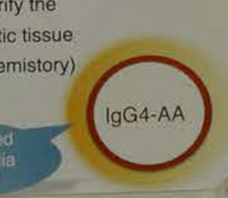

Case selection for subgroups

IgG4-related AAA (IgG4-AA)
Serum IgG4 135 mg/dL<
Pathological IgG4+cells 80/hpf< and IgG4/IgG ratio80%<
Adventitial thickening 2mm<

Non-IgG4-reraled Inflammatory AAA (non-IgG4-AAA)
Serum IgG4 and IgG4+ cells within the normal range
Adventitial thickening 2mm<

Atherosclerotic AAA (aAAA)
Serum IgG4 and IgG4+ cells within the normal range
Adventitial thickening 0.1mm>

Autopsy controls (no dilation, mild atherosclerosis)

Summary of subgroups

Subgroup	Age (years)	Gender (M/F)	Adventitia (mm)	Serum IgG4	Pathologic IgG4(/hpf)
IgG4-AA (10 cases)	71.4 (63-79)	8/2	4.1 (2.0-9.0)	221.0 (137-559)	109 (82-145)
Non-IgG4-AAA (5 cases)	77.0 (68-92)	5/0	3.9 (2.0-9.0)	42.3 (32-59)	32 (14-56)
aAAA (10 cases)	76.5 (95-85)	9/1	0.6 (0.1-1.3)	33.3 (12-59)	20 (0-45)
Autopsy (10 cases)	70.5 (59-81)	8/2	0.2 (0.1-0.5)	37 (12-80)	1.1 (0-0.3)

Methods 1

1. Measuring serum cytokines for ELISA
All sera used in this study were collected before treatment or at the time of autopsy and were stored at −20 °C until tested.

Human IL-4 Ultra sensitive immunoassay kit, AGC TECHNO GLASS
Human IL-10 Ultra sensitive immunoassay kit, AGC TECHNO GLASS
Human IL-13 ELISA, COSMO BIO
Human INF-γ kit, Bender Med systems
Detectable normal ranges of these assays were as follows: IL-4 ≤ 3.02 pg/mL, IL-10 <7.05 pg/mL, IL-13 <28.6 pg/mL, and IFN-γ <20.6 pg/mL.

Usual laboratory methods were used to measure serum IgG, IgG4, and IgE.

Methods 2

2. Histology and Immunohistochemistry (IHC)
Using surgical or autopsy specimens, the adventitial thickness from the lowest elastic fiber of the media to the lowest part of the adventitia was calculated on Elastica van Gieson-stained sections using a microscopic measure.

Immunohistochemical staining was performed in accordance with the manufacturer's instructions.
IL-4 (Abcam, polyclonal, clone ab9622, x200)
IL-10 (Abcam, polyclonal clone ab34843, x200)
IL-13 (Abcam, polyclonal clone ab64000, x100)
INF-γ (Abcam, polyclonal clone ab9652, x200)

Methods 3

3. In situ hybridization using RNAscope
RNAscope® is capable of reliably detecting transcriptionally active genes in formalin-fixed, paraffin-embedded (FFEP) tissue samples mounted on slides. The stained slides could be Visualized using a bright field microscope. Detecting cytokine mRNA by RNA scope® is thought to be more effective because mRNAs are intracellularly localized; thus, detecting these proteins.

3-1) Cytokine mRNAs
IL-4 mRNA, IL-10 mRNA, IL-13 mRNA and INF-γ mRNA

3-2) Cytokine producing cells
Above Cytokine mRNAs and tissue immune cells mRNA (CD34 mRNA, c-kit mRNA and CD163 mRNA)

Statistical Methods

The Kruskal–Wallis analysis of variance was used to statistically compare the four groups. Spearman's correlation coefficients were used to test associations between continuous variables. All analyses were performed using the SPSS version 20 software (IBM). Values of $p < 0.05$ were considered statistically significant.

Ethics

The present study was approved by the Human Investigation Review Committee of the Kanazawa Medical Center (NO. 24-63, NO.26-17) and conformed to the principles outlined in the Declaration of Helsinki. Informed consent was given prior to the patients in this study.

Results 1) Serum cytokine levels

IL-4 levels were within normal range in all patients. Two of 10 (20%) patients with IgG4-AA showed elevated IL-10 levels more than 7.0 pg/dL, whereas all of the remaining patients tested in this study showed very low IL-10 levels (<1.0 pg/dL). Median value of IL-10 levels in IgG4-AA were significantly higher than other 3 controls. Serum IL-13 were elevated in two patients, who were IgG4-AA. Five of ten (50%) patients with IgG4-AA also showed elevated levels of IFN-γ.

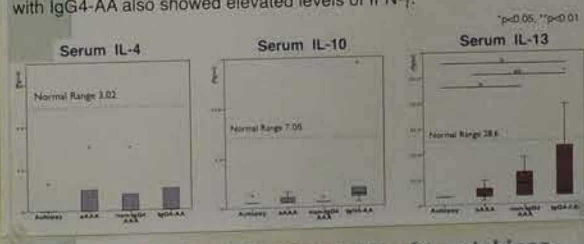

Results 2) Immunohistochemistory for cytokines

IL-4 immunopositive cells were spindle cells and plasmacyte-like cells, and were significantly frequently observed in IgG4-AA (median 45.9/hpf) than aAAA group, median 2.3/hpf, p=0.001) and autopsy group (median 13.0/hpf, p=0.001), however there was no significant difference of IL-4 expression between IgG4-AA and non-IgG4-AAA (median 31.9/hpf, p=0.266).

Results 2) Immunohistochemistory for cytokines

IL-10 immunopositive cells were mostly plasmacyte-like cells. The median count of IL-10 immunopositive cells increased in IgG4-AA (13.0/hpf) compared with other controls groups (non-IgG4-AAA, 2.0/hpf, p=0.009; aAAA, 0.5/hpf, p=0.001; autopsy, 3.0/hpf, p=0.002, respectively).

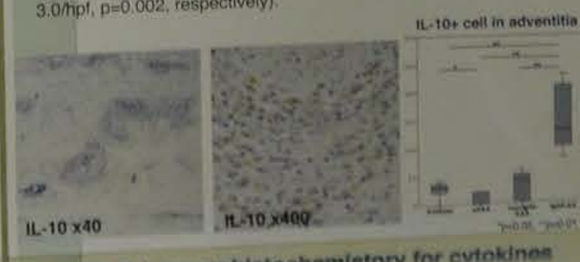

Results 2) Immunohistochemistory for cytokines

IL-13 immunopositive cells were polygonal to spindle cells distributed in the media to adventitia, and significantly frequently detected in IgG4-AA (median 102.6/hpf) than the cases of aAAA and autopsy (median 57.5hpf, p=0.004 and 20.0/hpf, p=0.002, respectively).

Results 2)Immunohistochemistory for cytokines

IFN-γ positive cells were detected sparsely in the lymphoid follicles in several cases of all groups and no differences were seen around each group.

Results 3)mRNA detection using RNA scope

A few numbers of labeling of IL-10 mRNA and IL-13 mRNA detected in spindle cells in 4 cases of IgG4-AA, but not detected in other 3 control groups. A few number of IL-4 mRNA signaling were detected in the same cases. Using 2plex RNA scope, IL-13 and CD34 mRNAs or IL-13 and CD163 mRNAs were also seen in the several numbers of polygonal cells. Coexpression of cytokines and c-kit were not detected.

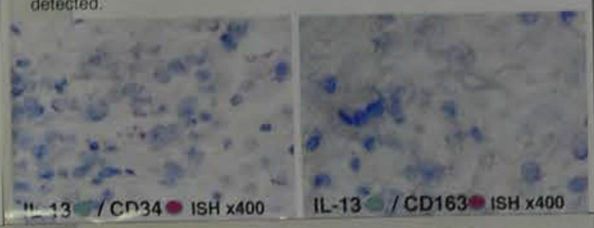

Results 4)Correlations between cytokine concentration and other parameters

In all 35 patients in this series, whether serum cytokines did not correlate with any clinicopathological parameter, immunopositive cell of IL-4, IL-10 and IL-13 in the adventitia showed significant positive correlations with adventitial thickness, serum IgG4 and IgG4 immunopositive cells of IgG4. Additionally, among 10 cases of IgG4-AA, immunopositive cell of IL-4 and IL-13 showed significant positive correlations with serum IgG4 ($R = 0.561$, $p = 0.02$; $R = 0.644$, $p = 0.03$).

Among 35 patients	Adventitial thickness (mm)	IgG4 serum (pg/mL)	IgG4+ cells (/hpf)
IL-4+ cells (/hpf)	R=0.694 (p<0.001)	R=0.644 (p=0.001)	R=0.533 (p=0.006)
IL-10+ cells (/hpf)	R=0.513 (p<0.001)	R=0.631 (p=0.001)	R=0.724 (p<0.001)
IL-13+ cells (/hpf)	R=0.492 (p<0.001)	R=0.671 (p=0.001)	R=0.496 (p=0.014)

Summary of Results

(1) Elevations of serum IL-10 and IL-13 were only observed in IgG4-AA, but not in the other vascular controls. Serum IL-4 were under normal limit in all cases. Serum IFN-γ elevated in half cases of IgG4-AA.

(2)IL-10 positive cells were significantly higher in IgG4-AA than in vascular controls. IL-4 and IL-13 positive cells were more frequent in the IgG4-AAA. INF-γ positive cells were sparsely detected in several cases.

(3)IL-4, IL-10 and IL-13 immunopositive cells in the aortic adventitia significantly correlated with serum IgG4 and IgG4 immunopositive cells and adventitial thickening.

(4)Co-expression of IL-13-mRNA and CD34-mRNA or CD168 mRNA was detected in the same cells in the adventitia of IgG4-AA. A few number of IL-4 mRNA signaling were detected. INF-γ mRNA signals were not found.

Discussion

Th2 and Treg appear to play a central role in IgG4-RD. Treg cells are activated by excessive immune reactions to prevent a Th2-type immune response in allergic diseases. This condition of suppressive allergic Th2 response has been termed "modified Th2 response." In this condition, IgG4 behaves as a regression antibody, IL-13 produces IgG4 and IgE and IL-10 can direct B cells to switch from IgE to IgG4 production. Slight increase of serum IL-10 and IL-13 in IgG4-AA suggested the partial Th2 and Treg cytokine production, related to the "modified Th2 response." The local upregulation of IL-10 in IgG4-AA was confirmed using immunohistochemistry. A few signals of IL-10 mRNA in IgG4-AA, but not in other controls, would support this suggestion. The local upsynthesis of IL-13 in IgG4-AA was also proposed. IL-13 immunopositive cells in IgG4-AA were more abundant than that in non-IgG4-IAAA. In addition, several IL-13 mRNA signals in CD34mRNA labeling mesenchymal cells and CD163mRNA labeling histiocytes were detected.

Immune-cells infiltration and Cytokine upregulation in the adventitia of IgG4-AA

Conclusion

In conclusion, upregulation of IL-4, IL-10, and IL-13 in the aortic adventitia would reflect the Th2 predominant and Treg immune-reactions in IgG4-AA, and be related with the pathogenesis or progression of IgG4-AA, similar to previous reports with other organs of IgG4-RD.

Acknowledgement
This work was supported by Grant-in-AID for Scientific Research (C) (JSPS KAKENHI) Grant Number 26462119. The authors would like to thank Mr Yutaka Yamaguchi, Ms Mitoko Mizuno, Mr Katsumasa Ishida, Ms Aiko Matsuda Ms Youko Amazawa and Mr Rei Kasashima for their special technical assistance.

Disclosure/Conflict of Interest
The authors declare no conflict of interest.

---

eration of tissue
on of nail specimen

JI KIM, SUNGCHUL HONG, SEUNGWOO HAN
G MEDICAL CENTER

e diagnosis of nail h histological important to ty slides.

of the components is difficult to cut ty slide, so it is a nd there is a well. In addition, rmly, the impact of s of softening the ory factor in special of softening nail ful attention.

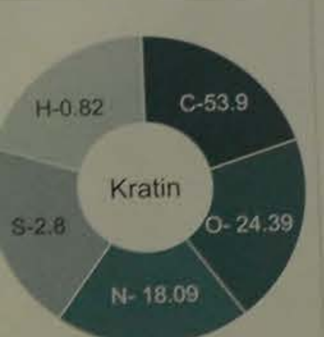

Nail components

psy form

l gross

ocess of preparing nail mon to soften tissues in d cut them into pieces is study prepared tissue out stain.

g the process as ening in 10% HCL and 1 micro microtome

Post-softening	Thickness
NON	1 µm
4% KOH, 1 hour	1 µm
10% HCL, 30 min	1 µm

Results I

In addition, in preparing sections, there w wide differences in the falling off of the tissues on the slide, according to their thickness, but surface softening in HCL solution, too, should be done in the shorte possible time for other types of staining.(H

Group1

Group2

Group3

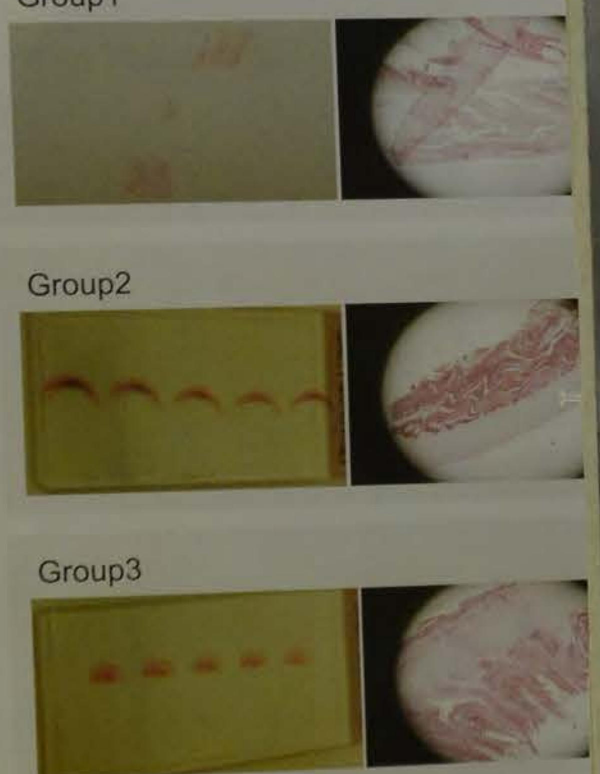

Results II

There was a falling off of the fungal colon the slide in the existing process of softeni using KOH solution; however, the fungal colony remained intact on the slide in the process of softening using HCL solution. (H&E)

	Total	Fungus +	Cancer	Abn %
2013	337	165	6	50.7
2014	344	190	6	55.2

Statistics

Discussion

Thus, the production of tissue sections o specimens requires quite difficult conditior unlike the existing softening processing d so observations by histopathologic examination are needed, but in credibility of the histological exan is not high.

Therefore, it is judged that it is imp medical laboratory technologist to prepare good tissue sections by repeatedly improv research and experiment on it so as to ha a good effect on diagnosis and treatment.

SAMSUNG MEDICAL

Pathology
PE-09

Case Report: F
tenax in an Elc

Introduction

Empyema is one of the potential complica Infections of the pleural space are usually empyema can be the result of microorganism empyema caused by *Trichomonas canistomae*

Patients & methods

A case of an 83-year-old female patient wit who complained of cough with sputum and help in March 29, 2016. At ER, physical e breath sound, wheezing and lower leg pittin not show anemia (Hgb: 10.2g/dl); in contra with left shift and impaired renal function (B effusion (Fig. 1) and chest CT showed RLL pigtail insertation was done. The pleural flu count reached 83308/ul.

Results

A wet mount of the pleural fluid show demonstrating tumbling motility. A Liu's s demonstrated small, pale staining, flagellat species with size and morphology most co confirmed as evidenced by presence of tw extracted from empyema fluid by using PC After sequencing of the PCR product of identified to be *T. canistomae* with 91% ide (Fig 3, 4)It is likely that the patient acquire

Fig01.
right pleural effusion

Fig03.
Trichomonas canistomae trophozoite (arrow) with anterior flagellate (red arrow head) by Liu's stain at 1000 X magnification

Discussion

We denied any history of smoking, alcoho for further evaluation and management d The bacterial staining of pleural fluid antibiotics of Crevit was given. On April right pleural by using thoracoscopic dec

Pathology
PE-09

Taipei Tzu Chi Hospital, Buddhist Tzu Chi Medical Foundation

Case Report: Empyema Caused by *Trichomonas tenax* in an Elderly Female Taiwanese

Hsin-Chieh Lu[1] | Hsiang-Lin Wan[2] | Chia-Kwung Fan[3*]

[1,3]Department of Laboratory Medicine, Taipei Tzu Chi Hospital, Buddhist Tzu Chi Medical Foundation, New Taipei City, Taiwan
[2]Department of Molecular Parasitology and Tropical Diseases, School of Medicine, College of Medicine, Taipei Medical University, Taipei, Taiwan
*Correspondence

Introduction

Empyema is one of the potential complications of lower respiratory tract infections or pneumonia. Infections of the pleural space are usually bacterial in origin; however, in predisposed individuals empyema can be the result of microorganisms other than bacteria. Here, we present a very rare case of empyema caused by *Trichomonas canistomae* from dog's mouth.

Patients & methods

A case of an 83-year-old female patient with type II diabetes mellitus for more than 20 years history who complained of cough with sputum and dyspnea for days went to the emergency room to seek for help in March 29, 2016. At ER, physical examination showed tachypnea respiration rate, decrease breath sound, wheezing and lower leg pitting edema (3+). Vital sign was normal. Blood analysis did not show anemia (Hgb: 10.2g/dl); in contrast, the data showed leukocytosis (WBC count: 20890/ul) with left shift and impaired renal function (BUN/CRE:37/1.5 mg/dl). Chest x-ray showed right pleural effusion (Fig. 1) and chest CT showed RLL pulmonary abscess and right empyema (Fig. 2). So, right pigtail insertion was done. The pleural fluid was examined and showed red-brown color and WBC count reached 83308/ul.

Results

A wet mount of the pleural fluid showed many neutrophils and several flagellated organisms demonstrating tumbling motility. A Liu's stains of a cytocentrifuged preparation of the pleural fluid demonstrated small, pale staining, flagellated organisms consistent with a diagnosis of *Trichomonas* species with size and morphology most consistent with *T. tenax*. (Fig 3) It Although *T. tenax* was also confirmed as evidenced by presence of two bands of ~370 and ~400 bp which were seen in DNA extracted from empyema fluid by using PCR. (Fig 4)
After sequencing of the PCR product of this organism DNA, the sequence of this parasite was identified to be *T. canistomae* with 91% identity via BLAST, which this parasite exists in dog's mouth. (Fig 3, 4)It is likely that the patient acquired *T. canistomae* by accidental ingestion of the dog's saliva.

Fig01.
right pleural effusion

Fig02.
pulmonary abscess and right empyema

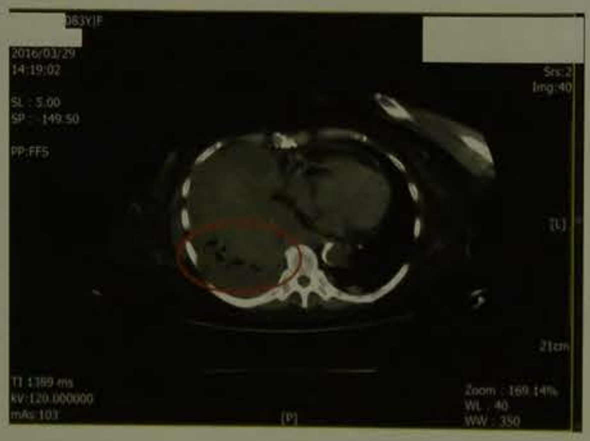

Fig03.
Trichomonas canistomae trophozoite (arrow) with anterior flagellate (red arrow head) by Liu's stain at 1000 X magnification

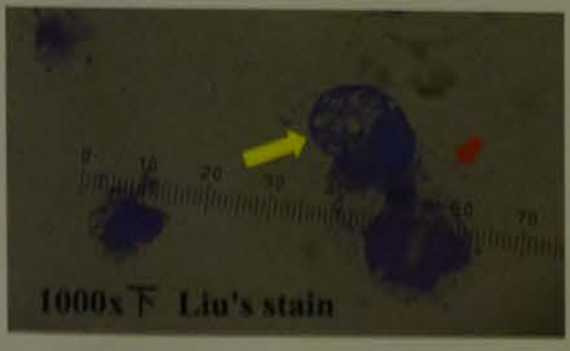

Fig04.
Two bands of ~370 and ~400 bp were seen in DNA extracted from empyema fluid

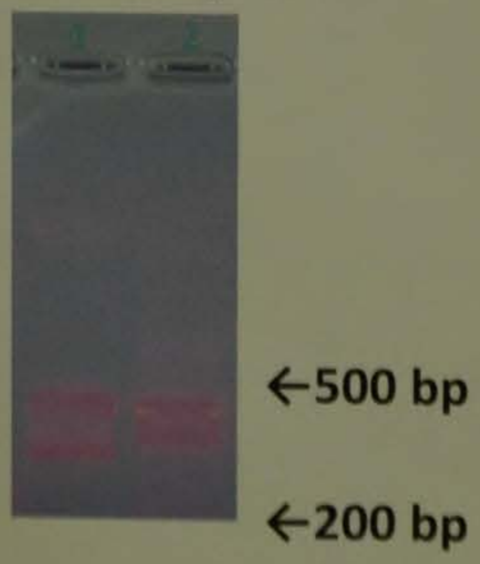

Discussion

She denied any history of smoking, alcohol, and betel nut chewing. She was admitted to ordinary ward for further evaluation and management due to suspected of pneumonia and acute respiratory failure. The bacterial staining of pleural fluid was identified to be G (+) *Streptococcus sanguinis* then antibiotics of Cravit was given. On April 1, she was undertaken a surgical operation in excision of the right pleural by using thoracoscopic decortication of pleura. Much peel was noted over right pleural cavity with purulent effusion. Simultaneously, one 32 Fr. straight chest tube was inserted via right 8th ICS and the other 32 Fr. curved tube was inserted via original tube thoracostomy. After changed ETT to single lumen, she was sent to MICU under stable condition. Pathological findings were shown abundant fibrinopurulent exudate and fibrin with no malignancy or granuloma found. On April 5, patient's condition has improved and discharged. Pulmonary infections with *Trichomonads* might be underestimated because of diagnostic difficulties. The utility of molecular biology for species identification is underlined and the pathogenicity of *Trichomonad* parasites in human lungs should not be ignored.

Pathology
PE-10

Text-mining application in clinical document record of lung cancer pathological staging: the influence factors of overall survival for early stage mucoepidermoid carcinoma of lung

Poster Number PE-10

Yung-Han Sun[1,2], Chih-Cheng Hsieh[1,3], Shih-Wei Lin[4,5]

[1]Division of Thoracic Surgery, Department of Surgery, Taipei Veterans General Hospital, Taipei, Taiwan
[2]Graduate Institute of Business and Management, Chang Gung University, Taoyuan, Taiwan
[3]School of Medicine, National Yang-Ming University, Taipei, Taiwan
[4]Department of Information Management, Chang Gung University, Taoyuan, Taiwan
[5]Stroke Center and Department of Neurology, Linkou Chang Gung Memorial Hospital , Taiwan

Background

- Text mining is an automated text-analysis process for identifying information hidden within large numbers of text documents.
- Pathology reports are pivotal elements in the staging of cancers because they are the most reliable source of cancer staging, that is an important step in cancer diagnosis, treatment and prognosis.
- In this study we applied text-mining techniques to automatically analyze the content of reports on pulmonary mucoepidermoid carcinoma (PMEC) pathology reports and to establish an automatic document classification.
- The aim of this application was identify factors influencing survival with clinical records of early stage of PMEC with text-mining techniques.

Methods

Materials

- From January 1991 to July 2015, pathology reports for 4567 patients undergoing surgery of lung cancer were collected.
- The medical records of patients with PMEC were extracted with text-mining techniques.

Text-mining

- Text mining techniques were used to analyze cancer staging related keywords in pathology reports.
- A pathology report contains sections labeled “PATHOLOGICAL” and “MICROSCOPIC” in the text file. Keywords related to cell type, N factors, and M factors appear mainly in the “PATHOLOGICAL” section, and those related to the T factor appear mainly in the “MICROSCOPIC” section.
- We took full advantage of this knowledge by extracting keyword vectors used in training the classifiers of cell type, N factors, and M factors from the “PATHOLOGICAL” sections, and extracting those used to train T factor classifiers from the “MICROSCOPIC” sections of pathology reports. Research flowchart of text-mining for pathology reports in Figure 1 and Figure 2.

Statistics

- The overall survival (OS) was day of surgery to the date of death from any cause.
- All the statistical analyses were performed using SPSS 20.0.

Research flowchart

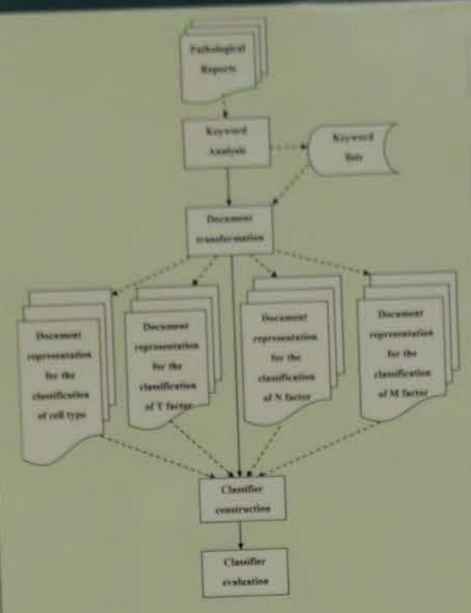

Figure 1. Research flowchart of text-mining for pathology

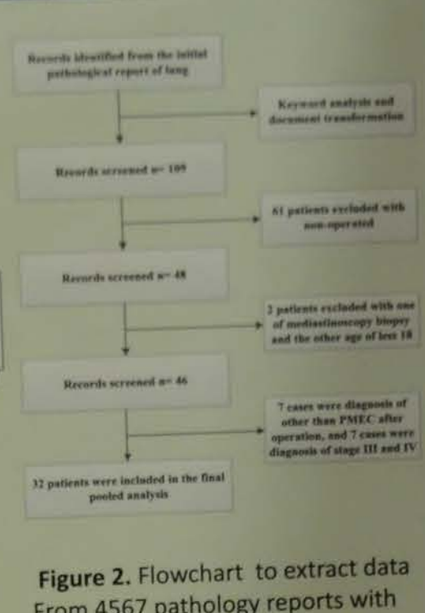

Figure 2. Flowchart to extract data From 4567 pathology reports with text-mining.

Results

Table 1. Univariate and multivariate analysis of prognostic factors influencing overall survival (OS) after surgical resection.

Variable		Number of patients	Univariate analysis 5-year survival rate (%)	p-value	Multivariate analysis Hazard ratio (95% CI)	p-value
Age				0.005	1.231 (1.035-1.463)	0.019
	<65 years	15	90.9			
	>65 years	17	56.4	0.096		0.754
Gender					1	
	Male	23	67.5		0.557 (0.014-21.634)	
	Female	9	87.5	0.066		0.783
Smoking					1	
	No	15	84		0.705 (0.058-8.507)	
	Yes	17	64.9	0.672		
Location						
	Right	16	79			
	Left	16	68.1	0.407		
Surgical method						
	Open thoracotomy	22	76.8			
	VATS	10	70	0.776		
Resection						
	Pneumonectomy and bilobectomy	5	60			
	Lobectomy	31	62.5			
	Wedge resection	5	25	0.098		0.072
Tumor size					1	
	≤ 3 cm	21	84		6.462 (1.078-60.716)	
	>3 cm	11	48.2	0.092		0.142
T status					1	
	T1	12	90.9		6.775(1.014-45.251)	0.048
	T2	19	57.8			0.999
	T3-4	1	100	0.564		
N status						
	N0	26	72.8			
	N1	6	75	0.898		
Pathological stage						
	I	21	76			
	II	11	69.3	0.444		
Tumor grade						
	Low	9	76.2			
	High	23	72.6	0.022		0.099
Angiolymphatic invasion					1	
	No	25	82.2		5.785 (0.720-46.433)	
	Yes	7	0	0.359		
Postoperative treatment						
	No	24	70.5			
	Yes	8	80			

CI, confidence interval; VATS, video-assisted thoracoscopic surgery.

Finding

- The mean age of the patients was 61.6 years and the median follow-up time of the 32 surviving patients was 53.7months. The 5-year OS rate was 73.8%. The influence factors of overall survival for early stage mucoepidermoid carcinoma of lung result was showed in Table 1 and Figure 3.

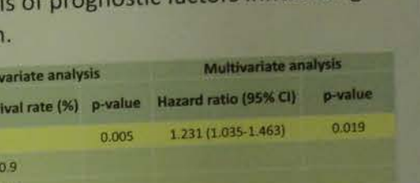

Figure 3. The prognostic factors influencing overall survival after surgical resection were age and angiolymphatic invasion.

Conclusion

Text mining techniques were apply to analyze text records related keywords in medical reports. In this study, we successfully applied an automatic classification model to cancer staging for PMEC.

Pathology

PE-11

orld Congress of Biomedical Laboratory Science (IFBLS). August 31–September 4, 2016, Kobe, Japan.

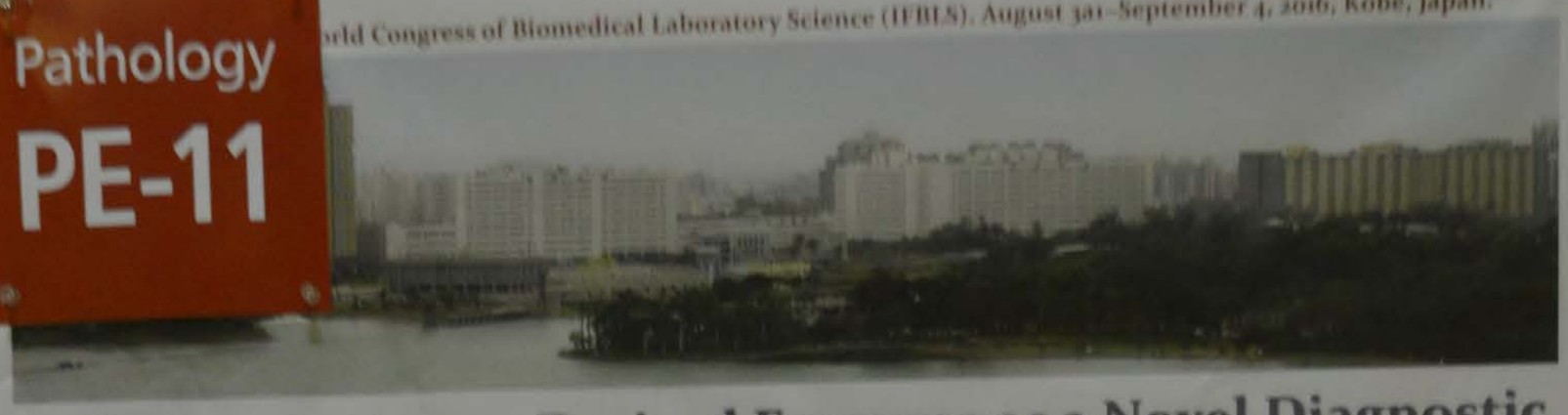

MiRNA-21 in Tumor-Derived Exosome as a Novel Diagnostic Biomarker for Oral Squamous Cell carcinomas.

Ching-Mei Chen[1], Chih-Yen Chien[2], Chao-Cheng Huang[3]

[1]Department of Laboratory medicine, [2]Department of Otolaryngology, [3]Department of Pathology, Kaohsiung Chang Gung Memorial Hospital, Kaohsiung, Taiwan

Background

- Oral cancers are the fourth most common cancer in Taiwan and the sixth most common cancer worldwide. The majority of oral cancers are squamous cell carcinoma (SCC) in histology, and the main risk factors for these cancers are tobacco, alcohol, and areca-nut use in Taiwan. Following diagnosis of oral cavity cancer, **5-year relative survival is close to 40%**. Although better combinations of multidiscipline approach have improved the quality of life in oral cancer patients, the **overall 5-year survival rate has not improved** much over the past decades. These reasons are attributed **to lack of suitable markers for screening**, presentation of the disease at an advanced stage, and failure of advanced lesions to respond to treatment.
- Exosomes are **30~100 nm cell-derived vesicles** that are present in many biological fluids, including cultured medium of cell cultures, blood and urine. Exosomes are either released from the cell when multivesicular bodies fuse with the plasma membrane or they are released directly from the plasma membrane. Exosomes contain DNA, RNA, miRNA, proteins, lipids and metabolites that is reflective of the cell type of origin. Exosomes have specialized functions and play a key role in intercellular signaling, angiogenesis, cell proliferation, cell survival and waste management. **Exosomes may be potentially used as biomarkers for prognosis, therapy, and early detection of diseases.**
- MicroRNAs constitute a recently discovered class of non-coding RNAs that play key roles in the regulation of gene expression. Acting at the post-transcriptional level, these fascinating molecules may fine-tune the expression of as much as 30% of all mammalian protein-encoding genes. microRNAs have been implicated in a number of diseases including a broad range of cancers, heart disease and neurological diseases. Consequently, **microRNAs are intensely studied as candidates for diagnostic and prognostic biomarkers and predictors of drug response**.
- miR-21 is one of the most frequently upregulated miRNAs in many pathological conditions. The human microRNA-21 gene is located on plus strand of chromosome 17q23.2 within a **coding gene TMEM49** (also called vacuole membrane protein). miR-21 is considered to be a typical 'onco-miR', which acts by inhibiting the expression of phosphatases, which limit the activity of signaling pathways such as AKT and MAPK. **miR-21 can be transcriptionally activated by NF-κB and downregulate phosphatases PDCD4 and PTEN**. Post studies evaluated circulating miR-21 as a biomarker of various carinomas, finding it has potential as a tool for early diagnosis.

Purpose

1. The objective of this study was to explore whether analysis of miRNA isolated from the exosomes of patients with oral squamous cell carcinomas could provide clinically useful information and whether they have the potency for the development of a new diagnostic approach.
2. To investigated the expression of circulating miRNAs in patients with oral squamous cell carcinomas by using whole microRNAome microarray analysis and RT-qPCR.
3. To discover potential signaling of exosomal miRNA-21, we employed a co-culture system of non-neoplastic epithelial cell lines and the exosomal miRNA-21 isolated from oral squamous cell carcinomas cell line, to study their effect on tumorigenesis.

Methods

1. Exosomes were isolated from the conditioned media from 3 OSCC cells and the non-cancerous cell by ultracentrifugation and inspected by electron microscopy. Total RNA was isolated and microRNAs were analyzed by microarray analysis and real time RT-PCR. MicroRNA microarray analysis revealed that the microRNA profile of OSCCs released exosomes was evaluated the expression of exosomal miRNAs in OSCCs.
2. Real-time RT-PCR analyses of miRNAs in exosome-enriched fractions of serum samples from 23 primary OSCC patients and 6 healthy controls were performed.
3. Transfer the exosomal miR-21 to the culture medium of the non-neoplastic epithelial cell lines. The expression level of endogenous and exosomal miRNAs were examined by real time PCR and the expression level of target proteins were detected by western blot. Functional significance of exosomal miR-21 was estimated by invasion and apoptosis assays.

Results

1. 21 miRNAs were upregulated in the exosomes of OSCC tissue as compared with those of keratinized gingival tissue.

Table 1. Differential expression of exosomal miRNAs between primary cell culture media of neoplastic and keratinized gingival tissues of OSCCs.

Range of fold change	Number	miRNA
-5~-10	5	hsa-miR-126c, hsa-miR-190, hsa-miR-200, hsa-miR-32, hsa-miR-362-3p
-2~-5	26	hsa-let-7a, hsa-miR-101, hsa-miR-1257, hsa-miR-2159, hsa-miR-1266, hsa-miR-1297, hsa-miR-1300, hsa-miR-203, hsa-miR-30, hsa-miR-379, hsa-miR-411, hsa-miR-424, hsa-miR-582-5p, hsa-miR-587, hsa-miR-590-3p, hsa-miR-592, hsa-miR-593, hsa-miR-609, hsa-miR-644, hsa-miR-648, hsa-miR-769-3p, hsa-miR-886-3p, hsa-miR-889, hsa-miR-9, hsa-miR-922, hsa-miR-95
2~5	21	hsa-miR-155, hsa-miR-1205, hsa-miR-1274b, hsa-miR-1275, hsa-miR-1277, hsa-miR-138-2, hsa-miR-182, hsa-miR-187, hsa-miR-188-3p, hsa-miR-200a, hsa-miR-204, hsa-miR-208b, hsa-miR-542, hsa-miR-548e, hsa-miR-571, hsa-miR-589, hsa-miR-597,hsa-miR-605, hsa-miR-920-2, hsa-miR-21, hsa-miR-205

2. The expression of hsa-miR-155, miR-21 and hsa-miR-205 increased and the expression of hsa-miR-126, hsa-miR-20a, hsa-miR-32, hsa-miR-362 and hsa-miR-101 decreased in OSCCs serum relative to healthy serum.

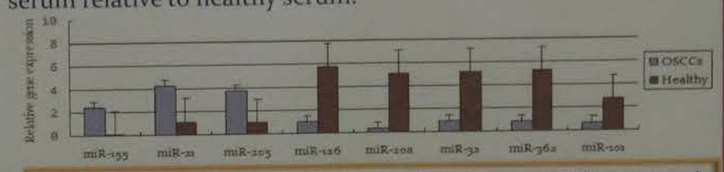

Figure 1. Relative expression levels of 8 selected miRNAs in serum of OSCC patients and healthy analyzed by real-time quantitative RT- PCR.

3. Exosomal miR-21 was potential early diagnosis signature for OSCCs.

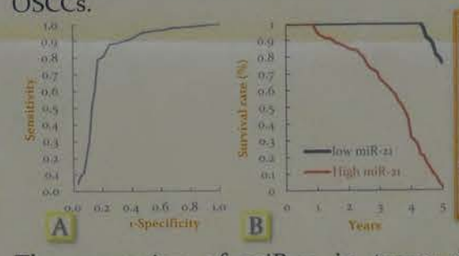

Figure 2A. The selected cut-off value of exosomal miR-21 showed 87.2% sensitivity and 89.5% specificity with an AUC of 0.856 for distinguishing OSCC patients from healthy controls.
Figure 2B. Survival was analysed in correlation to the expression levels of miR-21.

4. The expression of miR-21 in tumor-derived exosomes was significantly up-regulated in OSCC patients.

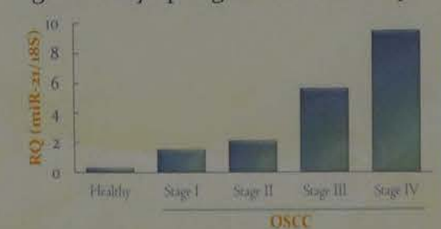

Figure 3. Real-time RT-PCR of miR-21 expression in differential stage oral cancer - derived exosomes. Exosomal miR-21 was correlated with the TNM stage. (r= 0.832; P=0.017)

5. MicroRNA-21 represses tumor suppressor PTEN and promotes cell proliferation, cell cycle progression, cell invasion and colony formation, while suppress cell apoptosis.

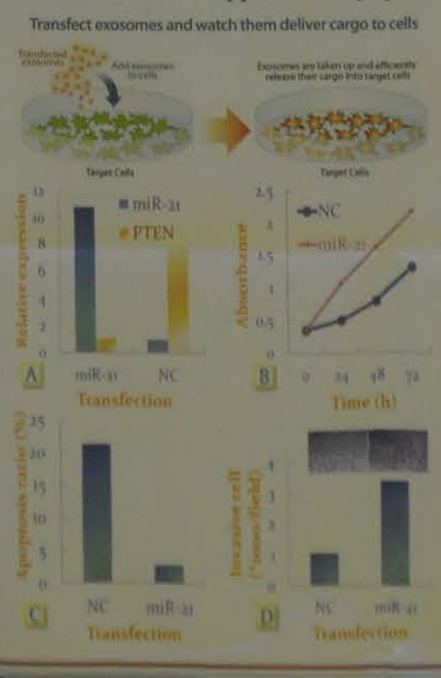

Figure 4A. Real-time RT-PCR was performed to detect the expression of miR-21 and PTEN in non-neoplastic gingival cells after treatment with exosomes.
Figure 4B. Cell Counting Kit was performed to analyze the effect of miR-21 on cell proliferation of non-neoplastic gingival cells. Ectopic expression of miR-21 promotes cell proliferation.
Figure 4C. The influence of miR-21 on cell apoptosis was analyzed using cell apoptosis assays. Transfection with miR-21 showed those cells inhibited early apoptosis.
Figure 4D. miR-21 promotes cell invasion through the membrane.

Conclusions

1. Tumor-derived exosomes are emerging as a new type of cancer biomarker. Further validation of exosomes as noninvasive, liquid equivalents of tumor biopsies are necessary.
2. These data demonstrated that exosomal microRNA acts as a oncogene or tumor suppressor in OSCC cells.
3. miR-21 post-transcriptionally down-regulates the expression of tumor suppressor PTEN and stimulates growth and invasion in OSCCs. It may be a potential therapeutic target for OSCCs.

C-3 C-3

Pathology

PE-12

PE-12

Immunohistochemical Analyses of Human Atrioventricular Node using Paraffin Sections

Muyasar Abdusalam,[1,2] Yurie Soejima,[2] Masanobu Kitagawa,[1] Motoji Sawabe[2]

[1]Department of Comprehensive Pathology, Graduate School of Medical and Dental Sciences, Tokyo Medical and Dental University, 1-5-45 Yushima, Bunkyo-ku, Tokyo 113-8519 Japan

[2]Department of Molecular Pathology, Graduate School of Health Care Sciences, Tokyo Medical and Dental University

Objective: Normal cardiac contraction critically depends on electrical impulses generated and conducted by the cardiac conduction system (CCS), which consists of sinus node, atrioventricular node, His bundle and bundle branches. As it is often difficult to identify the CCS, especially atrioventricular node, on usual HE sections, we try to search for useful immunohistochemical markers applicable to paraffin sections.

Materials and method: The subjects were ten normal human hearts taken from autopsy cases at Tokyo Medical and Dental University Medical Hospital. The method of the cutting is shown in Figure 1 and 2. Immunohistochemical study was performed on paraffin sections using antibodies against CCS-specific maker proteins, including Connexin 40 (Cx40), Connexin 43 (Cx43), HCN4 and Tbx3.

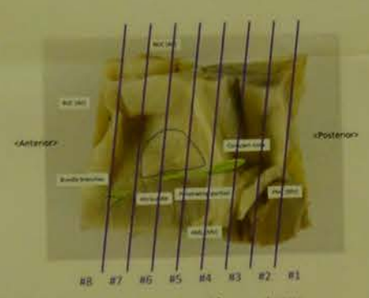

Fig1. The tissue block resected from autopsy heart and seen from the left. The suspected location of AV node and His bundle is shown in green.

Fig2. Eight 5 mm-thick tissue blocks seen from the posterior. AM, arterial muscle; MV, mitral valve; NCC, non-coronary cusp of aortic valve; RCC, right coronary cusp, TV, tricuspid valve

Results:

Cx40: The positive membranous expression of Connexin 40 in CCS cells was observed in AV node (6/9 cases; 66.6%) and in His bundle (8/10; 80%) (Figure 3 and Table 1).

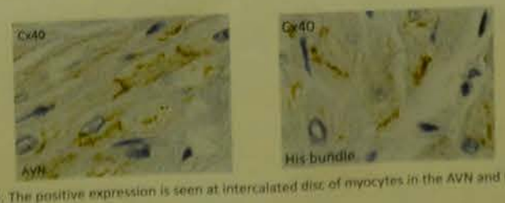

Fig 3. The positive expression is seen at intercalated disc of myocytes in the AVN and His bundle.

Table 2. Immunohistochemical staining of connexin40

Connexin40	Arterial muscle (n=9)	Atrioventricular node (n=9)	His bundle (n=10)	Ventricular muscle (n=10)
Positive	6(75%)	4(45.5%)	5(55%)	5(50%)
Partially positive	0	2(22.2%)	3(30%)	0
Negative	2(25%)	3(33.3%)	2(20%)	5(50%)

COI disclosure:
The authors and their families have nothing to disclose.

Cx43: The negative membranous expression of Connexin 43 was present in AV node (7/9; 77.7%) and in His bundle (5/10; 50%). The Connexin43 was abundantly expressed in the working myocardial cells (Figure4 and Table2).

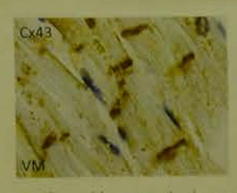

Fig 4. The positive expression is seen at intercalated disc of working myocytes of ventricle.

Table2 Immunohistochemical staining of connexin43

Cx43	Arterial muscle (n=9)	Atrioventricular node (n=9)	His bundle (n=10)	Ventricular muscle (n=10)
Positive	9(100%)	2(22.2%)	5(50%)	10(100%)
Partially positive	0	3(33.3%)	5(50%)	0
Negative	0	4(44.4%)	0	0

HCN4: The positive cytoplasmic expression of HCN4 was found in AV node (10/10; 100%) and in His bundle (7/10; 70%) (Figure 5 and Table 3).

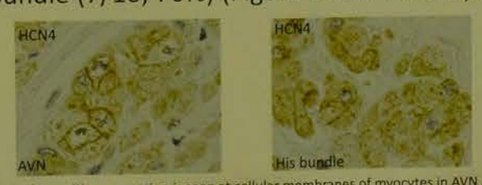

Fig 5. The positive expression is seen at cellular membranes of myocytes in AVN and His bundle.

Table 3 Immunohistochemical staining of HCN4

HCN4	Arterial muscle (n=9)	Atrioventricular node (n=10)	His bundle (n=10)	Ventricular muscle (n=10)
Positive	4(44.4%)	8(80%)	6(60%)	2(20%)
Partially positive	4(44.4%)	2(20%)	1(10%)	5(50%)
negative	1(11.1%)	0	3(30%)	3(30%)

Tbx3: The positive expression of Tbx3 was observed in AV node (4/8; 50%) and in His bundle (5/9; 55.5%) (Figure 6 and Table 4).

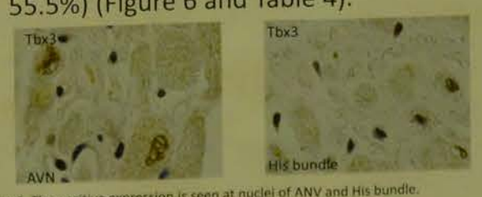

Fig 6. The positive expression is seen at nuclei of ANV and His bundle.

Table 4 Immunohistochemical staining of Tbx3

Tbx3	Arterial muscle n=(8)	Atrioventricular node n=(8)	His bundle n=(9)	Ventricular muscle n=(8)
Positive	4(50%)	4(50%)	5(55.5%)	5(62.5%)
Partially positive	4(50%)	4(50%)	4(44.4%)	3(37.5%)

Conclusion: We succeeded in identifying CCS-specific immunohistochemical markers applicable to paraffin sections (especially Cx43). Negative results warrants further study to search for more specific markers.

Reference

[1] Anderson RH, Yanni J, Boyett MR, Chandler NJ, Dobrzynski H. The anatomy of the cardiac conduction system. J Clinical anatomy. 2009; 22(1):99-113.

[2] Liang X, Evans SM, Sun Y. Insights into cardiac conduction system formation provided by HCN4 expression. J Trends Cardiovasc Med. 2015; 25(1):1-9.

[3] Severs NJ, Bruce AF, Dupont E, Rothery S. Remodelling of gap junctions and connexin expression in diseased myocardium. J Cardiovasc Res. 2008; 80(1):9-19.

[4] Severs NJ, Bruce AF, Dupont E, Rothery S. Remodelling of gap junctions and connexin expression in diseased myocardium. J Cardiovasc Res. 2008; 80(1):9-19.

Validation of inter-laboratory differences and improvements using clinical specimens

Introduction

Methods

Results

Pathology

PE-15

Clinical impact on HER2-FISH results by the 2013 ASCO/CAP Guideline

Hidehiro IWATA, Aya UMEMURA, Yoshiaki MIZUNO, Kenji NITTA, Hiroe MIZUSHIMA
Hiroyuki OSADA, Shuko SEKO, Yota MURASE, Nagako MAEDA, Toyonori TSUZUKI
Japanese Red Cross Nagoya Daini Hospital, Nagoya, Japan
Aichi Medical University Hospital, Nagakute, Japan

Objectives

The guideline American Society of Clinical Oncology/ College of American Pathologists was revised in 2013 (2013 ASCO/CAP guideline). The FISH criteria for HER2 status in breast cancer have been changed. Major changes are as follows: Positive threshold of HER2 signal to HER2/CEP17 ratio become more than 2.0, which was 2.2 previously. Average HER2 copy number is more than 6.0 also become positive even if HER2/CEP17 ratio less than 2.0. The new criteria for equivocal cases is HER2 copy number is 4.0 to less than 6.0 in case with less than 4.0 HER2 copy number. (Figure 1 and Table1) The aim of this study is to elucidate how 2013ASCO/CAP guideline influences on current clinical breast cancer practice.

Methods

From April 2014 to March 2016, we corrected 226 breast cancer biopsy cases which HER2-FISH tests were performed. According to the 2013 ASCO/CAP guideline, we reevaluated the results of HER2-FISH tests and compared with those of the original reports. We compared the HER2 FISH results according to the 2007 and 2013 ASCO/CAP Guideline. The comparison was analyzed by using the Fisher exact test. We also investigated the result of estrogen receptor (ER), progesterone receptor (PgR), HER2 test by immunohistochemistry.

Results

The data are shown in Figure 2 and Table 2. Of the 226 cases, 37 (16.4%) cases were positive by the 2013 ASCO/CAP guideline. Two of 37 positive cases were HER2/CEP17 ratios were less than 2.0, but HER2 copy numbers were more than 6.0, which had been negative, previously. Twenty-four (10.6%) cases were equivocal, which had been negative, previously. The equivocal cases by the 2013 ASCO/CAP guideline significantly increased compared to those of the original reports. (P<. 05) Among these cases, 2 (2/2, 100%) cases and 3 (3/24, 12.5%) cases were diagnosed as positive and equivocal by 2013 ASCO /CAP guideline, which were originally diagnosed triple negative (ER (-), PgR (-), HER2 (-)) breast cancers by 2007 ASCO/CAP guideline.

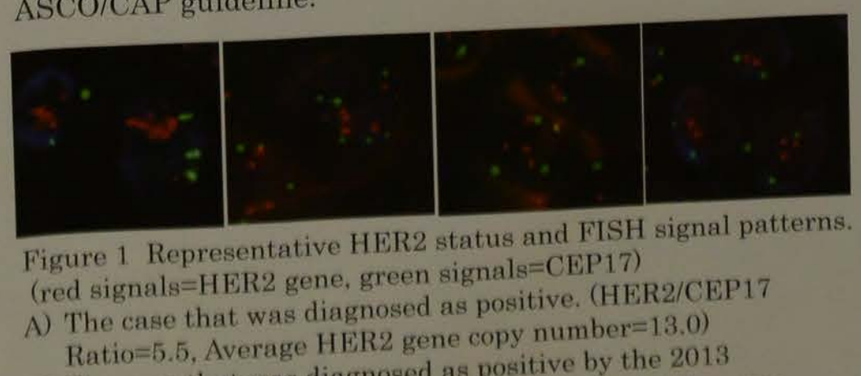

Figure 1 Representative HER2 status and FISH signal patterns. (red signals=HER2 gene, green signals=CEP17)
A) The case that was diagnosed as positive. (HER2/CEP17 Ratio=5.5, Average HER2 gene copy number=13.0)
B) The case that was diagnosed as positive by the 2013 ASCO/CAP guideline. (HER2/CEP17 Ratio=1.1, Average HER2 gene copy number=6.5) This case was diagnosed as negative by the previous criteria.
C) The case that was diagnosed as equivocal by the 2013ASCO/CAP guideline. (HER2/CEP17 Ratio=1.1, Average HER2 gene copy number=4.3) This case was diagnosed as negative by the previous criteria.
D) The case that was diagnosed as negative. (HER2/CEP17 Ratio=1.1, Average HER2 gene copy number=2.3)

Conclusions

The number of additional positive and equivocal cases increased in HER2-FISH testing were increased by using 2013 ASCO/CAP guideline. The increased cases were diagnosed as negative by the 2007 ASCO/CAP guideline. Not negligible cases became equivocal by the 2013 ASCO/CAP guideline. In addition, 2 positive cases and 3 equivocal cases might be candidates for HER2-targeted therapy by the 2013 ASCO/CAP guideline, which were originally diagnosed as "Triple negative" by the 2007 ASCO/CAP guideline. Our data suggest that the 2013 ASCO/CAP guideline can expand candidates for patients receiving HER2-targeted therapy.

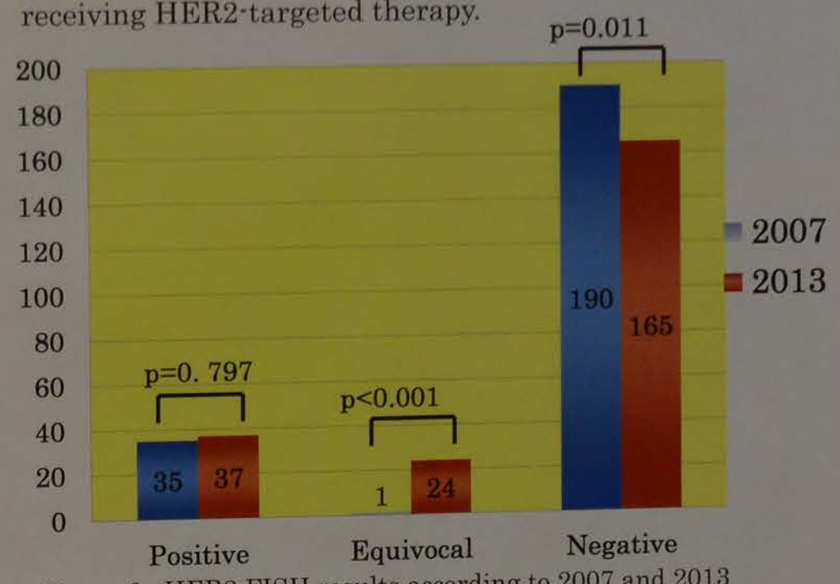

Figure 2 HER2 FISH results according to 2007 and 2013 ASCO/CAP Guideline. (n=226)
※Fisher's exact test; Significant, p<. 05

Table 2 Correlation between ER, PGR and HER2-IHC and HER2-FISH status in cases newly diagnosed as HER2-FISH results by the 2013 ASCO/CAP guideline.

	Cases with change in the HER2-FISH results	
	Negative to Positive (n=2)	Negative to Equivocal (n=24)
ER(+), PgR(+), HER2-IHC(−)	0(0.0%)	19(79.2%)
ER(+), PgR(+), HER2-IHC(−)	0(0.0%)	2(8.3%)
ER(+), PgR(+), HER2-IHC(−)	2(100.0%)	3(12.5%)

Table 1 HER2-FISH criteria of 2007 and 2013 ASCO/CAP Guideline

	2007	2013
Positive	R≧2.2	R≧2.0 or 2.0>R and HER2 N≧6.0
Equivocal	2.2>R≧1.8	2.0>R and 6.0>HER2 N≧4.0
Negative	1.8>R	2.0>R and 4.0>HER2 N

R: HER2/CEP17 Ratio, HER2 N: Average HER2 gene copy number

Pathology

PE-16

Secretagogin, a newly found Ca2+ binding protein, containing neurons in the striatum

Seiko Yasuda

Dept. of Medical Technology and Sciences, school of Health Sciences at Fukuoka, International Univ. of health and welfare

Introduction and Aim

Calcium binding proteins such as parvalbumin (PV), calretinin (CR), and calbindin D28k (CB) are considered to be valuable chemical markers to reveal the neuronal organization of various parts of the nervous system. Interestingly, the distributions of these calcium-binding protein occasionally show a considerable species differences.

Secretagogin (Scgn) is a recently discovered calcium binding protein of the EF hand family, cloned from b cells of pancreatic island of Langerhans and endocrine cells of the gastrointestinal gland (Wagner et al., 2000). Secretagogin expression has been also shown in developing and adult neurons (Alpár et al., 2012).

In this study, we examined the expression of Scgn in the striatum of rats and mice. Particularly we assessed the co-localization of Scgn with known chemical markers of striatal interneurons, choline acetyltransferase (ChAT), nitric oxide synthase (NOS), parvalbumin (PV) and calretinin (CR).

Materials and methods

1. Animals and tissue preparation

All of the experiments were carried out in accordance with the institutional guidance for animal welfare (the Guidelines for Animal Experiment in International University of Health and Welfare). Every experimental procedure was approved by the Committee of the Ethics on Animal Experiment in International University of Health and Welfare. Five adult male C57BL/6J mice (8 weeks old) and five male Wistar rats (8weeks old) were used in this study. Animals were deeply anesthetized with 2.5% isoflurane and perfused transcardially with phosphate-buffered saline (PBS, pH7.4) followed by 4% paraformaldehyde in 0.1M phosphate buffer (PB, pH7.2-7.4). The brains were left in situ for 1-2 hours at room temperature and then removed from the skull. From each brain, coronal, parasagittal, and horizontal 50μm thick sections were cut on a vibratome.

2. Immunohistochemistry

Free floating sections were processed for fluorescent triple immunolabeling using various combinations of the following primary antibodies.

- Rabbit or sheep anti-secretagogin (SCGN)
- Mouse or rabbit or guinea-pig anti-parvalbumin (PV)
- Mouse or rabbit or goat anti-calretinin(CR)
- Goat anti-choline acetyl transferase (ChAT)
- Sheep anti-nitric oxide synthase (NOS)

Fluorochromes conjugated to secondary antibodies (Jackson Labo.) were FITC, Cy3 and AMCA.

3. Image analysis

The distribution and strucutrtal features of labeled neurons were examined with a fluorescence stereoscopic microscope (Leica) equipped with a digital camera (Olympus DP70) and a fluorescence microscope (Olympus B) equipped with a digital camera (Olympus DP73). For the analyses of the colocalization relationships among makers each of three channels were separately obtained using X20 or X40 objective, then color-merged and analysed using the image-analysis software (Olympus cellSens software).

Results

Strial Scgn-positive neurons showed prominent species differences between rats and mice. In rats numerous Scgn-positive neurons were scattered throughout the whole striatum, which were nearly comparable with PV-positive neurons in number (Fig.1A, C, D), whereas in mice Scgn-positive neurons were small in number. Scgn-positive neurons in the rat striatum were heterogeneous in their structural features; one type was relatively large, and the other was relatively small and mainly located in the peripheral portion of the striatum. The co-localization analyses revealed that Scgn-positive neurons were apparently different from chemically-defined 4 types of interneurons previously reported, although they overlapped PV-, ChAT- and CR-positive ones to some extent (Fig.2-7).

In the mouse striatum, Scgn-positive neurons were far smaller in number and they appeared to correspond to the smaller type of neurons in the rat striatum (Fig.1B). Scgn-positive neurons in the mouse striatum also overlapped ChAT- and CR-positive ones to some extent, but were distinct from PV- and NOS-positive ones (data not shown).

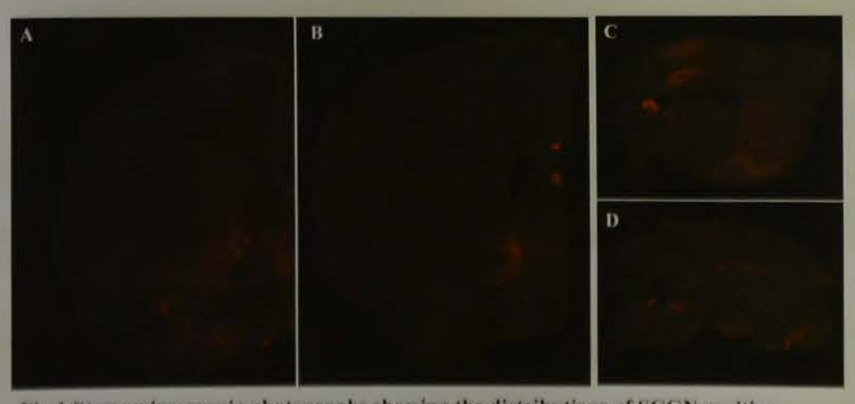

Fig.1 Stereomicroscopic photographs showing the distributions of SCGN positive neurons. (A) Rat, coronal section. (B) mouse, coronal section. In septal nuclei and basal forebrain, there are SCGN positive neurons in both rat and mouse. In contrast numerous SCGN positive neuron are seen in the rat striatum, whereas only a few positive neurons in the mouse striatum. (C) Rat, parasagittal section. (D) Rat, horizontal section.

Fig.2 Photomicrographs of the rat striatum triple-immunostained for SCGN (red), PV (green), and NOS (blue). (A) coronal section. (B) parasagittal section. (C) horizontal section. The higher magnification images of part of (B) are shown in Fig.3.

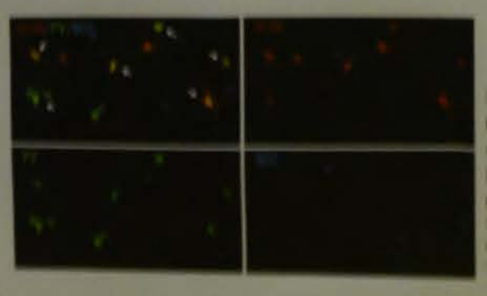

Fig.3 The higher magnification images of part of Fig.2B, showing merged and individual channel images. SCGN (red), PV (green), and NOS (blue). Arrows indicate the colocalization of SCGN and PV. In this image no neurons show the colocalization of SCGN and NOS, or of PV and NOS.

Fig.4 Photomicrographs of the rat striatum triple-immunostained for SCGN (red), PV (green), and ChAT (blue). (A) coronal section. (B) parasagittal section. (C) horizontal section. The higher magnification images of part of (A) are shown in Fig.5.

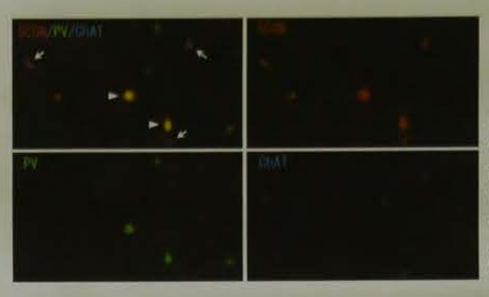

Fig.5 The high-magnification images of Fig.4A, showing merged and individual channel images. SCGN (red), PV (green), and ChAT (blue). Arrows indicate the colocalization of SCGN and ChAT. Arrowheads indicate the colocalization of SCGN and PV.

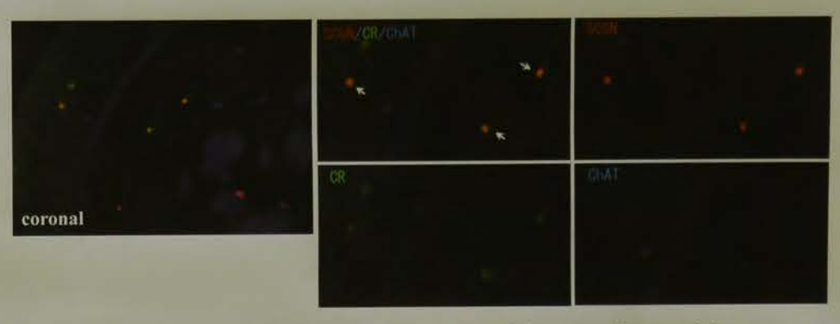

Fig.6 The low- and the high-magnification images of the rat striatum triple-immunostained for SCGN (red), CR (green), and ChAT (blue). Coronal section. The high-magnification images show the merged and individual channel images. Arrows mark indicate the colocalization of SCGN and CR.

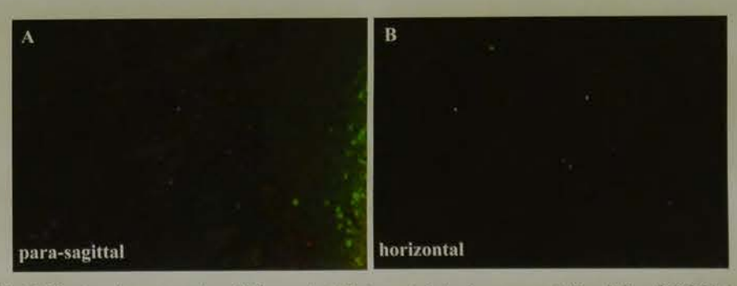

Fig.7 Photomicrographs of the rat striatum triple-immunostained for SCGN (red), PV (green), and CR (blue). (A) coronal section. (B) horizontal section.

Discussion

In the present study we examined the distribution of Scgn-positive neurons in the striatum of rats and mice. Our results indicated the followings;

1) There is a prominent species difference between rats and mice in the Scgn expression in the striatum.

In the progress of genetic engineering methods, now the mouse nervous system is one of the major targets of the analysis. On the other hand the rat nervous system has been analyzed in detail with rather classical methods. Frequently the data obtained from rats and mice have been considered to be compartible with each other, although there reported some differences between rats and mice in, for example, chemical properties of some types of neurons such as hilar mossy cells. Scgn neurons in the striatum are also an additional example of species differences between rats and mice.

2) Scgn positive striatal neurons might be a novel group of interneurons different from known 4 major groups of striatal interneurons, although they overlap those to some extent.

The present immunocytochemical analyses indicated that Scgn positive neurons did not coincide with any of the four major striatal interneurons, but overlapped PV, ChAT and CR positive neurons to some extent. These observations indicate that Scgn positive neurons might be different from previously reported four major striatal interneuron groups, but a novel group of interneurons in the rat striatum.

Conclusion

In this study, we showed that Scgn neurons were rather numerous in the rat striatum and presumed to be the fifth group of interneurons. Furthermore they showed prominent species differences between rats and mice. Future studies should aim to study the structural and functional features of these striatal Scgn neurons in detail.

Pathology
PE-18

Developing techniques for differentiating between squamous cell carcinoma and keratoacanthoma by using iCCD.

●Emmy Yanagita (CT)
Ryosuke Mastuoka (MD), Tomoo Itoh (MD),
Department of Diagnostic Pathology
Kobe University Graduate School of Medicine

Background 1

■ Keratoacanthoma and squamous cell carcinoma are characterized by similar clinical presentations that are hard to differentiate.

■There two diseases require distinct regimens of therapy similarity, differentiation between them is crucial.

Background 2

■ We developed a multiplex immunohistochemical method that can simultaneously stain cells in the G1 and S/G2/M phases and undergoing apoptosis using 3 markers CDT1, Geminin, and H2A.X.

Method & Protocol

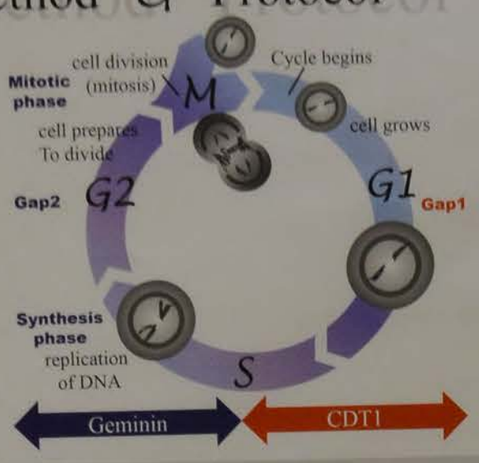

CDT-1
- A key licensing factor
- Specifically expressed in G1 phase
- Function to license DNA by foming the pre-replicative complex (pre-RC)

Geminin
- DNA replication inhibitor
- Specifically expressed in S/G2/M phases

H2A.X
- phosphorylated form of H2A.X
- Appears during apoptosis

1. **Deparaffinization**
2. **Heat-induced antigen retrieval with (HIAR) for 9min with pH6.0 citrate buffer**
3. **Blocking with 3% hydrogen peroxide in methanol for 10 min**
4. **Washing with Tris buffer(TBS)**
5. **Anti-Geminin rabbit polyclonal antibody RA 40min**
6. **Washing with TBS**
7. **Secondary antibody (MACH 2 Double Stain) RA 30 min**
8. **PermaBlue/AP RA 3min**
9. **Washing with TBS**
10. **Ab inactivation & HIAR 3min**
11. **Washing**
12. **Anti-CDT1 rabbit polyclonal antibody RA 60min**
13. **Washing**
14. **Secondary antibody (MACH 2 Double Stain) RA 40 min**
15. **Washing**
16. **PermaRed/AP RA 10min**
17. **Washing**
18. **Ab inactivation 5min**
19. **Washing**
20. **Anti-P-Histone H2A.X rabbit polyclonal antibody RA 80min**
21. **Washing**
22. **Secondary antibody (MACH 2 Double Stain) RA 40 min**
23. **DAB RA ~10min**

CDT1	x80	(Gene Tex#GTX109663)
Geminin	x40	(Prointech Group#10802-1-AP)
H2A.X	x20	(Cell Signaling#2577S)
PermaBlue/AP		(DBS#K051)
PermaRed/AP		(DBS#K049)
DAB		(Dako#K3468)

TBS : Tris-buffer saline
HIAR : indicates heat-induced antigen retrival

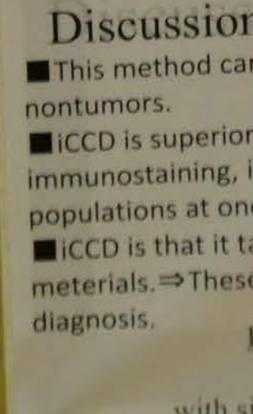

■ In the skin, a large concentration of Geminin-positive cells was found immediately above the basal cells.

■H2A.X-positive cells were abundantly observed limited to the surface layer, and a concentration of CDT1-positive cells was evident in the prickle cell layer.

Immunohistochemistry-based Cell Cycle Detection (iCCD):
A Novel System to Visualize Cell Kinetics on Formalin-fixed Paraffin-embedded Tissue.
Am J Surg Pathol 2012;36:796-773

Results

Normal skin & keratoacanthoma

■ In the skin, a large concentration of Geminin-positive cells was found immediately above the basal cells.

■H2A.X-positive cells were abundantly observed limited to the surface layer, and a concentration of CDT1-positive cells was evident in the prickle cell layer.

■Specimens from normal skin and keratoacanthoma showed organized staining patterns of cells positive for these cell cycle markers unlike those of squamous cell carcinoma.

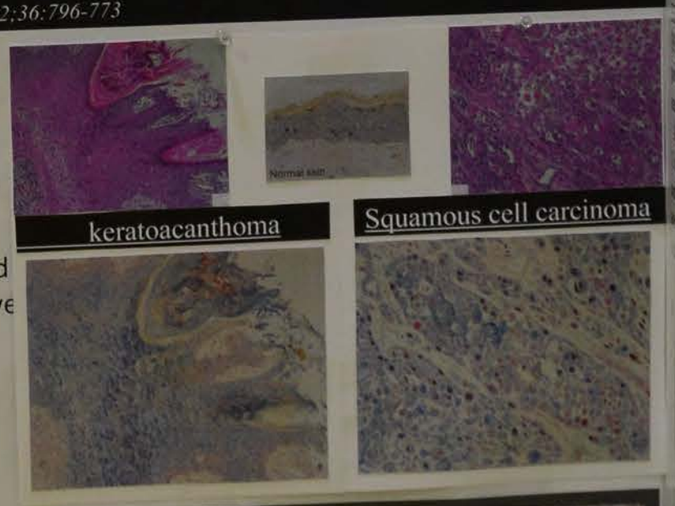

squamous cell carcinoma

■Random distribution of CDT1-positive, Geminin-positive, and H2A.X-positive cells in squamous cell carcinoma.

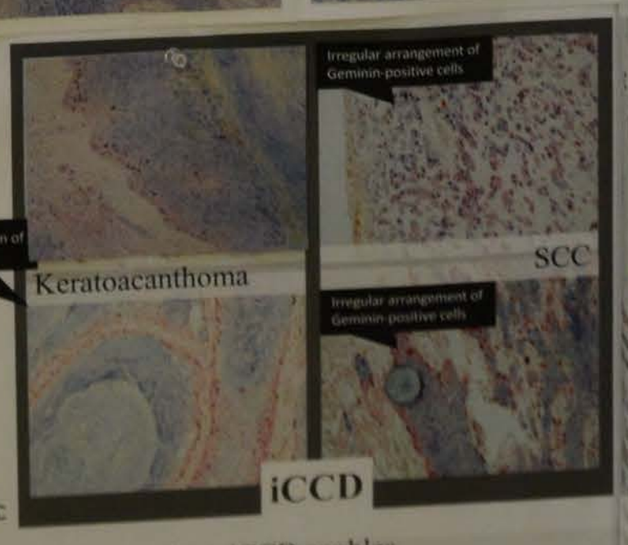

Discussion

■This method can help to distinguish tumors from nontumors.

■iCCD is superior to conventional single-color immunostaining, it allows examination for multi-cell populations at one time.

■iCCD is that it targets formalin-fixed, paraffin-embedded meterials.⇒These materials are routinely used in pathologic diagnosis.

In conclusion, the multicolor immunostaining method such as iCCD enables the differentiation between two distinct pathologies with similar the differentiations, such as karatoacanthoma and squamous cell carcinoma.

Pathology

PE-19

Evaluation of High-Resolution-Melting-Analysis (HRMA) as a diagnostic tool to detect KRAS, NRAS, and BRAF mutations with DNA extracted from formalin-fixed paraffin-Embedded (FFPE) specimens of colorectal cancer

○Tomoya Minami [1], Shinichiro Matsuki [1], Shumpei Mizuta [1], Takao Komai [1], Makiro Ishibashi [2]

1 Department of clinical laboratory , Hyogo prefectural Amagasaki general medical center, Japan

2 Department of clinical laboratory , Hyogo prefectural Kaibara hospital, Japan

【Introduction】

Anti-EGFR monoclonal antibodies such as cetuximab and panitumumab inhibit cell growth and proliferation in colorectal cancer. Recent studies showed that somatic mutations in KRAS, NRAS (All RAS) and BRAF are predictors of resistance to the anti-EGFR monoclonal antibodies, because these genes participate in downstream of EGFR in the signal transduction cascade (Figure1). Additionally, it has been reported that patients harboring these mutations not only do not benefit from but may be harmed by anti-EGFR therapy. Thus, the rapid and accurate screening of All RAS and BRAF mutations is valuable.

High-Resolution-Melting-Analysis (HRMA) is a recently developed methodology for mutation screening in double strand DNA by analyzing the difference of melt curve. It is simple, fast, and cost-effective relative to other screening techniques such as direct sequencing and PCR-rSSO.

【Method】

We described a HRMA for mutation screening of All RAS (codon12/13, codon59/61, codon117, codon146), and BRAF exon15 with DNA extracted from formalin-fixed paraffin-embedded (FFPE) specimens of 43 colorectal cancers, and analyzed the results of mutation screening by HRMA compared with the results by PCR-rSSO or direct sequencing analysis.

HRMA and direct sequencing analysis were performed with the same primer pairs (Table1). We designed primer pairs for screening KRAS codon117 and NRAS codon117 mutation with primer 3 software. For screening other mutation sites in All RAS and BRAF, we used primer pairs described in other articles.

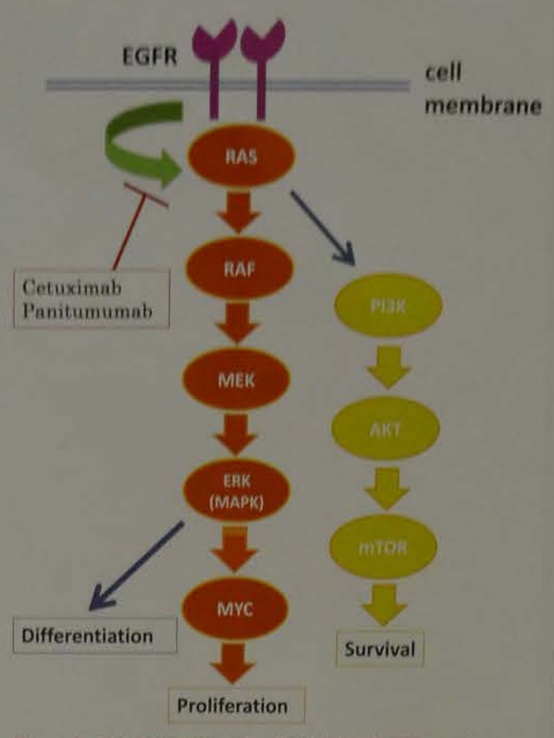

Figure1. RAS/RAS/MAPK and PIK3/AKT/mTOR pathway.
Regulation of cell growth, survival, and differentiation.

Gene	Forward primer	Reverse primer	Amplicon size
KRAS codon12/13	AAGGCCTGCTGAAAATGACTG	GGTCCTGCACCAGTAATATGCA	165bp
KRAS codon59/61	CCAGACTGTGTTTCTCCCTT	CACAAAGAAAGCCCTCCCCA	155bp
KRAS codon117	TCTTTCCCAGAGAACAAATTAAAAGA	ACTTCTTGCTAAGTCCTGAG	128bp
KRAS codon146	GACACAAAACAGGCTCAGGA	TGATTTTGCAGAAAACAGAT	120bp
NRAS codon12/13	GGTGTGAAATGACTGAGTAC	GGGCCTCACCTCTATGGTG	128bp
NRAS codon59/61	AAACAAGTGGTTATAGATGGT	CACAGAGGAAGCCTTCGCCT	118bp
NRAS codon117	TGTACCTATGGTGCTAGTGGGA	CCCGTAACTCTTGGCCAGTT	91bp
NRAS codon146	TTTGCCAACAAGGACAGTTG	CTTGCACAAATGCTGAAAGC	124bp
BRAF exon15	ATGAAGACCTCACAGTAA	CCTCAATTCTTACCATCC	120bp

Table1 : KRAS, NRAS, BRAF primer sequences and amplicon length.

【Results】

To determine the sensitivity of HRMA for detecting KRAS codon117 and NRAS codon117 mutation, dilution series of 20%, 10%, 5%, 1% of mutated DNA in wild-type DNA were analyzed. The tests revealed our HRMA protocol to be detectable at 5% mutation frequency, whereas the 1% dilution was not distinct from wild-type DNA (Figure2).

Then, we analyzed 43 diagnostic specimens from patients with colorectal cancer. All analysis results by HRMA corresponded with results by PCR-rSSO analysis (Figure3). The similar results was also obtained by performing direct sequencing analysis with several samples (Figure4).

Among samples, 18 harbored in KRAS codon12/13, and 1 harbored in KRAS codon146, and 2 harbored in NRAS codon59/61 (Figure5). BRAF mutation was detected in 4 samples among 23 samples not harboring All RAS mutation.

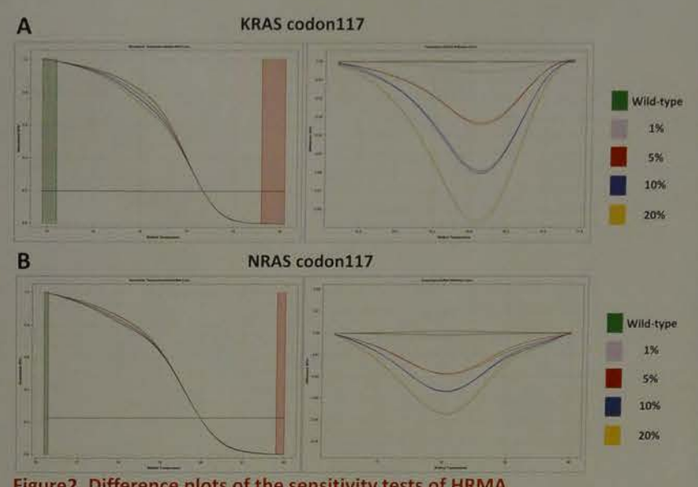

Figure2. Difference plots of the sensitivity tests of HRMA.
In order to determine the sensitivity of HRMA, mutated DNA were serially diluted with wild-type DNA at the rate of 20%, 10%, 5%, 1%. Although the 1% dilution was not distinct from wild-type DNA, the 5% dilution was detectable. A) KRAS K117N in wild-type DNA. B) NRAS K117N in wild type DNA. All samples are displayed in duplicate.

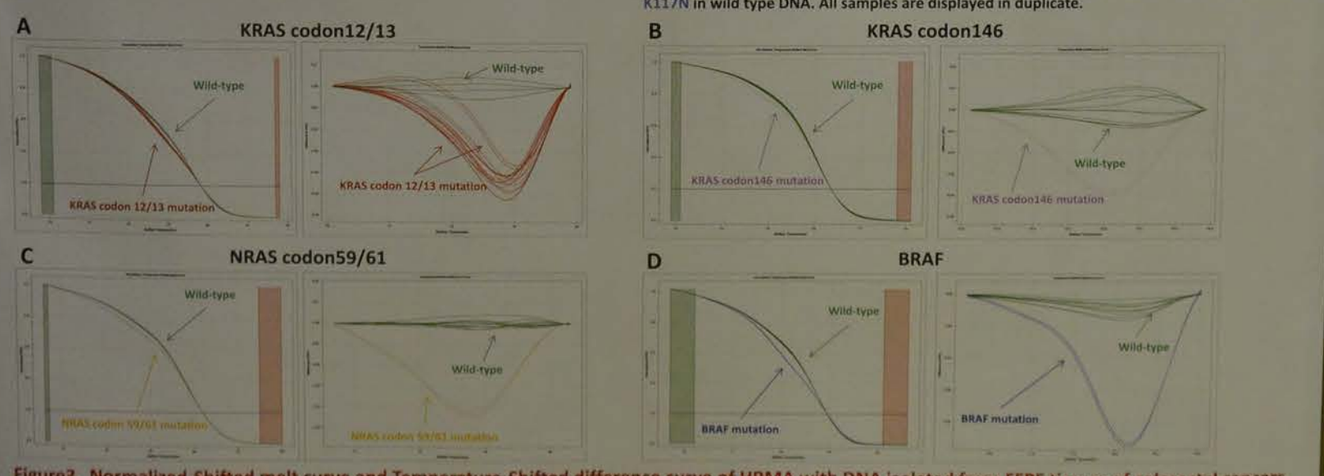

Figure3. Normalized-Shifted melt curve and Temperature-Shifted difference curve of HRMA with DNA isolated from FFPE tissues of colorectal cancers.
Samples with each mutation in A): KRAS codon12/13, B): KRAS codon146, C): NRAS codon59/61, D): BRAF were distinct from samples not harboring mutation (Wild-type).
All samples are displayed in duplicate.

【Conclusion】

In this study, we detected all mutation using HRMA with the each plasmid harboring mutation in 8 sites of All RAS. However, with diagnostic specimens from colorectal carcinoma patients, we could confirmed All RAS mutation in only 3 of 8 sites by HRMA. It is necessary to detect All RAS and BRAF mutations in more diagnostic specimens.

Thus, our study suggests that HRMA is an extremely high specific and sensitive method for mutation screening in genes with various mutation patterns such as All RAS and BRAF. In addition, HRMA enables us to detect somatic mutations in these genes more simply and efficiently.

Conflict of interest of principal presenter
The 32nd World Congress of Biomedical Laboratory Science

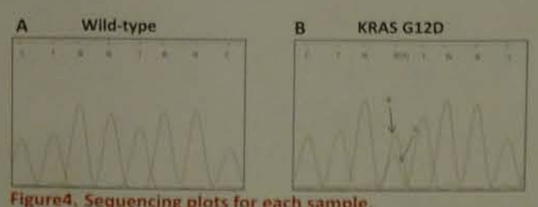

Figure4. Sequencing plots for each sample.
A): Wild-type , B) KRAS G12D. The sequence trace for B) showed the presence of a 12 G>A mutation.

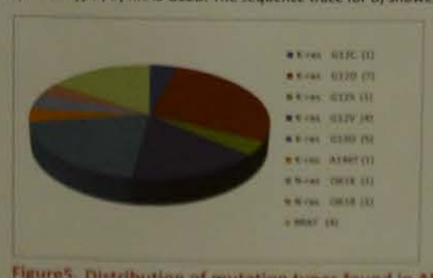

Figure5. Distribution of mutation types found in All RAS and BRAF .

D-3

Pathology
PE-20

Development of the efficient FISH signal detection by the FISH method using the immunostaining specimen.

Akikazu Endo, Emmy Yanagita, Hiroshi Yamada
Ryuko Tsukamoto, Tomoo Itoh

Department of Diagnostic Pathology
Kobe University Hospital

athology
PE-18

Developing techniques for differentiating betwee squamous cell carcinoma and keratoacanthoma by

●Emmy Yanagita (CT)
Ryosuke Mastuoka (MD), Tomoo Itoh (MD),
Department of Diagnostic Pathology
Kobe University Graduate School of Medicine

Background 1

■ Keratoacanthoma and squamous cell carcinoma are characterized by similar clinical presentations that are hard to differentiate.

■ There two diseases require distinct regimens of therapy similarity, differentiation between them is crucial.

Background 2

■ We developed a multiplex immuno that can simultaneously stain cells in t phases and undergoing apoptosis usin Geminin, and H2A.X.

Method & Protocol

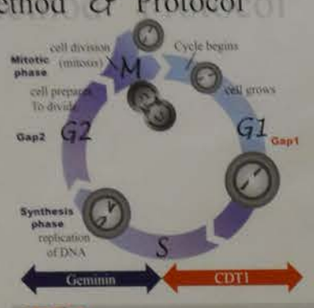

CDT-1
- A key licensing factor
- Specifically expressed in G1 phase
- Function to license DNA by foming the pre-replicative complex (pre-RC)

Geminin
- DNA replication inhibitor
- Specifically expressed in S/G2/M phases

H2A.X
- phosphorylated form of H2A.X
- Appears during apoptosis

1. Deparaffinization
2. Heat-induced antigen retrieval with (HIAR) for 9min
3. Blocking with 3% hydrogen peroxide in methanol for
4. Washing with Tris buffer(TBS)
5. Anti-Geminin rabbit polyclonal antibody RA 40
6. Washing with TBS
7. Secondary antibody (MACH 2 Double Stain) RA 30
8. PermaBlue/AP RA 3min
9. Washing with TBS
10. Ab inactivation & HIAR 3min
11. Washing
12. Anti-CDT1 rabbit polyclonal antibody RA 60mi
13. Washing
14. Secondary antibody (MACH 2 Double Stain) RA 40
15. Washing
16. PermaRed/AP RA 10min
17. Washing
18. Ab inactivation 5min
19. Washing
20. Anti-P-Histone H2A.X rabbit polyclonal antibo
21. Washing
22. Secondary antibody (MACH 2 Double Stain) RA 40
23. DAB RA ~10min

CDT1	x80	(Gene Tex#G
Geminin	x40	(Prointech G
H2A.X	x20	(Cell Signalin
PermaBlue/AP		(DBS#K051)
PermaRed/AP		(DBS#K049)
DAB		(Dako#K346

TBS : Tris-buffer saline
HIAR : indicates heat-induced antigen retrival

■ In the skin, a large concentration of Geminin-positive cells was found immediately above the basal cells.

■ H2A.X-positive cells were abundantly observed limited to the surface layer, and a concentration of CDT1-positive cells was evident in the prickle cell layer.

Immunohistochemistry-based Cell Cycle Detection (iCCD): A Novel System to Visualize Cell Kinetics on Formalin-fixed Paraffin-embedded Tissue. Am J Surg Pathol 2012;36:796-773

Results

Normal skin & *keratoacanthoma*

■ In the skin, a large concentration of Geminin-positive cells was found immediately above the basal cells.

■ H2A.X-positive cells were abundantly observed limited to the surface layer, and a concentration of CDT1-positive cells was evident in the prickle cell layer.

■ Specimens from normal skin and keratoacanthoma showed organized staining patterns of cells positive for these cell cycle markers unlike those of squamous cell carcinoma.

squamous cell carcinoma

■ Random distribution of CDT1-positive, Geminin-positive, and H2A.X-positive cells in squamous cell carcinoma.

Discussion

■ This method can help to distinguish tumors from nontumors.

■ iCCD is superior to conventional single-color immunostaining, it allows examination for multi-cell populations at one time.

■ iCCD is that it targets formalin-fixed, paraffin-embedded meterials.⇒These materials are routinely used in pathologic diagnosis.

In conclusion, the multicolor immunostaining method such as iCCD enab the differentiation between two distinct pathologies with similar the differentiations, such as karatoacanthoma and squamous cell c

Background

The FISH method often hesitates about a judgement to observe it under dark field using a fluorescent microscope whether it's the cell which we should count.

We usually judge the cell which we should count in reference to an H&E staining specimen. However , we don't necessarily serve as a reference because a slice slide is different from an H&E staining specimen with the FISH specimen.

When there are few neoplastic cells in particular, it is concerned about being judged to be with a normal epithelium cell or stroma cell by mistake.

Therefore the count of the FISH method is difficult and must perform it carefully.

Purpose

We examined it to find the method that could enforce the FISH method where had high precision than before.

We can judge the cell which we should count from only a fluorescent microscope without an H&E staining specimen exactly.

Method

It enforced the FISH method to an immunohistochemistry staining specimen developed by DAB.
Immunohistochemistry stained an auto immunity staining device.---Ventana XT system benchmark(Roche) , Bond Max(Leica)

1.Immunohistochemistry stain it.

2.The FISH method according to a protocol to recommend.
1)Digest proteins using Pepsin
※We do not perform the heating step. ---Because we have already heated by immunostaining.
2)Dehydrate the slides
3)Put on the slides probe hybridization mixture
4)Denaturation and hybridization
5)Wash the slides
6)Put on the slides mounting medium with DAPI

3. We observe it with a fluorescent microscope.

Results

Immunohistochemistry stain : AE1/AE3 + FISH probe : *her2*

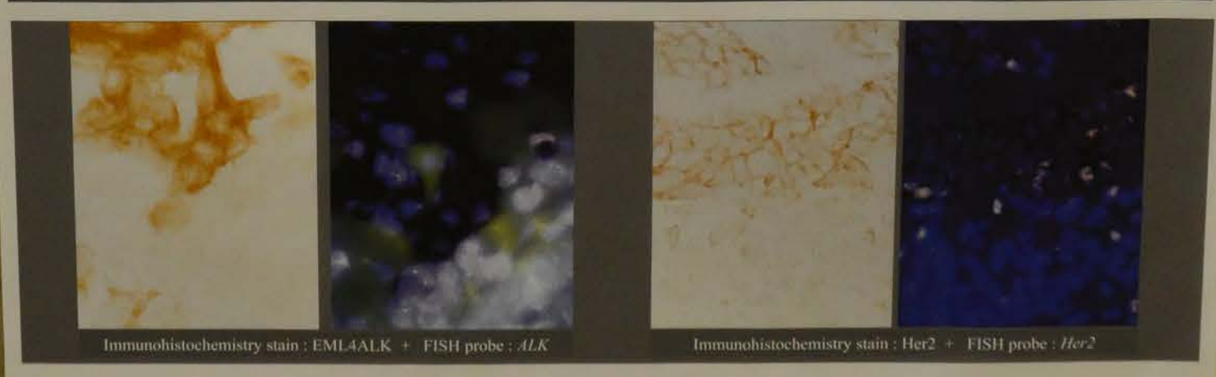

An immunohistochemistry stained specimen became able to judge the cell which we should count only in a fluorescent microscope by enforcing an FISH method.
Fading of DAB was not seen by the operation of the FISH method , and the cell fusion was not seen,too. The judgement of the cell which we should count was easy.

Pathology

PE-21

Study of rapid FISH method using the IQ Buffer.

Ohkazu Endo, Emmy Yamagina, Hiroshi Yamada
Ryuko Tsukamoto, Tomoo Itoh

Department of Diagnostic Pathology
Kobe University Hospital

Background

The conventional FISH method spend overnight on hybridization, it is performed for two days. We often reexamine the FISH method by various reasons such as the nonspecific reaction of the background being too strong or a signal is weak or it's not detected.

In late years hybridization buffer which hybridization finished in 60-120 minutes was released, and the FISH method became able to be finished in 3 hours. A result report was enabled on the day even if we carried out reexamination.

Purpose

We diluted other companies probes using IQ FISH FAST Hybridization Buffer(IQ buffer) and performed the FISH method according to the FISH method for 3 hours protocol and performed the examination that a signal could detect.

Method

Using several kinds of other companies probes, we diluted it in hybridization buffer to recommend each and carried out the FISH method according to a protocol to recommend. We performed the FISH method according to the protocol of the FISH method for 3 hours when the same probe was recommended in diluted form using IQ buffer(G9415A,Agilent technologies).

In the already probe that is diluted, mixed equal amounts of probe mix and IQ buffer.

Protocol *Use reagents from the Dako Histology Accessory Kit(K5799,Dako)*

1. De-paraffinize the samples
2. Pre-treat the samples with Dako Pre-Treatment Solution
   for 10 minutes at 98 degrees
3. Allow the slides to cool in the Pre-Treatment Solution
   for 15 minutes at room temperature
4. Digest proteins using Pepsin
   for 5 minutes(3-18 minutes) at 37 degrees
5. Dehydrate the samples
6. Prepare the probe hybridization mixture
   Labeled FISH probe 1 : IQ buffer 9
7. Denaturing and Hybridizing the Probe and Chromosomal DNA
   Denature for 10 minutes at 80 degrees
   Hybridization for 90minutes(60-120 minutes) at 45 degrees
8. Wash the slides
   for 10 minutes at 63 degrees
9. Dehydrate the samples
10. DAPI
    VECTASHIELD Hard set mounting medium with DAPI
    (H-1500,VECTOR)

Results

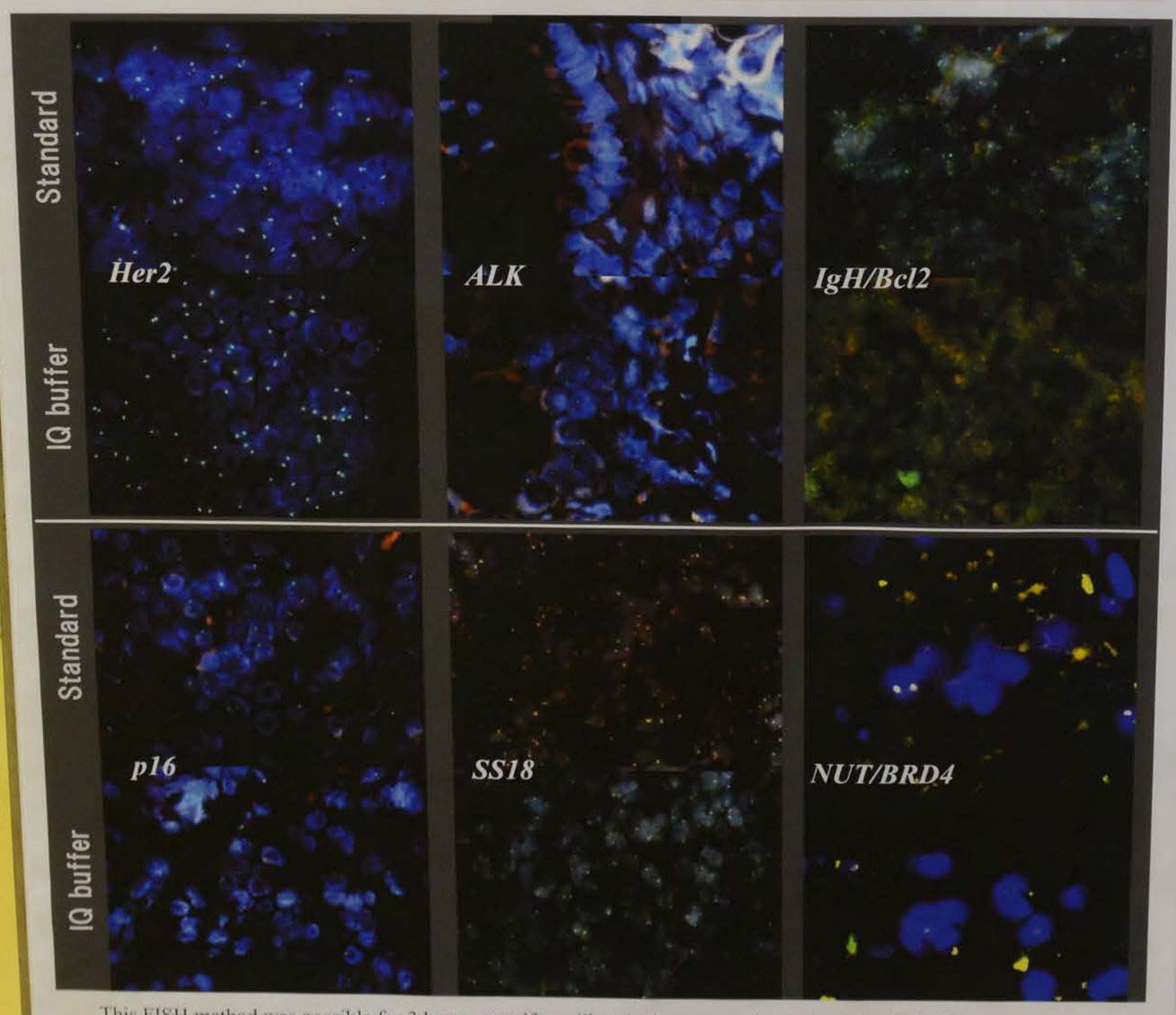

This FISH method was possible for 3 hours even if we diluted other companies probe using IQ buffer.
And by some probes, the signal that one using IQ buffer was clear was provided.

Pathology

PE-22

Study of the efficient FISH signal detection and rapid FISH method.

Akikazu Endo, Emmy Yamagita, Hiroshi Yamada
Ryuko Tsukamoto, Tomoo Itoh

Department of Diagnostic Pathology, Kobe University Hospital

Background

In late years various molecular target drugs are developed , immunohistochemistry staining and the FISH method are indispensable to the adaptation.
However , We need 2 days before a result is given by the conventional FISH method.
In addition , we must carry out reexamination because a signal is not often seen depending on a specimen.

The fine adjustment of the preprocessing process is necessary for this reexamination and needs 2 days extra.
Furthermore , the FISH method is observation under the dark field , and it's difficult to distinguish the cell which we should count.
Therefore we spend time with great labor to look for the signal of the objective cell and must count it.

Purpose

We shortened time to spend it for the FISH method and performed the examination that could not distinguish the cell which we should count more under dark field.

Method

Protocol

1. Immunohistochemistry staining
2. The FISH method
   1) Digest proteins using Pepsin for 5 minutes(3-18minutes) at 37 degrees
   2) Dehydrate the specimen
   3) Hybridize probes using IQ buffer
      labeled FISH probe 1μl : IQ buffer 9μl
      pre-mix FISH probe 5μl : IQ buffer 5μl
   4) Denature the probe and chromosomal DNA in IQ buffer for 10 minutes at 80 degrees
   5) Hybridize the probes to the chromosomal DNA in IQ buffer for 90 minutes(60-120 minutes) at 45 degrees
   6) Wash the slides
   7) Dehydrate the specimen
   8) DAPI
      VECTASHIELD Hard set mounting medium with DAPI (H-1500,VECTOR)

We diluted a probe using IQ FISH Fast Hybridization buffer(IQ buffer,G9415A,Agilent Technologies) and carried out the FISH method according to protocol of 3 hours.

We used the specimen which carried out immunohistochemistry staining because the effective detection of the FISH signal was enabled by performing the FISH method using an immunostaining specimen developed by DAB.

Immunostaining : an auto immunity staining device and hand method----------Ventana XT system benchmark(Roche) ,Bond Max(Leica)

The FISH method : Using reagents from Dako Histology Accessory Kit(K5799,Dako)

Results

We could distinguish only the signal of the objective cell under dark field, and the report was enabled as a result of the FISH method in half day.

Conclusion

By this technique, we can give molecular pathological diagnosis and treatment quickly.
In addition, we think that we can contribute to the life convalescence of the patient very much.

Pathology

PE-23

Three dimensional imaging analysis of the promotion process from β-catenin accumulated crypts to colonic adenomas in mice model

Kazuo Kase[1)3)], Nobuko Saito[1)], Yuji Sato[1)], Kenzo Hiroshima[2)], Yukari Okita[3)], Yukihide Watanabe[3)], Hiroyuki Suzuki[3)], Mituyasu Kato[3)]

[1)]Edogawa Medical Laboratory Center, [2)]Tokyo Women's Medical University Yachiyo Medical Center, [3)]Department of Experimental Pathology, Faculty of Medicine, University of Tsukuba

Summary

Early process of colon adenoma formation is not fully understood , though cancer cells as well as tumor microenvironment are thought to have important roles.

In this study, we examined cell proliferation status of neoplastic cells and microvascular structures during the process of early adenoma development from β-catenin accumulated crypt (BCAC) in mice models.

Dextran sodium sulfate (DSS) was given to $Apc^{Min/+}$mice at 5 weeks of age in drinking water for 7days to induce colonic inflammation and adenoma formation. $Apc^{Min/+}$mice have multiple BCAC in the colon but BCAC rarely develop to colon adenoma. DSS initiated adenoma formation and visible adenoma with multiple branching structures were developed within 3-4 weeks. Increase of Ki-67 positive cells in BCAC was observed on 5th day during DSS treatment and reached to 90% of the total cell numbers in 3-4 weeks. Then, protruding tumors were formed during 1-4 weeks after DSS. At the same time, in the surrounding , neovascular formation and increase of spindle shaped stromal cells were also detected during the early time point of adenoma formation.

Introduction

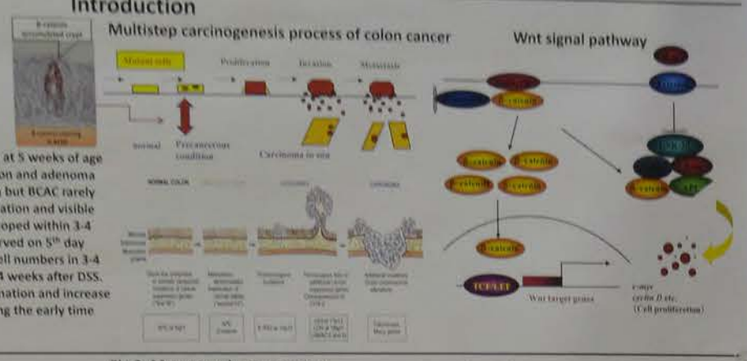

Materials and Methods

Fig 1, Experimental Procedures

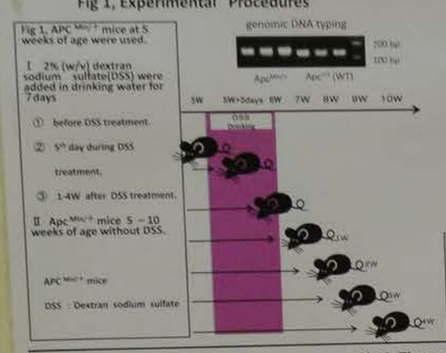

Fig 1, $APC^{Min/+}$ mice at 5 weeks of age were used.

I 2% (w/v) dextran sodium sulfate(DSS) were added in drinking water for 7 days

① before DSS treatment.

② 5th day during DSS treatment.

③ 1-4W after DSS treatment.

II $Apc^{Min/+}$ mice 5 – 10 weeks of age without DSS.

$APC^{Min/+}$ mice

DSS : Dextran sodium sulfate

Fig 2, Macroscopic appearance

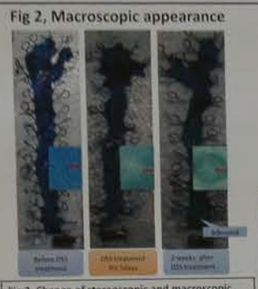

Fig 2, Change of stereoscopic and macroscopic appearance of BCAC in the large intestine.
Methylene blue staining.
Before DSS : BCAC normal formation.
DSS for 5 days : expanded BCAC that it around ulcer formation.
3 weeks after DSS : elevated adenoma formation.

Fig 3, Three dimensional imaging analysis

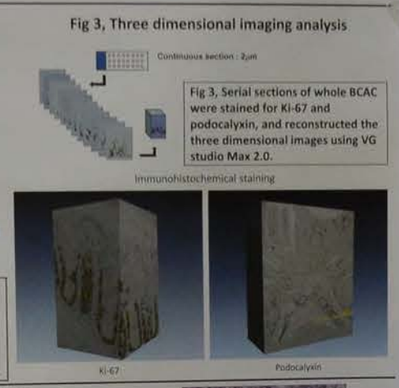

Fig 3, Serial sections of whole BCAC were stained for Ki-67 and podocalyxin, and reconstructed the three dimensional images using VG studio Max 2.0.

Results

Fig 4, Time course of Hematoxylin eosin staining in the colon

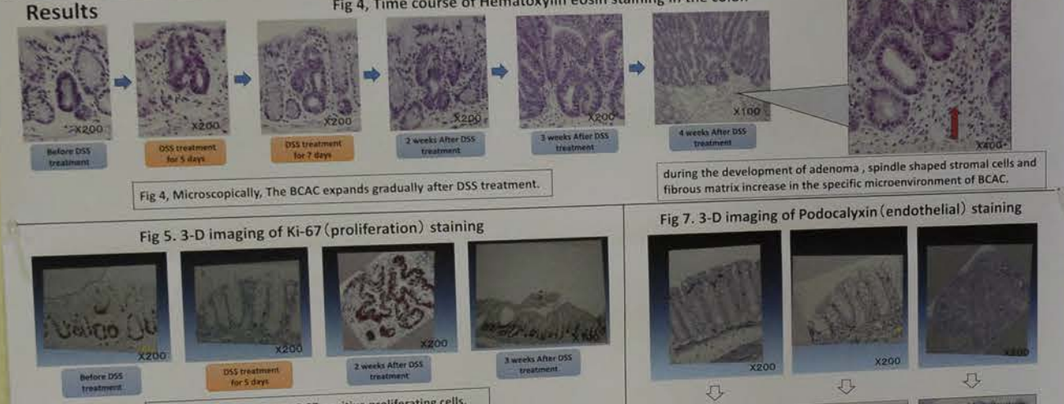

Fig 4, Microscopically, The BCAC expands gradually after DSS treatment.

during the development of adenoma , spindle shaped stromal cells and fibrous matrix increase in the specific microenvironment of BCAC.

Fig 5. 3-D imaging of Ki-67(proliferation) staining

Fig 5, 3-D imaging of the Ki-67 positive proliferating cells.

Fig 7. 3-D imaging of Podocalyxin(endothelial) staining

Fig7, The microvascular structure changed from loop to mesh structure in the microenvironment of BCAC treatment.

Fig 6. Time course of proliferating cell number in BCAC

Fig 6, Increase of Ki-67 positive cell ratio in BCACs was observed as early as 5th day during DSS treatment and reached to 90% of the total cell number in 3-4 weeks. Then, protruding tumors were formed during 1 to 4 weeks after DSS.

Conclusion

DSS treatment induced development of BCAC to adenomas in the colon of $Apc^{Min/+}$mice.
During this process , neovascular formation and increase of spindle shaped stromal cells accompany to adenoma formation from the early time points.

Pathology

PE-24

Assessment of Lgr5 expression in colorectal neuroendocrine tumors

Tamayuki Nakajima[1], Takeshi Uehara[1], Yuko Ono[1], Yasuhiro Maruyama[1], Yukihiro Kobayashi[1], Takayuki Honda[1]

[1]Department of Anatomic Pathology, Tokyo Medical University, Tokyo, Japan

Background

Materials & Methods

Results

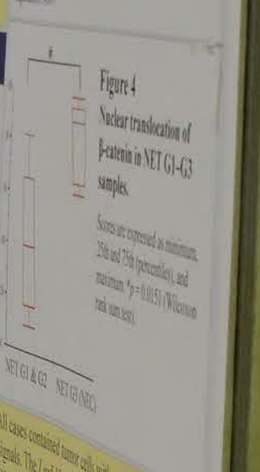

Figure 1 Immunohistochemical staining of Ki-67, β-catenin, and combination of Lgr5 RNA in situ hybridization with synaptophysin immunohistochemistry for NET G1-G3.

Figure 4 Nuclear translocation of β-catenin in NET G1-G3 samples.

Conclusion

Pathology

PE-25

Immunohis... integrins in...

Yurie Soejima[1,2], Toshio Fukusato[3]

[1]Department of Molecular... [2]General Medical Educat... [3]Department of Human P...

Intrahepatic cholangiocarcinoma

- Intrahepatic cholangiocarcinoma (ICC) is epithelial tumor which occurs in bile duct. Anatomically, intrahepatic bile duct is defined as peripheral side from the second bile duct bifurcation. About the localization, ICCs arising from large bile ducts which consist of the first to third branches are called perihilar type, while ICCs arising from small bile ducts or bile called peripheral type. According to macroscopic growth patterns, ICC as mass forming type (MF), periductal infiltrating type (PI), intraductal (IG). Histologically, ICCs compose of adenocarcinoma which forms a g structure and are classified into well, moderately, poorly differentiated g *Pancreat Sci , 2014*), but a pathway of carcinogenesis is unclear. Following progress in the study of hepatic progenitor/stem cells, a need for re-cla classification of ICCs is now increasing.
- ICCs have various biological behaviors and prognosis (*Ariizumi S et al. Pancreat Sci , 2014*), but a pathway of carcinogenesis is unclear. Following progress in the study of hepatic progenitor/stem cells, a need for re-cla classification of ICCs is now increasing.

We analyzed the expression of β4 and β6 integrin in ICCs immunoh... expressions of extracellular matrix.

Tissue samples of 48 ICC cases were obtained from surgical specimens at Tokyo Me... Dental University hospital.

Table 1. Clinical and pathological characteristics of ICC cases

	Intrahepatic cholangiocarcinoma (48 cases)
Male / Female	36 / 12
Age (mean)	70.5 (39-84)
Tumor size (mm)	58.8 (18-220)
HBV / HCV / None	6 / 8 / 35
NL / CH / LC	30 / 11 / 7
Peripheral / Perihilar	38 / 10
MF / MF+PI / PI / IG+PI	42 / 4 / 1 / 1
Well / Moderate / Poor	6 / 29 / 13

MF : mass forming type, PI: periductal infiltrating type, IG: intraductal growth type, HBV+HCV: one case

Table 3. Evaluation of β4, β6 integrin expressions by immunohistochemistry

Intensity	0: negative	1: weak	2: moderate	3: strong	
Percentage	0: negative	1: 1-25%	2: 26-50%	3: 51-75	4: 76-100%
Score (Multiply)	0-4 : negative~low		6-12 : high		

1. Expressions of β4, β6 integrin in intrahepatic cholangiocarcinoma

Figure 1. β4, β6 integrin immunohistochemistries in intrahepatic cholangiocarcinoma

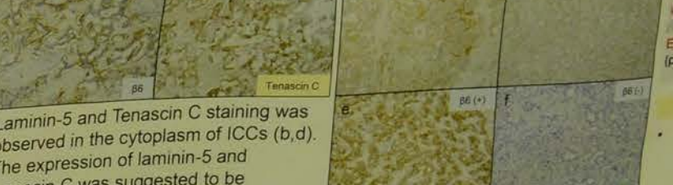

- Positive staining for β4 or β6 integrin was demonstrated in 46(96%) and 35(73%
- The predominant pattern for the β4, β6 integrin was classified as a basal lamina pattern(b,c), cell membrane pattern(d) and cytoplasmic pattern.

Figure 2. β4, β6 integrin expressions and the localization type

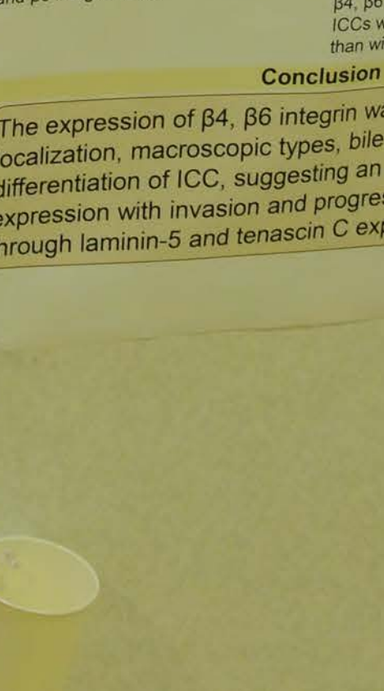

Figure 3. β4 integrin expression and gross type

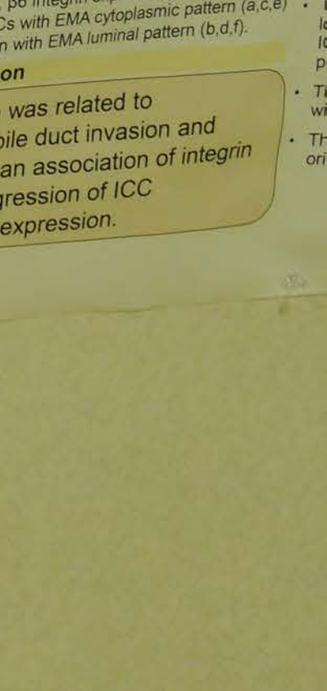

- β4, β6 integrin expression levels were higher in perihilar type(a,b) than in peripheral type(c,d) (Figure 2).
- β4 integrin expression is higher in a PI IG (a) than a MF(b) (Figure 3).

2. Relation to extracellular matrix and EMA expression

Figure 4. Expressions of β4, β6 integrin, laminin-5 and tenascin C

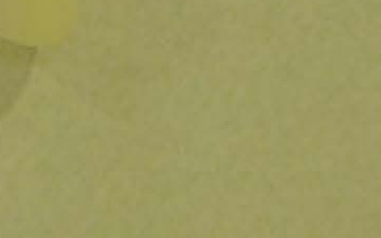

Laminin-5 and Tenascin C staining was observed in the cytoplasm of ICCs (b,d). The expression of laminin-5 and tenascin C was suggested to be associated with the expression of β4 and β6 integrin (a,c).

Figure 5. Expressions of β4, β6 integrin and EMA

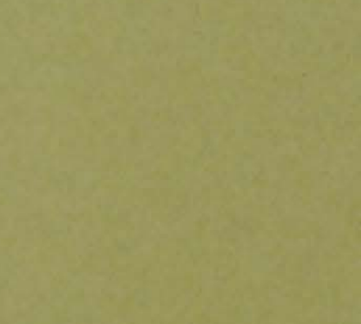

β4, β6 integrin expression was stronger in ICCs with EMA cytoplasmic pattern (a,c,e) than with EMA luminal pattern (b,d,f).

Conclusion

The expression of β4, β6 integrin was related to localization, macroscopic types, bile duct invasion and differentiation of ICC, suggesting an association of integrin expression with invasion and progression of ICC through laminin-5 and tenascin C expression.

Pathology

PE-24

Assessment of *Lgr5* expression in colorectal neuroendocrine tumors

Tomoyuki Nakajima[1], Takeshi Uehara[1], Yuko Otani[3], Yasuhiro Maruyama[2], Yukihiro kobayashi[1], Takayuki Honda[1]

[1]Department of Laboratory Medicine, [2]Gastroenterology, Department of Medicine, Shinshu University School of Medicine, Matsumoto, Japan , and [3]Niigata Prefectural Central Hospital, Niigata, Japan

Background

Leucine-rich repeat-containing G-protein-coupled receptor 5 (*Lgr5*) is a putative intestinal stem cell marker. *Lgr5* is also expressed in various tumors. In this study, we have investigated *Lgr5* expression in colorectal neuroendocrine tumor (NET) samples, and analyzed associated pathological characteristics.

Materials & Methods

We evaluated the clinicopathological features of 8 NET grade 1 (G1), 4 NET grade 2 (G2), and 8 NET grade 3 (G3; also termed neuroendocrine carcinoma (NEC)) cases. We also measured *Lgr5* expression using RNAscope®, a newly developed RNA *in situ* hybridization technique, and a tissue microarray of NET samples. *Lgr5* staining in individual tumor cells was scored semi-quantitatively using an H-score scale. Ki-67, β-catenin, and synaptophysin were also detected in all cases by immunohistochemistry. We also performed a combination of *Lgr5* RNA *in situ* hybridization and synaptophysin immunohistochemistry.

Results

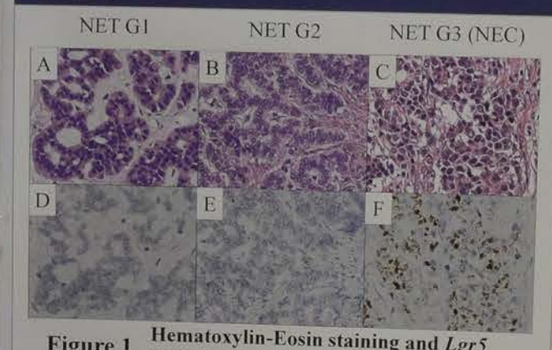

Figure 1 **Hematoxylin-Eosin staining and *Lgr5* RNA *in situ* hybridization detection in NET samples.**

A–C: Hematoxylin-Eosin staining of NET G1–G3 samples. D–F: Identification of *Lgr5* (brown dot)-positive cells in NET G1–G3 samples. Original magnification: 400×

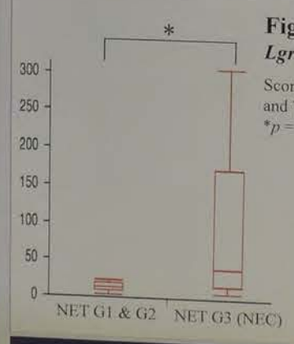

Figure 2 ***Lgr5* H-scores in NET G1–G3.**

Scores are expressed as minimum, 25th and 75th (percentiles), and maximum. *$p = 0.0491$ (Wilcoxon rank sum test).

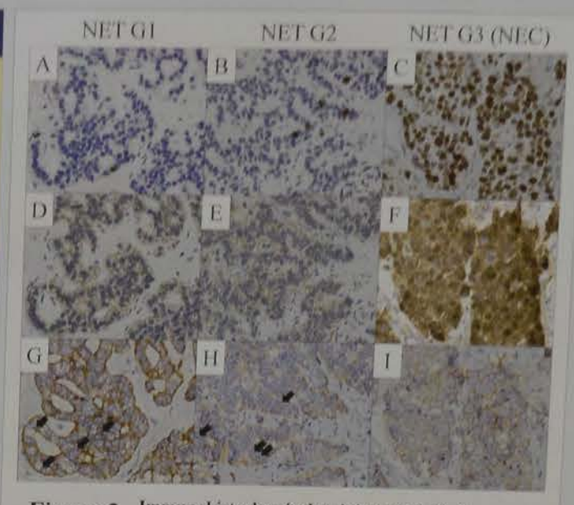

Figure 3 **Immunohistochemical staining of Ki-67, β-catenin, and combination of *Lgr5* RNA *in situ* hybridization with synaptophysin immunohistochemistry for NETG1–G3.**

A–C: Staining of Ki67-positive cells. D–F: Staining for nuclear translocation of β-catenin positive cells. G–H: Identification of *Lgr5*-positive (red dot) and synaptophysin-positive (brown) cells in NET G1–G3. Double-positive cells are indicated (black arrows). Original magnification: 400×

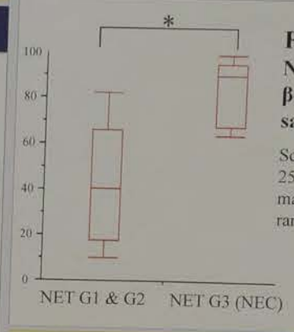

Figure 4
Nuclear translocation of β-catenin in NET G1–G3 samples.

Scores are expressed as minimum, 25th and 75th (percentiles), and maximum. *$p = 0.0151$ (Wilcoxon rank sum test).

All cases contained tumor cells with some *Lgr5*-positive signals. The *Lgr5* H-score was significantly higher in NET G3 (NEC) samples compared with those of NET G1 and G2. Both *Lgr5*-positive and synaptophysin-positive cells were observed in most cases. In all cases, *Lgr5* H-scores showed a positive correlation with nuclear β-catenin expression ($r = 0.6662$, $p = 0.0013$). There was no correlation between *Lgr5* H-score and Ki-67 expression. In the NET G1 and NET G2 groups, there was also no correlation between *Lgr5* H-score and Ki-67 expression, or between *Lgr5* H-score and β-catenin expression. In NET G3 (NEC) there was a strong positive correlation between *Lgr5* H-score and β-catenin expression ($r = 0.8333$, $p = 0.0102$).

Conclusion

Lgr5 expression might be affected by β-catenin expression in NET and especially in NET G3 (NEC) lesions. The presence of *Lgr5* and synaptophysin double-positive cells suggests that *Lgr5*-positive cells may be also stem cells in NEC, as is the case in colon adenocarcinoma. A further study with a larger number of NEC cases is warranted to confirm these findings.

Pathology

PE-25

Immunohistochemical studies of beta4 and beta6 integrins in intrahepatic cholangiocarcinoma

Yurie Soejima[1,2], Motoji Sawabe[1], Takumi Akashi[3], Yoshinobu Eishi[3], Toshio Fukusato[2]

1) Department of Molecular Pathology, Graduate School of Health Care Sciences, Tokyo Medical and Dental University
2) General Medical Education and Research Center, Teikyo University
3) Department of Human Pathology, Graduate School of Medical and Dental Sciences, Tokyo Medical and Dental University

Introduction

Intrahepatic cholangiocarcinoma

- Intrahepatic cholangiocarcinoma (ICC) is epithelial tumor which occurs in bile duct. Anatomically, intrahepatic bile duct is defined as peripheral side from the second bile duct bifurcation. About the localization, ICCs arising from large bile ducts which consist of the first to third branches are called perihilar type, while ICCs arising from small bile ducts or bile ductules are called peripheral type. According to macroscopic growth patterns, ICCs are classified as mass forming type (MF), periductal infiltrating type (PI), intraductal growth type (IG). Histologically, ICCs compose of adenocarcinoma which forms a glandular structure and are classified into well, moderately, poorly differentiated grade.
- ICCs have various biological behaviors and prognosis (*Ashima S. et al. J Hepatobiliary Pancreat Sci., 2014*), but a pathway of carcinogenesis is unclear. Following the recent progress in the study of hepatic progenitor/stem cells, a need for re-evaluating the classification of ICCs is now increasing.

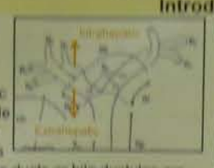

Integrins

Integrins are cell surface receptors that connect the cytoskeleton to the extracellular matrix and regulate cell adhesion and movement. Integrins compose of α and β subunits, forming 24 αβ heterodimeric members. They contribute to tumor progression and metastasis.

β4, β6 integrin

- α6β4 (β4) integrin is expressed on normal bile duct and cholangiocarcinoma. It is a receptor for laminin-5.
- αvβ6 (β6) integrin is upregulated during tissue remodeling or in cancers, however no expression is shown in normal adult epithelia. It is a receptor for fibronectin and tenascin C.
- We have reported that **the expression of β4, β6 integrins were significantly higher in ICC than in cholangiolocellular carcinoma and Hepatocellular carcinoma.**

(Y. Soejima et al. Hepatology Research, 2014)

Aim

We analyzed the expression of β4 and β6 integrin in ICCs immunohistochemically and compared the results with the clinicopathological characteristics and the expressions of extracellular matrix.

Materials & Methods

Tissue samples of 48 ICC cases were obtained from surgical specimens at Tokyo Medical and Dental University hospital.

Table 1. Clinical and pathological characteristics of ICC cases

	Intrahepatic cholangiocarcinoma (48 cases)
Male / Female	36 / 12
Age (mean)	70.5 (39-84)
Tumor size (mm)	58.8 (18-220)
HBV / HCV / None	6 / 6 / 35
NL / CH / LC	30 / 11 / 7
Peripheral / Perihilar	38 / 10
MF / MF+PI / PI / IG+PI	42 / 4 / 1 / 1
Well / Moderate / Poor	6 / 29 / 13

MF: mass forming type, PI: periductal infiltrating type, IG: intraductal growth type, HBV+HCV: one case

Table 3. Evaluation of β4, β6 integrin expressions by immunohistochemistry

Intensity	0: negative	1: weak	2: moderate	3: strong	
Percentage	0: negative	1: 1-25%	2: 26-50%	3: 51-75	4: 76-100%
Score (Multiply)	0-4: negative-low		6-12: high		

1. The diagnosis of ICC was performed with H-E stain, immunostain for CK7, HepPar1 and EMA and alcian blue mucin stain (Table 2).
2. Immunohistochemistry of β4, β6 integrin, laminin-5 and tenascin C was conducted on formalin-fixed paraffin-embedded tissue sections (Table 2).

Table 2. Primary antibodies and antigen retrieval methods

Antibody	Clone	Dilution	Antigen retrieval	Source
β4 integrin		1:200	pH9, 95°C, 40min	Santa Cruz
β6 integrin	442.5C4	1:400	Proteinase K, 10min	Calbiochem
Laminin-5	4G1	1:50	pH9, 95°C, 40min	DAKO
Tenascin C	E-9	1:50	pH9, 121°C, 15min	Santa Cruz
CK7	OV-TL12/30	1:60	pH9, 95°C, 40min	DAKO
Hep Par-1	OCH1E5	1:60	pH6, 95°C, 40min	DAKO
EMA	E29	1:200	pH6, 95°C, 40min	DAKO

3. The intensity and percentage of β4, β6 integrin expressions were semi-quantitatively scored (Table 3). Then the relationships between β4 or β6 integrin expressions and clinicopathological parameters were evaluated by using a final score.

Results

1. Expressions of β4, β6 integrin in intrahepatic cholangiocarcinoma

Figure 1. β4, β6 integrin immunohistochemistries in intrahepatic cholangiocarcinoma

- Positive staining for β4 or β6 integrin was demonstrated in 46(96%) and 35(73%) ICCs
- The predominant pattern for the β4, β6 integrin was classified as a basal lamina pattern(b,c), cell membrane pattern(d) and cytoplasmic pattern.

Figure 2. β4, β6 integrin expressions and the localization type

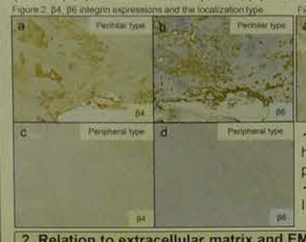

Figure 3. β4 integrin expression and gross type

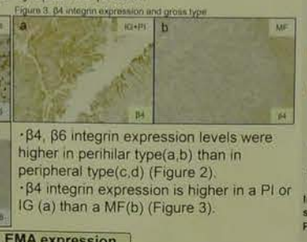

- β4, β6 integrin expression levels were higher in perihilar type(a,b) than in peripheral type(c,d) (Figure 2).
- β4 integrin expression is higher in a PI or IG (a) than a MF(b) (Figure 3).

2. Relation to extracellular matrix and EMA expression

Figure 4. Expressions of β4, β6 integrin, laminin-5 and tenascin C

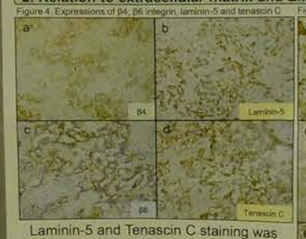

Laminin-5 and Tenascin C staining was observed in the cytoplasm of ICCs (b,d). The expression of laminin-5 and tenascin C was suggested to be associated with the expression of β4 and β6 integrin (a,c).

Figure 5. Expressions of β4, β6 integrin and EMA

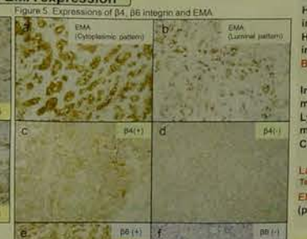

β4, β6 integrin expression was stronger in ICCs with EMA cytoplasmic pattern (a,c,e) than with EMA luminal pattern (b,d,f).

3. Clinicopathological features and expressions of β4, β6 integrin in ICC

Table 4. Clinicopathological features and expressions of β4, β6 integrin in intrahepatic cholangiocarcinoma

		Number of Cases (n=48)	β4 integrin expression: Negative-low (n=36)	β4 integrin expression: High (n=12)	β4 integrin expression: P value	β6 integrin expression: Negative-low (n=36)	β6 integrin expression: High (n=12)	β6 integrin expression: P value
Gender	Male	36	24	12	0.13	26	10	0.36
	Female	12	5	7		10	2	
Age			71.6(46-84)	69.0(39-83)	0.39	70.4(39-84)	71.1(51-82)	0.83
Tumor size (mean) (mm)			60.1 (18-220)	56.8 (22-110)	0.77	61.9 (18-220)	49.4 (23-100)	0.20
Localization type	Peripheral type	38	26	12	0.033	31	7	0.054
	Perihilar type	10	3	7		5	5	
Macroscopic type	MF	42	29	13	0.0022	31	11	0.52
	MF+PI, IG+PI, PI	6	0	6		5	1	
Differentiation	Well	6	3	3	0.023	3	3	0.031
	Moderate	29	14	15		20	9	
	Poor	13	12	1		13	0	
Growth type	Expansive growth type	23	18	5	0.015	20	3	0.065
	Infiltrative growth type	25	11	14		16	9	
HBV	Positive	6	5	1	0.22	6	0	0.15
	Negative	42	24	18		30	12	
HCV	Positive	8	6	2	0.31	6	2	0.68
	Negative	40	23	17		30	10	
Invasion of the serosa	+	24	12	12	0.14	17	7	0.36
	-	24	17	7		19	5	
Portal vein invasion	+	39	23	16	0.49	29	10	0.60
	-	9	6	3		7	2	
Hepatic vein invasion	+	21	10	11	0.11	15	6	0.61
	-	27	19	8		21	6	
Hepatic artery invasion	+	4	2	2	0.52	2	2	0.25
	-	44	27	17		34	10	
Bile duct invasion	+	26	11	15	0.0053	17	9	0.089
	-	22	18	4		19	3	
Intrahepatic metastasis	+	21	10	11	0.11	14	7	0.20
	-	27	19	8		22	5	
Lymph node metastasis	+	14	6	8	0.11	9	5	0.93
	-	34	23	11		27	7	
Cirrhosis	+	7	4	3	0.58	6	1	0.43
	-	41	25	16		30	11	
Laminin-5(β4) Tenascin C(β6)	≦25%	21	20	1	0.0000	26	4	0.016
	>25%	27	9	18	14	10	8	
EMA (predominant type)	Luminal pattern	11	10	1	0.018	11	0	0.027
	Cytoplasmic pattern	37	19	18		24	12	

Discussion

- There are some reports that the expression of β6 integrin is positive in Gallbladder carcinomas (4/4) (*E. Patsenker et al. Journal of Hepatology, 2010*), and no positivity is observed in 21/23 cholangiolocellular carcinomas (*soejima*). The enhanced expression of β4 integrin is associated with a migratory and invasive phenotype and the progression of cholangiocarcinoma (*Ding YB et al. Dig Dis Sci, 2013*).
- The present study indicated that the expression of β4, β6 integrin was related to localization, macroscopic types, growth types, bile duct invasion and differentiation of ICC. In addition, β4 and β6 integrin expression was associated with the expression patterns of EMA and suggested to be related to laminin-5 and tenascin C expression.
- These results suggested that the expressions of β4, β6 integrin might be associated with invasion and progression of ICC.
- The biological behaviors of ICC might be different between subtypes of large bile duct origin and small bile duct origin.

Conclusion

The expression of β4, β6 integrin was related to localization, macroscopic types, bile duct invasion and differentiation of ICC, suggesting an association of integrin expression with invasion and progression of ICC through laminin-5 and tenascin C expression.

Pathology

PE-23

Three dimensional imaging analysis of the promotion proces β-catenin accumulated crypts to colonic adenomas in mice r

Kazuo Kase[1)3)], Nobuko Saito[1)], Yuji Sato[1)], Kenzo Hiroshima[2)], Okita[3)], Yukihide Watanabe[3)], Hiroyuki Suzuki[3)], Mituyasu Katc

[1)]Edogawa Medical Laboratory Center, [2)]Tokyo Women's Medical University Yachi Center, [3)]Department of Experimental Pathology, Faculty of Medicine, University

Summary

Early process of colon adenoma formation is not fully understood , though cancer cells as well as tumor microenvironment are thought to have important roles.

In this study, we examined cell proliferation statve of neoplastic cells and microvascular structures during the process of early adenoma development from β-catenin accumulated crypt (BCAC) in mice models.

Dextran sodium sulfate (DSS) was given to Apc$^{Min/+}$mice at 5 weeks of age in drinking water for 7days to induce colonic inflammation and adenoma formation. Apc$^{Min/+}$mice have multiple BCAC in the colon but BCAC rarely develop to colon adenoma. DSS initiated adenoma formation and visible adenoma with multiple branching structures were developed within 3-4 weeks. Increase of Ki-67 positive cells in BCAC was observed on 5th day during DSS treatment and reached to 90% of the total cell numbers in 3-4 weeks. Then, protruding tumors were formed during 1-4 weeks after DSS. At the same time, in the surrounding , neovascular formation and increase of spindle shaped stromal cells were also detected during the early time point of adenoma formation.

Introduction

Multistep carcinogenesis process of colon cancer

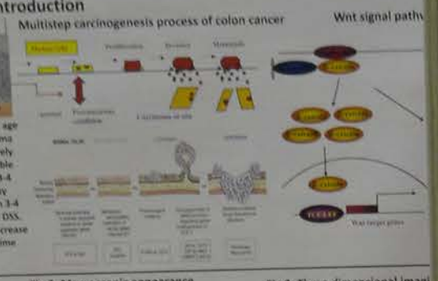

Materials and Methods

Fig 1. Experimental Procedures

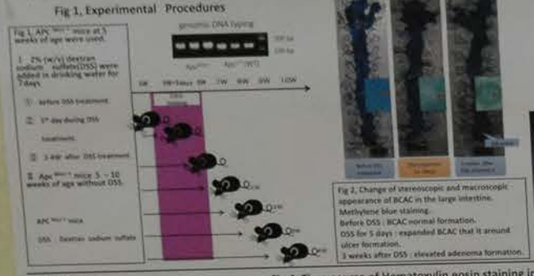

Fig 2, Macroscopic appearance

Fig 2, Change of stereoscopic and macroscopic appearance of BCAC in the large intestine. Methylene blue staining.
Before DSS : BCAC normal formation.
DSS for 5 days : expanded BCAC that it around ulcer formation.
3 weeks after DSS : elevated adenoma formation.

Fig 3, Three dimensional imagi

Fig 3, Serial sect were stained for podocalyxin, an three dimensior studio Max 2.0.

Results

Fig 4, Time course of Hematoxylin eosin staining in the colon

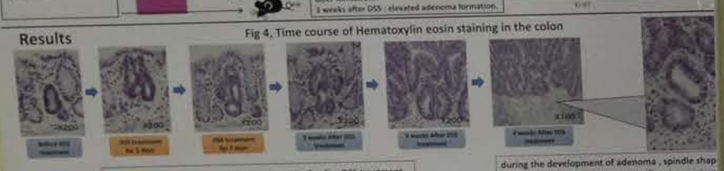

Fig 4, Microscopically, The BCAC expands gradually after DSS treatment.

during the development of adenoma , spindle shap fibrous matrix increase in the specific microenviron

Fig 5, 3-D imaging of Ki-67(proliferation) staining

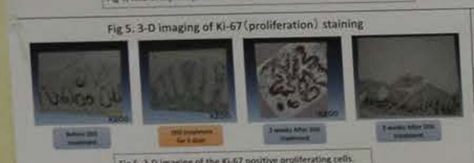

Fig 5, 3-D imaging of the Ki-67 positive proliferating cells.

Fig 7, 3-D imaging of Podocalyxin(endoth

Two dimensional projection structure

Fig7, The microvascular structure changed from loop to microenvironment of BCAC treatment.

Fig 6. Time course of proliferating cell number in BCAC

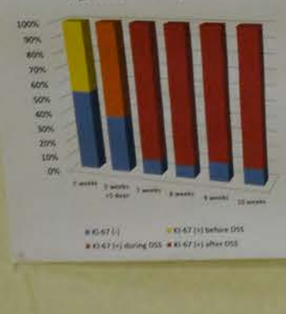

Fig 6, Increase of Ki-67 positive cell ratio in BCACs was observed as early as 5th day during DSS treatment and reached to 90% of the total cell number in 3-4 weeks. Then, protruding tumors were formed during 1 to 4 weeks after DSS.

Conclusion

DSS treatment induced development of BCAC to adenomas in the colon of Apc$^{Min/+}$. During this process , neovascular formation and increase of spindle shaped stroma to adenoma formation from the early time points.

hara[1], Yuko Otani[1],
ashi[1], Takayuki Honda[1]

nent of Medicine, Shinshu University School of
al Central Hospital, Niigata, Japan

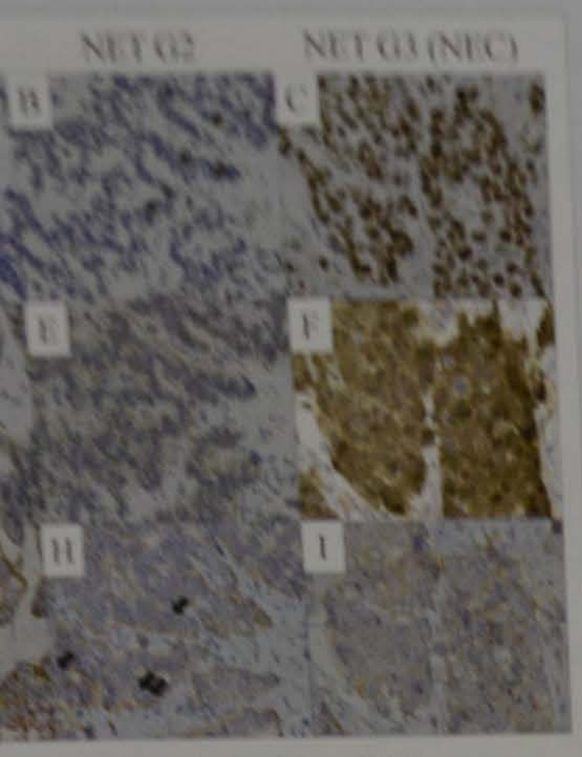

mmunohistochemical staining of Ki-67, β-atenin, and combination of *Lgr5* RNA *in situ* ybridization with synaptophysin mmunohistochemistry for NETG1–G3.

Ki67-positive cells. D–F: Staining for nuclear β-catenin positive cells. G–H: Identification of *Lgr5*- and synaptophysin-positive (brown) cells in NET G1–tive cells are indicated (black arrows). Original 00×

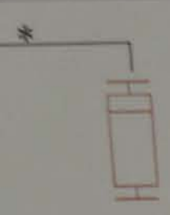

Figure 4
Nuclear translocation of β-catenin in NET G1–G3 samples.

Scores are expressed as minimum, 25th and 75th (percentiles), and maximum. *$p = 0.0151$ (Wilcoxon rank sum test).

e G2 NET G3 (NEC)

ontained tumor cells with some *Lgr5*-positive e *Lgr5* H-score was significantly higher in NET samples compared with those of NET G1 and G2. -positive and synaptophysin-positive cells were in most cases. In all cases, *Lgr5* H-scores showed a orrelation with nuclear β-catenin expression (r = = 0.0013). There was no correlation between *Lgr5* and Ki-67 expression. In the NET G1 and NET G2 here was also no correlation between *Lgr5* H-score 7 expression, or between *Lgr5* H-score and β- expression. In NET G3 (NEC) there was a strong correlation between *Lgr5* H-score and β-catenin ion ($r = 0.8333$, $p = 0.0102$).

clusion

xpression might be affected by β-catenin expression in nd especially in NET G3 (NEC) lesions. The presence 5 and synaptophysin double-positive cells suggests that positive cells may be also stem cells in NEC, as is the n colon adenocarcinoma. A further study with a larger er of NEC cases is warranted to confirm these findings.

Pathology
PE-26

Improved Azan staining protocol and the utility –clear color contrast and short staining time–

Shigenobu Tatsumi, Takeshi Nishikawa, Hisae Suzuki, Mao Takeuchi
Yushimasa Fukui, Kyouko Tanaka, Yayoi Umeki
Hospital Pathology, Nara Medical University Hospital

Introduction

It is difficult for Azan staining to secure staining accuracy. Therefore, a mordant such as chromic acid is required in Japan. However, the procedure is not standardized sufficiently. Our recent studies suggested that picric acid can be a useful mordant for Azan staining, better differentiating tissue components.

Our previous studies

our Azan staining protocol

1) deparaffinize in xylene, rehydrate in a graded series of alcohol, and rinse with distilled water (DW)
2) incubate in picric acid at 60℃ for 30min and rinse in DW
3) soak azocarmin G at room temperature (RT) for 60min and rinse briefly in DW
4) soak in 5% phosphotungstic acid at RT for 30min and rinse briefly in DW
5) soak in Mallory's aniline blue orange G stain sol. at RT for 15min
6) rinse and dehydrate through pure alcohol, clear through xylene, and coverslip

Tatsumi S et al.: Usefulness of picric acid as mordant: with the heating of picric acid, the efficiency of Azan staining is improved. Jpn J Med Technol; 2016; 69(1): 78-83

□ Our previously reported Azan staining can differentiate tissue components better.

- Collagen fibers can be distinguished from muscle fibers on vascular structures by using our Azan staining (＊).
- Cellular components can't be stained by aniline blue (○).

Objectives

We tried to further improve our picric acid-using method for Azan staining by making it more time-efficient. Additionally, we investigated whether Azan staining done by our method could be combined with other stains

Materials

◆Samples
Liver, heart, kidney, skin and artery fixed with 10% neutral buffered formalin were adopted.

◆Reagents
- Picric acid (Nacalai Tesque, Japan)
- Azo Carmine GFM (azocarmin G) (C.I.No.18134, Chroma, USA)
- 12-tungsto (VI) phosphoric acid n-hydrate (PTA)(Nacalai Tesque)
- Mallory's aniline blue orange G stain sol. (Muto Pure Chemicals, Japan)
- Maeda's Resorsin Fuchsin Solution for staining elastic fibers (Muto Pure Chemicals)

Methods

Based on our previously reported Azan staining, we examined

[1] Effects of picric acid on Azan staining
[2] Improved Azan staining
[3] Elastica improved Azan staining.

[1] Effects of picric acid on Azan staining

□ **Effects of picric acid on azocarmin G and aniline blue**

We soaked slides in only azocarmin G (①) and Mallory's aniline blue orange G stain sol. (②) respectively after picric acid.

[2] Improved Azan staining

We integrated procedures of picric acid and azocarmin G, and made the mixed solution. We soaked slides in this solution at 60℃ for 30min.

the mixed solution of picric acid and azocarmin G
: 100ml
- saturated aqueous solution of picric acid: 100ml
- azocarmin G : 0.1g

Improved Azan staining

1) deparaffinize, rehydrate, and rinse with DW
2) **incubate in the mixed solution of picric acid and azocarmin G at 60℃ for 30min**
3) rinse briefly in DW
4) soak in 5% PTA at RT for 30min and rinse briefly in DW
6) soak in Mallory's aniline blue orange G stain sol. at RT for 15min
7) rinse and dehydrate, clear, and coverslip

[3] Elastica improved Azan staining

Before the mixed solution of picric acid and azocarmin G, we soaked slides in Resorsin Fuchsin at RT for 50min and dipped in 1% hydrochloric acid・70% alcohol at 10~15 times.

Elastica improved Azan staining

1) deparaffinize and rehydrate
2) soak in Resorsin Fuchsin at RT for 50min
3) dip in 1% hydrochloric acid・70% alcohol at 10~15 times and rinse in DW
4) follow improved Azan staining (soak in Mallory's aniline blue orange G stain sol. at RT for 30min when stain kidney biopsies)

Results

【1】Effects of picric acid on Azan staining

□ **Effects of picric acid on azocarmin G and aniline blue**

1) Picric acid **doesn't compete with azocarmin G**.
2) Picric acid **competes with aniline blue**.

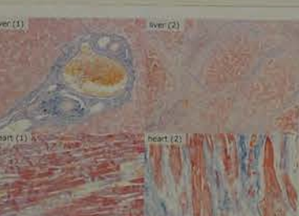

Azocarmin G may be able to be mixed with picric acid.

【2】Improved Azan staining

- This staining can get **the clearer color contrast** between collagen fibers and other tissue components due to brilliant red of cellular components.
- **Collagen fibers** are blue by aniline blue, **cellular components** are red by azocarmin G, **nuclei** are deep red by azocarmin G, and **erythrocytes** are yellow or orange by picric acid or orange G.
- This staining requires about 1.5 hours totally, which **is shorter about more than an hour at least than conventional Azan staining**.

【3】Elastica improved Azan staining

- This staining can get **the clear color contrast** as same as improved Azan staining.
- Elastic fibers are black by resorsin fuchsin.
- This staining can **stain cellular components and collagen fibers more clearly** than EVG staining.
- This staining requires about 2.5 hours totally.

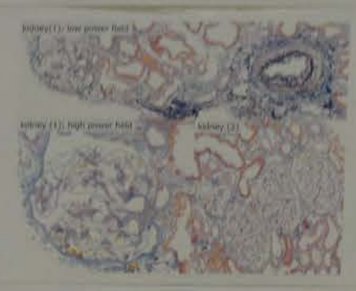

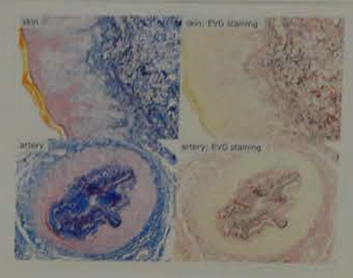

Conclusion

- **Picric acid can be a useful mordant for Azan staining**, better differentiating tissue components.
- **Mordanting by picric acid can be done simultaneously with the staining by azocaemin G**, thereby simplifying the whole procedure.
- **Elastic staining can be added** to the Azan staining done by our picric acid-using method.

The 32nd World Congress of Biomedical Laboratory Science

Conflict of Interest (COI)

the Principal Presenter: Shigenobu Tatsumi

No potential COI to disclose

C-1

Pathology

PE-27

Glyoxal fixation is useful for histological evaluation.

A comparative analysis of tissue fixation with formaldehyde and glyoxal.

Fuminori Sakanashi, Mami Mizuno, Misaki Uehara, Koji Tateishi, Masazumi Tsuneyoshi
Fukuoka Sanno Hospital, Fukuoka, Japan
(E-mail address : sakanashi@kouhoukai.or.jp)

Introduction

Formalin has been the leading fixative in histopathological examination.
However, carcinogenic of formaldehyde was pointed out by World Health Organization(WHO) in 2004, and now the use and disposal of formalin are monitored and regulated strictly in Japan.

Glyoxal, a non-formaldehyde-containing histological fixative, is one of the most popular substitutes for formalin, and said to have the advantage of being less hazardous than formaldehyde.

Our purpose of this study is to verify the usefulness of glyoxal fixed specimens, especially focusing on histological staining.

Materials and Methods

Biopsy specimens obtained from the same organs of the same patients (47 cases).

Some of them were fixed with 10% neutral buffer formalin(NBF), and the others with glyoxal-based fixative(GBF) for 18-24 hours.

Histological stains were performed in the same protocol to determine the difference in dyeability.

- Hematoxylin and Eosin(HE) stain
- 4 kinds of Special stains
- 11 kinds of Immunohistochemical(IHC) stains
  6 were for cytoplasm or cell membrane
  5 were for nucleus

Results 1

There weren't significant differences between the two fixation methods in **HE stain, Special stain, IHC stain for cytoplasm or cell membrane**

Erythrocytes were lysed in GBF fixed specimens.

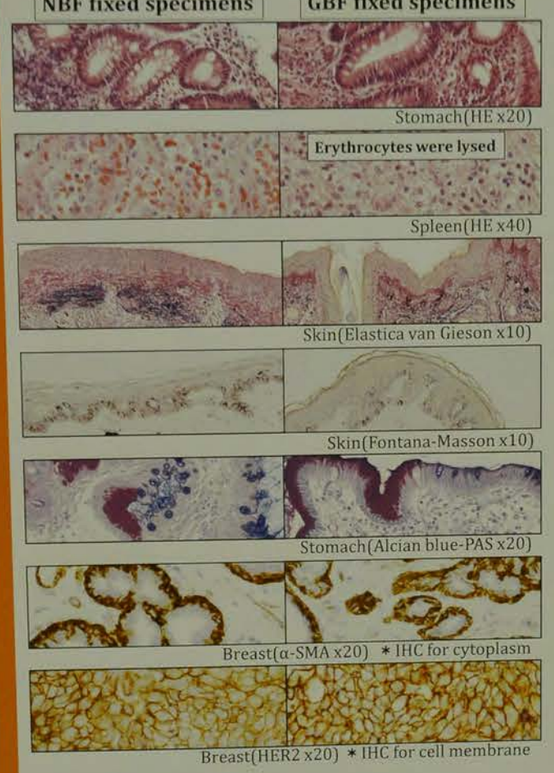

Stomach(HE x20)
Spleen(HE x40)
Skin(Elastica van Gieson x10)
Skin(Fontana-Masson x10)
Stomach(Alcian blue-PAS x20)
Breast(α-SMA x20) ✶IHC for cytoplasm
Breast(HER2 x20) ✶IHC for cell membrane

In contrast, for **IHC stain for nuclear**, both the intensity of staining and the frequency of stained cells were attenuated (or disappeared) with GBF fixed specimens as compared to NBF-fixed.

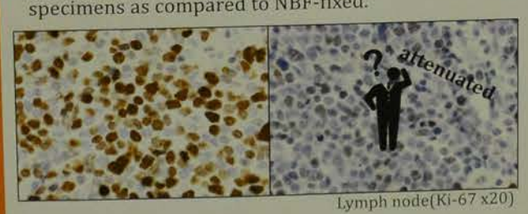

Lymph node(Ki-67 x20)

Results 2

Why "attenuated or disappeared " ??

- Imidazole reaction between glyoxal and the guanidinium group of arginine (occur much more in nucleus than cytoplasm)

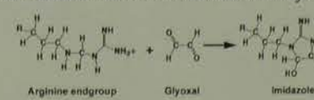

- irreversible with usual heat-induced epitope retrieval(HIER).

·· need stronger HIER ??

(GBF fixed specimens) Ki-67, with routine protocol

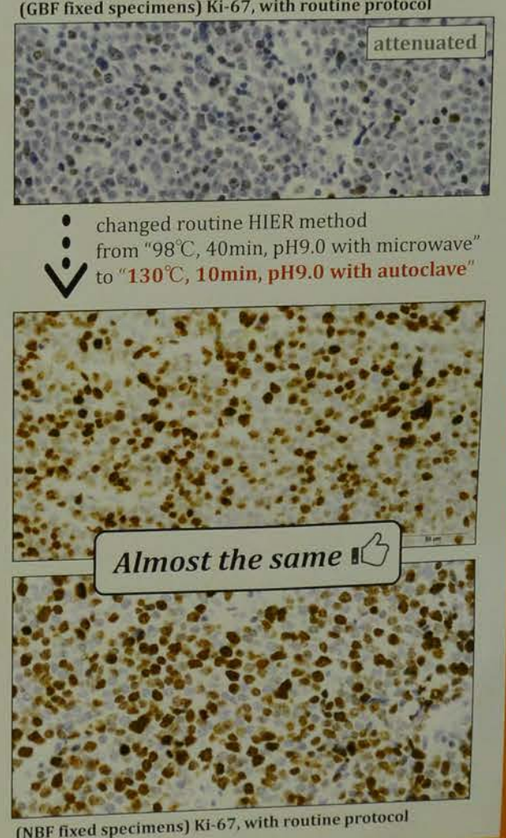

(NBF fixed specimens) Ki-67, with routine protocol

Conclusion

Considering the environmental and health concerns, the non-formaldehyde-containing tissue fixative "glyoxal" is a useful substitute fixative for histological evaluation in pathology laboratories.

The 32nd World Congress of Biomedical Laboratory Science (IFBLS2016) Aug 31-Sep 4,2016 Kobe, Japan

Pathology

PE-28

Development and Utility of Improved Silver Protein

Nobuo Kuninaka[1,2], Yuko Sato[1], Yoshiyuki Umeto[1], Masanobu Higo[2], Shigeo Murayama[3], Yuko Saito[1]

1) National Center of Neurology and Psychiatry
2) National Hospital Organization Yokohama Medical Center
3) Tokyo Metropolitan Geriatric Hospital & Institute of Gerontology

Introduction

The Bodian stain has been widely used, with numerous modifications, and its staining power is determined by silver protein[1]. In Japan, Albumose silver (Merck co.) had popularly been used, but stopped in 2009. At our hospital in 2009, we used the silver protein (Chroma co.) as a substitute and confirmed its staining performance. However, the same product was corrupted in 2012, because the properties of the reagents were changed. Herein, we undertook the development of our own silver protein solution according to the procedure reported by Hattori[2] and found that this solution (traditional solution) could stain as well as the Merk's.[3] However, it took a lots time and labor to freshly prepare oxidized silver nitrate ($AgNO_3$) before each usage[2,3]. The differences caused by preparation also trouble us.

Purpose

This study aimed to investigate a modified solution whether the use of commercially available silver oxide, replacing the freshly prepared $AgNO_3$, would simplify the pre-procedural preparation and yield more consistent staining.

Materials

We used the paraffin-embedded sections of central and peripheral sural nerves, fixed for 2 weeks in a 10% formalin solution (FS) or a 15% formalin neutral buffer solution (FNB) or for 2 days in a 4% paraformaldehyde solution (PFA). Cerebellar sections were used as a normal control for comparison with the Merck product. The staining performance was assessed on tissue sections from cases with Alzheimer disease, progressive supranuclear palsy, Pick disease, and multiple sclerosis.

Table 1 Bodian stain - Silver Protein Process

Deparaffinization→Washing with tap water
Wash distilled water 1 times per 1 min.
1% Silver Protein Solution (12-18hours)
Wash distilled water 2 times per 1 min.
Reduced solution* Treatment 10 min. (*: Distilled Water100ml, Hydroquinone 1g, Formalin 5 ml)
Washing with tap water 3～5 min. →Washing distilled water
1% Gold chloride Process 40~60 min.
Wash distilled water 2 times per 1 min.
1% Oxalic Acid Process 5 min.
Wash distilled water 2 times per 1 min.
2% Sodium thiosulfate (hypo) process 1 min.
Washing with tap water 3 min.
Dehydrate, Clear and Sealed

Table 2

	per 100ml	conventional method	modified solution X1	X2	X3	X4
	Peptone (g)	0.1	0.1	0.1	0.1	0.1
	Arginine (g)	0.1	0.1	0.1	0.1	0.1
	Casein (g)	0.6	0.8	0.6	0.8	0.4
	Ovalbumin (g)	0.4	0.4	0.4	0.4	0.6
	Silver Oxide(g)	—	0.1	0.1	0.08	0.1
Cerebellum	axon in the cortex	A	A	A	A	C
	axon in the medulla	B	A	A	A	A
	purkinje cell	A	B	A	A	A
	granular layer	A	A	A	A	A
	cortical color	A	B	B	B	A
Cerebrum	senile plaque	A	A	A	A	A
	amyloid core	A	A	A	A	A
	neurofibrillary tangle	A	A	A	A	A
	Points	75	70	75	75	70

Very good :A(10point) Good :B(5point) Bad :C(0point)

Table 3

		10% FS	15% NFB	4% PFA
Cerebellum	axon in the cortex	Black	Black	Black
	purkinje cell	Purplish Red	Purplish Red	Purplish Red
	granular layer	Purplish Red	Purplish Red	Dark Red
	cortical color	Pale Purplish Red	Gray or Purplish Red	Purplish Red
Cerebrum	axon in the cortex	Black	Black	Black
	senile plaque	Purplish Red	Purplish Red	Purplish Red
	amyloid core	Red	Red	Red
	neurofibrillary tangle	Purplish Red	Purplish Red	Purplish Red

Methods

1) Process to prepare the modified solution

Pepton and L-arginine, 0.1 g each, were dissolved in 100 ml of distilled water. While the solution was heated at approximately 70°C, 0.4 g of casein was added., It was cooled to room temperature, then 0.4 g of ovalbumin and 0.08 to 0.1 g of silver oxide added. Reheat the solution up to 80°C until it turned dark brown. After being cooled to room temperature, it was filtered to be a reaction solution.

2) Staining method

In a Coplin staining jar (50 ml capacity), 50 ml of silver protein solution was mixed with 4 g of copper shot. A deparaffinized sample was placed in the solution and incubated at 40°C overnight. Staining method are shown in Table 1 .

3) Comparison between the conventional and modified solutions

To assess the modified solution, we compared the background colors of cerebellar cortex/medullary axons and the cortex, as well as the staining of Purkinje cells, the granular layer, axons and neurofibrillary tangles (NFTs) of the cerebral cortex.

4) Examination of various fixative solutions

The impacts of fixative solutions on staining performance were assessed in sections of central nerves fixed in 10% FS, 15% FNB, or 4% PFA, and in sections of sural nerves fixed only in 4% PFA.

5) Comparison between the modified solution and the Merck product

The modified solution and the Merck product were compared for staining performance on the neuropathological samples employed in this study.

Figure 1 a-c: Cerebellum, d-l: Cerebrum, j,k: Sural nerve Scale Bar:200μm

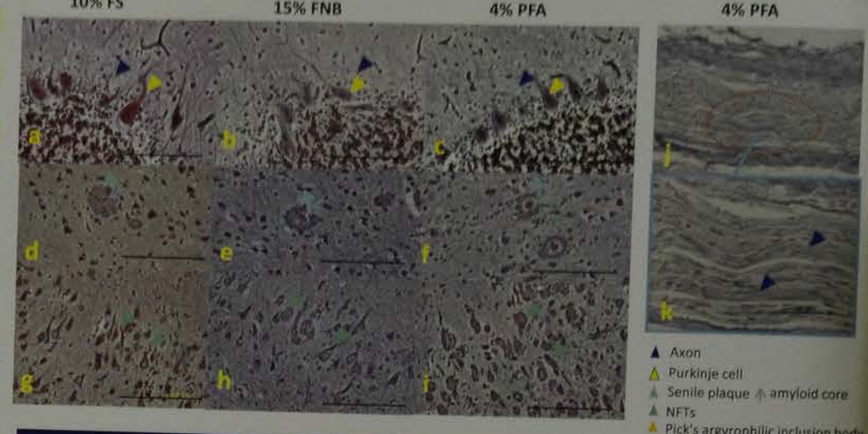

Figure 2 a-d: Merck (a. Cerebellum, b,c. Alzheimer disease, d. Pick disease) , e-h: Modified solution (e. Cerebellum, f,g. Alzheimer disease, h. Pick disease), i,j: multiple sclerosis (double staining with LFB) Scale bar:200μm

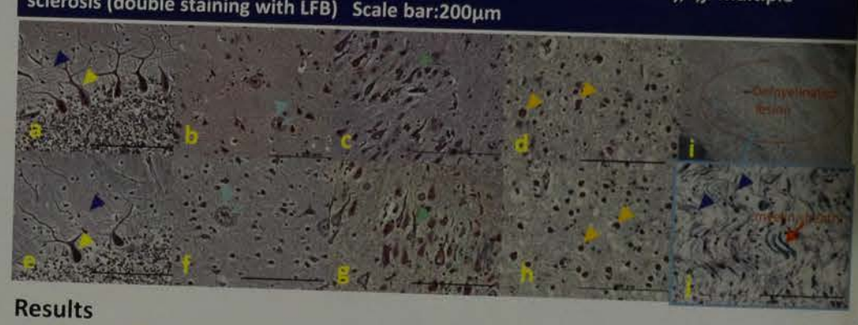

Results

1) The modified solutions generally stained as well as the conventional

For modified solutions X1–X3, medullary axons were more clearly stained a darker color with the modified solution than with the conventional solution. Although Purkinje cells were well stained with modified solutions X2, X3, and X4, the reddish-purple color, characteristic of the cerebellar cortex, was slightly paler with the modified solution than with the conventional solution. Moreover, there was no differences to stain NFTs, senile plaques, and amyloid cores between the conventional and modified solutions (Table 2).

2) Various fixative solutions make no great influence on the stains

The composition of the optimal modified solution (X3) was assessed with samples fixed in 10% FS and 15% FNB. No substantial differences in staining axons, senile plaques, NFTs, and others were observed between these fixative solutions (Table 3). However, the color of the cerebellar cortex appeared pale gray to reddish-purple in some of the samples fixed in 15% FNB. Taking the color of the cortex as priority, 10% FS was superior than others. Although the samples fixed in 4% PFA overall show darker staining, the axons, senile plaques, NFTs, and other structures were well stained. The axons of sural nerves were stained black, which facilitated observation. The modified solution was thus also applicable to staining of peripheral nerves (Figure 1).

3) The favorable modified solution X3 was as good as the Merck product

When tissues obtained from Alzheimer disease cases were stained with the modified solution, NFTs stained reddish-purple; the senile plaque margin stained black, making it clearly distinguishable from the amyloid core which stained red. Moreover, the argyrophilic inclusion bodies, indicative of Pick disease, stained reddish-brown. While demyelination was observed in cases with multiple sclerosis, residual axons were clearly stained. The modified solution was also applicable to double staining with Luxol fast blue (LFB) solution (Figure 2).

Discussion

1. Modified silver protein is consistent in quality

Silver protein is a colloidal silver compound in which silver oxide binds with proteins, such as peptone, casein, or albumin. Because casein is only soluble under alkaline conditions, it can be dissolved in a solution to which arginine has been added. Silver oxide was added after these proteins had been synthesized. This silver protein solution previously had to be freshly prepared before each usage and resulted in unavoidable differences. However, we used commercially available silver oxide as a modified solution, which is consistent in quality, enabled us to perform staining at a consistent level of quality.

2. Fixative solutions matter or not: it seems not an issue

Not only the Bodian stain but also other silver impregnation methods are known to be affected by fixative solutions and the duration of fixation. Bodian states that central nerves are not adequately stained by silver impregnation unless they are fixed in a mixture containing 5ml of FS, 5 ml of acetic acid, and 90 ml of 80% alcohol[1]. However, favorable staining was achieved with our modified solution on sections fixed in 10% FS, 15% FNB, or 4% PFA, making the use of any of these fixatives feasible. Particularly, sections fixed in 10% FS showed better staining than those fixed in the other fixative solutions.

3. Future prospects for the Bodian stain

While silver protein remains not easily available, there are more and more institutions where the Bodian stain is no longer performed or where they depend on immunohistochemical staining. If this condition persists, the Bodian stain will become obsolete. However, it remains one of the essential stains for institutions, such as ours, specialized in neuropathology. To meet this challenge, we developed a modified solution and demonstrated that it stained as well as the Merck product on axons, NFTs, senile plaques, Pick's argyrophilic inclusion bodies, and other structures. We have provided a practical, promising, and efficient method for the Bodian stain.

However, the disadvantages of the modified solution are that it has to be freshly prepared for each usage and cannot be stored because of its liquid form. Development of a freeze-dried form of silver protein solution is essential for achieving long-term storage. In a joint study conducted with Wako Pure Chemical Industries, Ltd. we succeeded in processing the solution into a powder form, which can be developed into a marketable product.

Conclusion

In this study, while silver protein suitable for the Bodian stain remains unavailable worldwide, we have developed a modified solution and demonstrated that it exhibits staining power which is both consistent and as good as that of the Merck product. Furthermore, commercialization of this modified solution will allow the Bodian stain, which would otherwise be destined to become obsolete, to still be performed in the future.

Reference

1.Bodian D: A new method for staining nerve fibers and nerve endings in mounted paraffin sections. Anat. Rec. 65; 89-97,1936

2.Hattori S: Improvement of Bodian's silver impregnation method. Ryinsho hyori 19, Suppl, 489, 1971.

3.Kuninaka N, et al. : Newly developed "protein silver" for Bodian staining. Neuropathology 33(6), 376 ,2013.

COI Disclosure Information

Trust research joint research funder: (jo+kyou-73) Wako Pure Chemical Industries, Ltd.

Pathology

PE-29

Using ultrasonic waves to infiltrate resin into electron microscopic specimens

- Mainly about skin sample -

Yamada Hiroshi, Yanagita Emmy, Morito Satoshi, Endo Akikazu, Tsukamoto Ryuko, Ito Tomoo

The Department of Diagnostic Pathology of Kobe University Hospital

1. Introduction

Epon resin that creates electron microscope samples is less penetrable than paraffin that creates pathological tissue samples. Ultra-thinly slicing and imaging of samples into which Epon resin penetrates less can be unclear and impossible to use. This tendency is especially evident in skin samples. Thus, we examined the penetration of Epon resin using the fixation, delipidation and decalcification device, Histra-DC (manufactured by Jokoh Co., LTD.), which uses ultrasonic waves.

2. About Histra-DC

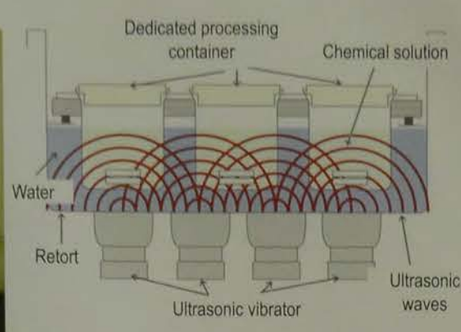

The vibration of minute bubbles caused by ultrasonic cavitation promotes filtration into cellular tissues. The increase in solution temperature resulting from ultrasonic waves occurring can be restrained with a cooling system; which enables setting it at a low temperature.

3. What is cavitation?

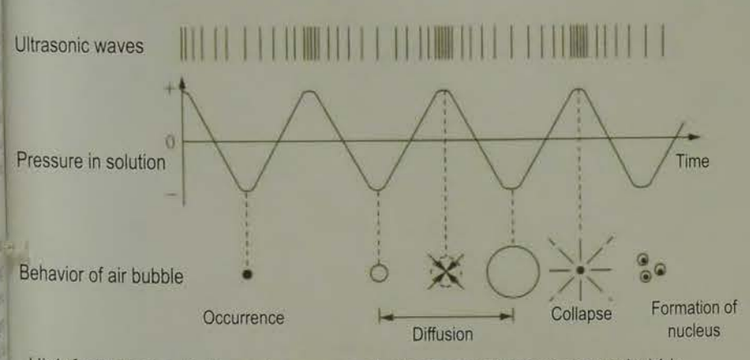

High frequencies of ultrasonic waves and strong sound waves cause bubble generation in a solution due to negative pressure. This phenomenon is called cavitation. Generated minute air bubbles collapse after repeated contraction and expansion. At that time, the temperature and pressure in air bubbles respectively reach thousands of degrees and thousands of units of atmospheric pressure. Vibrations of minute air bubbles stimulate cell membranes to enhance penetrability.

4. Method

In this hospital, electron microscope blocks are usually created in the following method:

Step	Reagent/time
1	1% osmium, 120 minutes (at 4°C)
2	50% ethanol, 5 minutes (at 4°C)
3	70% ethanol, 5 minutes (at 4°C)
4	80% ethanol, 10 minutes
5	90% ethanol, 10 minutes
6	95% ethanol, 10 minutes
7	99% ethanol, 10 minutes
8	80% pure ethanol, 20 minutes × 3 times
9	Propylene oxide (PO), 20 minutes × 3 times
10	PO: Epon resin = 1:1, 60 minutes
11	PO: Epon resin = 1:2, 60 minutes
12	Pure Epon resin, overnight
13	Epon resin embedding
14	Polymerization (35°C, 8 hours → 45°C, 8 hours → 60°C, 48 hours)

Approximately 1 mm square of sliced skin sample

Skin tissue immersed in Epon resin

The sample in Step 12 was compared with the one that was immersed overnight using Histra-DC.

Epon resin combination ratio
Mixed with the ratio of Quetol 812: MNA: DDSA: DMP30 = 472 mL: 281 mL: 247 mL: 1.5 mL

Pure Epon resin embedding 1
Suction for an hour with vacuum pump, and then, leaving overnight hermetically

Pure Epon resin embedding 2
Application of ultrasonic waves overnight at 24°C using Histra-DC

Then, creation of electron microscope block with use of polymerization device at 60°C

5. Sample comparison

Epon block after polymerization

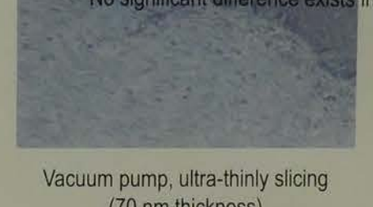

Slicing (Lieca)

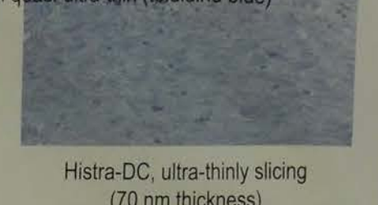

Vacuum pump, ultra-thinly slicing (block)

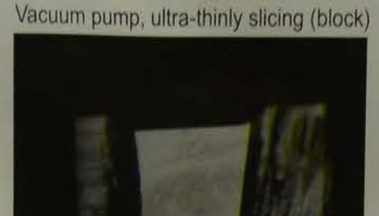

Histra-DC, ultra-thinly slicing (block)

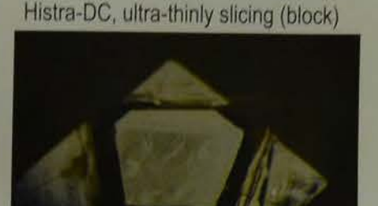

Vacuum pump, quasi-ultra-thin (toluidine blue)

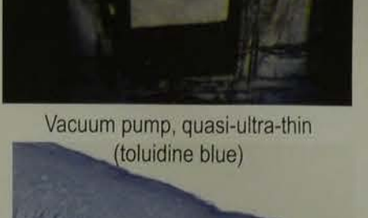

Histra-DC, quasi-ultra-thin (toluidine blue)

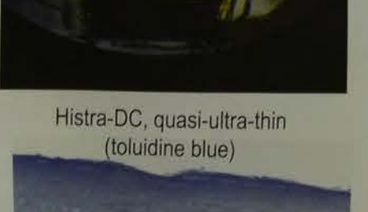

No significant difference exists in quasi-ultra-thin (toluidine blue)

Vacuum pump, ultra-thinly slicing (70 nm thickness)

Histra-DC, ultra-thinly slicing (70 nm thickness)

Regarding 70-nm ultra-thinly slicing, the subcutaneous tissue portion is compressed and becomes serpentine without forming a ribbon shape on the vacuum pump block side. To the contrary, sliced ribbons are connected in a straight manner on the Histra-DC block side.

Electron microscope/electron stain

Step	Reagent/time
1	Uranium acetate solution, 30 minutes
2	Wash in distilled water, 1 minute × 3 times
3	Lead acetate solution, 10 minutes
4	Wash in distilled water, 1 minute × 3 times
5	Dry

Vacuum pump, ultra-thinly slicing (70 nm thickness)

x5000 magnification
Intercellular bridge
Vacuum pump > Histra-DC
The intercellular on the vacuum pump side is larger.

x5000 magnification
Subcutaneous tissue (collagen fiber)
There are holes and broken fibers on the vacuum pump side, but even fiber flows are clear on the Histra-DC side.

Histra-DC, ultra-thinly slicing (70 nm thickness)

6. Discussion and Conclusions

According to the results mentioned above, poor Epon resin penetration on the vacuum pump side caused drifts, expanded gaps and holes in samples without withstanding electron beams in the observation using the electron microscope. The Epon resin penetration method using the fixation, delipidation and decalcification device, Histra-DC, which uses ultrasonic waves, is effective to improve the sample quality in creating electron microscope samples.

Pathology
PE-30
Reconstruction of the canine pelvic nerve
and its application to substitute bladder
○ Yuichiro Cho, Kenji Sato, Osamu Hoshi
Department of Anatomy and Physiological Science, Graduate School of Health Care Sciences
Tokyo Medical and Dental University, Tokyo, Japan
Reconstruction of the canine pelvic nerve and its application to substitute bladder
Yuichiro Cho, Kenji Sato, Osamu Hoshi
Department of Anatomy and Physiological Science, Graduate School of Health Care Sciences, Tokyo Medical and Dental University, Tokyo, Japan
Introduction 1
Nerve mechanism of urination
Introduction 2
When this occurs, cystoplasty with gastrointestinal elements, such as the ileum or sigmoid colon, is indicated for treatment.
Furthermore, when performing a total cystectomy for bladder cancer, the desired option is enterocystoplasty using gastrointestinal organs, such as the ileum, ileocecum, or sigmoid colon, for urinary diversion.
However, because bladder contractions during spontaneous voiding are mediated by the PN, PN reconstruction is important to ensure that the enterocystoplasty maintains effective voiding and improves the patient's quality of life.
Autonomic nerve of pelvic part
anatomical picture
anatomical chart
PN plexus
Materials and Methods
1. Creation of the colonic bladder substitute models (5 beagles)
2. Electrophysiology (After 18 months)
3. Histology
・light microscopy examination (3 beagles)
・transmission electron microscopy investigation (2 beagles)
Creation of the colonic bladder substitute models
Autonomic nerve of the colonic bladder substitute models
the colonic bladder substitute models
The colonic bladder substitute models
A : PN region
B : PN-HN suture region
C : Interposed HN region
D : HN-CN suture region
E : CN region
A' : Control PN
C' : Control HN
: sutured PN-HN-CN (sutured PN)
Electrophysiology (After 18 months)
Electrical stimulation
After 18 months, we repeated the laparotomy under general anesthesia.
Histology 1
Harvest of tissue specimens
Histology 2
Light microscopy examination (3 beagles)
Transmission electron microscopy investigation (2 beagles)
Results: Electrophysiology
Results: Histology
Photomicrographs of the typical regeneration of the sutured PN-HN-CN (Interposed HN region)
HE staining (x 600)
silver impregnation (x 600)
Optical microscopy of the nerve tissues (HE staining, silver impregnation)
Criteria of Silver impregnation 1
(−)
Nerve fibers were not observed
(+)
nerve fibers were observed (nerve fiber fascicles were not formed)
Criteria of Silver impregnation 2
(++)
nerve fibers were observed (nerve fiber fascicles were formed)
(G)
nerve ganglion (a small number of nerve cell bodies) were observed
Results of Silver impregnation for each of the sutured PN-HN-CN regions
Optical microscopy of the nerve tissues (Immunohistochemistry)
Criteria of Immunohistochemistry (anti-TH) 1
(−)
Positive rates: 0%
(+)
Positive rates: <10%
Criteria of Immunohistochemistry (anti-TH) 2
(++)
Positive rates: 10%–50%
(+++)
Positive rates: >50%
Results of Immunohistochemistry (anti-TH) for each of the sutured PN-HN-CN regions
Normal control autonomic nerves (TEM; x3,500)
A': Control PN
C': Control HN
PN region (TEM; x3,500)
PN-HN suture region (TEM; x3,500)
Interposed HN region (TEM; x3,500)
Distribution of nerve fiber axon diameter in the TEM photomicrographs
Conclusion
Thus, regeneration of PN tissue and reconstruction of PN function in sutured PN-HN-CN were confirmed.
The electrophysiological and histological results indicate that the function of PN can be restored to the colon as a substitute bladder after PN-HN-CN reattachment, and that the transplanted colon to bladder can become functionally advanced substitute bladder.
Pathology
PE-28
Development and Utility of Improved Si
Nobuo Kuninaka, Yuko Sato, Yoshiyuki Umeto, Masano
Shigeo Murayama, Yuko Saito
1) National Center of Neurology and Psychiatry
2) National Hospital Organization Yokohama Medical Center
3) Tokyo Metropolitan Geriatric Hospital & Institute of Gerontology
Introduction
Purpose
Materials
Table 1 Bodian stain - Silver Protein Process
Table 2
Table 3
Results
Methods
Discussion
Conclusion
Reference
COI Disclosure Information

Pathology

PE-31

Immunohistochemical study of PD-L1 expression and its clinicopathological correlation in invasive non-small cell lung cancers

Yuji Uno, Maiko Taira, Kanna Kishimoto, Naoko Akiyama, Masatoshi Sado, Naoyuki Miyokawa, Hidehiro Takei

Department of Pathology, Asahikawa Medical University Hospital

Introduction

Recently, immune checkpoint inhibitory approaches have shown considerable promise as innovative effective therapies for cancer patients. For lung cancers, especially non-small cell lung cancers (NSCLCs), two immune checkpoints, PD-1 and PD-L1, have emerged as important targets for immunotherapy. Our aim is to correlate immunohistochemical (IHC) expression of PD-L1 with clinicopathological parameters in NSCLCs.

Table 1. **Materials**

- Term	Jan/2014～Dec/2015
- Cases	99 NSCLCs
- Sex	63 males and 36 females
- Age	45～83 y/o
- Histology	41 SCCs and 58 ADCs

Figure 1. **Predominant histological subtypes of cases**

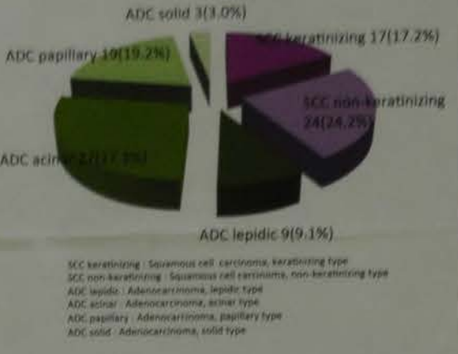

SCC keratinizing : Squamous cell carcinoma, keratinizing type
SCC non-keratinizing : Squamous cell carcinoma, non-keratinizing type
ADC lepidic : Adenocarcinoma, lepidic type
ADC acinar : Adenocarcinoma, acinar type
ADC papillary : Adenocarcinoma, papillary type
ADC solid : Adenocarcinoma, solid type

Materials and Methods

We examined 99 cases (63 males and 36 females) of invasive NSCLCs, including 41 squamous cell carcinomas (SCCs) and 58 adenocarcinomas (ADCs), resected in our institution in 2014 and 2015 (Table 1. & Figure 1.). One representative formalin-fixed paraffin-embedded tissue of each case was immunostained with anti-PD-L1 antibody (Table 2.). The extent of immunoreactive tumor cells and infiltrating intratumoral lymphocytes was respectively scored in a semiquantitative fashion. The proportion score (PS) , proportion of any immunoreactive tumor cells/lymphocytes out of all tumor cells/ lymphocytes, respectively, was statistically compared with multiple clinicopathological parameters (Table 3.). For the purpose of dichotomization, cases with PS >1% of tumor cells were considered IHC "positive".

Table 2. **Immunohistochemistry (IHC)**

IHC system	BOND-Ⅲ® (Leica Biosystems), Nussloch, DE
Detection kit	BOND Polymer Refine Detection® (Leica Biosystems)
Antigen retrieval solution	BOND Epitope Retrieval Solution 2® (Leica Biosystems)
Primary Antibody	Rabbit Anti-Human PD-L1/CD274 Monoclonal Antibody (Clone 142), Spring Bioscience, Pleasanton, CA

Table 3. **Clinicopathological parameters**

- Sex
- Age
- Histopathological types (SCC vs ADC)
- Tumor size
- Lymphovascular invasion
- pStage

Results

- PD-L1 immunoreactivity in tumor cells was significantly higher in SCCs than in ADCs (p=0.0154). (IHC "positive" cases were found 58.5 and 32.8% , respectively.)
- PD-L1 immunoreactivity in infiltrating intratumoral lymphocytes was also significantly higher in SCCs than in ADCs (p=0.0125) (Table 4.).
- Positive correlation between the pathologic stage and tumor cell PD-L1 immunoreactivity was found (p=0.0131) (Table 5.).
- No correlation was found between PS and gender (p=0.1846), PS and age (p=0.0700), PS and tumor size, or PS and lymphovascular invasion status (p=0.0928) (i.e., present or absent).

Table 4. **PD-L1 immunoreactivity in tumor cells and intratumoral lymphocytes**

		Tumor cells			Intratumoral lymphocytes		
Histology	N	Pos. Cases*1	Pos. Rate*2 (%)	p-value	Pos. Cases*3	Pos. Rate (%)	p-value
SCC*4	41	24	58.5	0.0154	39	95.1	0.0125
ADC*5	58	19	32.8		44	75.9	
Total	99	43	43.4		83	83.8	

*1 Positive cases, PS > 1%
*2 Positive rate (%)
*3 Positive cases, PS > 10% of infiltrating intratumoral lymphocytes
*4 Squamous cell carcinoma
*5 Adenocarcinoma

Table 5. **Tumor cells PD-L1 immunoreactivity in pStage*1**

pStage	N	Pos. Cases	Pos. Rate (%)	p-value
IA	53	17	32.1	
IB	16	9	47.4	
IIA	13	8	61.5	0.0131
IIB	3	2	66.7	
IIIA	14	7	50.0	
IIIB	0	0	0	
IV	0	0	0	
Total	99	43		

*1 Pathologic stage

Figure 2. **Squamous cell carcinoma, PD-L1 positive case**

A : H&E stain
B : Immunoreactive lymphocytes
C : Immunoreactive tumor cells

Figure 3. **Adenocarcinoma, papillary type, PD-L1 positive case**

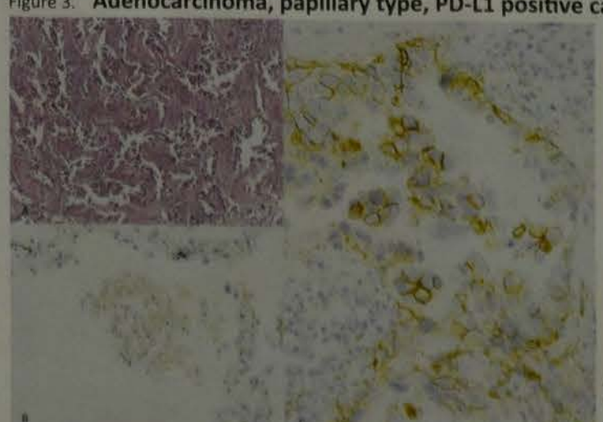

A : H&E stain
B : Immunoreactive alveolar macrophages
C : Immunoreactive tumor cells

Conclusions

PD-L1 expression was more significantly seen in higher pathologic stages of NSCLC cases, which might be associated with tumor immune evasion. This finding further supports the fact that the anti PD-1/ PD-L1 therapy could be of potential use in immunotherapy for patients with advanced NSCLC.

D-1 D-1

Pathology

PE-32

Immunohistological analysis of hMLH1 expression in carcinogenesis of endometrioid adenocarcinoma Grade 3.

Sayaka Kobayashi[1)], Otona Oikawa[2)], Mayu Kikuchi[2)], Tomomi Yoshida[1)], Toshio Fukuda[1)]

1) Department of Histopathology and Cytopathology, Graduate School of Health Sciences, Gunma University, Japan

2) School of Health Sciences, Faculty of Medicine, Gunma University, Japan

Objectives

We previously reported that hMLH1 expression loses at an early of Type-I carcinogenesis. On the other hand, occurrence of serous and clear cell adenocarcinoma of Type-II is reported to be caused by other cancer-causing mechanisms. However, G3 carcinogenesis is not understood. And there are coexistent G3 cases in G1, G2. Therefore, it is necessary to analyze separately Type- I, II. We assumed that G3 cases coexisted hyperplasia, G1 and G2 was Type-I (I-G3), and G3 cases not coexisted them was Type-II (II-G3). And we analyzed hMLH1 expression by immunohistochemistry in G1, G2 and G3 to analyze relationship between hMLH1 expression and I-G3 or II-G3 carcinogenesis.

Carcinogenesis model of Type I endometrial carcinoma (Type-I)

Nomal endometrium → Endometrial hyperplasia → Atypical endometrial hyperplasia → Endometrioid adenocarcinoma (EA) G1, G2 → EA G3

Loss of hMLH1 expression

Loss of hMLH1 expression is related ?

Carcinogenesis model of Type II endometrial carcinoma (Type-II)

Nomal endometrium → EA G3

Nomal endometrium → Serous adenocarcinoma, Clear cell adenocarcinoma

Other cancer-causing not hMLH1

Materials and Methods

Materials Endometrioid adenocarcinoma (EA) 73 cases

Histological grade (WHO 2003)

Histological grade	Cases
EA G1	32/73 (44%)
EA G2	21/73 (29%)
EA I-G3	14/73 (19%)
EA II-G3	6/73 (8%)

Possible cases of non-lesions

Histological grade	Cases
EA G1	23/32 (72%)
EA G2	15/21 (71%)
EA I-G3	9/14 (64%)
EA II-G3	4/6 (67%)

Mothod

Immunostaining was performed using formalin-fixed paraffin-embedded sections of the resected materials. Positive control sections (normal endometrium) were stained at the same time.

Antigen retrieval	autoclave 121℃, 10 minutes, citrate buffer(pH6.0)
Antibody	Anti hMLH1 monoclonal antibody
Clone	clone G168-15, PharMingen, 1:50 dilution

Evaluation

score	0	1	2	3	4
Percentage of positive tumor cells (**P**)	0%	1 to 10%	11 to 50%	51 to 80%	81 to 100%
Staining intensity (**I**)	no	weak	moderate	strong	

Grading of hMLH1 expression (G) ※ G= score P × score I :

Negative	Low	High
G※= 0	G = 1 ~ 6	G = 8 ~ 12

Results

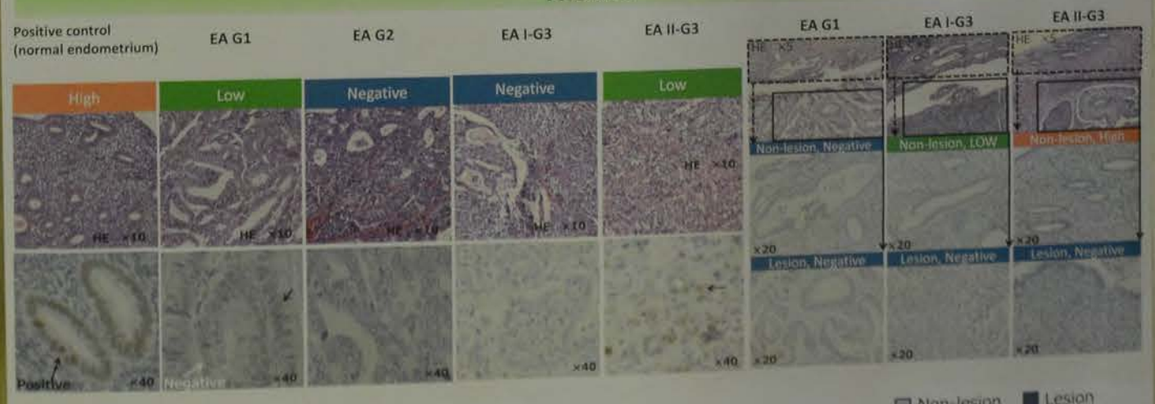

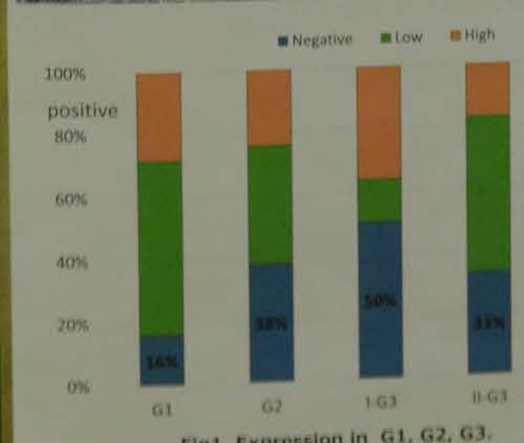

Fig1. Expression in G1, G2, G3.

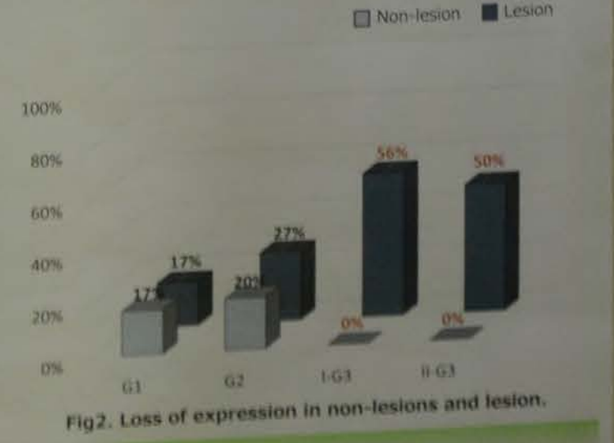

Fig2. Loss of expression in non-lesions and lesion.

Discussion

1. hMLH1 expression lost in 50% of I-G3 than G1, G2. However loss of hMLH1 expression was not observed in non-lesion of I-G3. Thus, hMLH1 expression lose after morphological changes in I-G3. And loss of hMLH1 expression might be related to the transition from G1, G2 to G3.
2. hMLH1 expression lost in 33% of II-G3. And loss of hMLH1 expression was not observed in non-lesion of II-G3. Thus, hMLH1 expression lose after morphological changes II-G3. And II-G3 may have different cancer-causing mechanism from Type-I as well as serous or clear cell adenocarcinoma.
3. Regardless of Type I or II, time of hMLH1 loss-expression in G3 were later than G1, G2.

Disclosure of Interest: None declared Presenters: Sayaka Kobayashi, IFBLS 2016

Pathology

PE-33

Use of immunohistochemistry with antibody cocktail of IgG subclasses instead of IgG in IgG4-related diseases

Rie Nakata[1], Takeshi Uehara[1], Yui Nakashima[1], Tomoyuki Nakajima[1], Yasuhiro Kinugawa[1], Yasuhiro Maruyama[2], Yukihiro Kobayashi[1], Takayuki Honda[1]

[1]Department of Laboratory Medicine and [2]Department of Gastroenterology, Shinshu University School of Medicine, Matsumoto, Japan
[3]Shonankamakura General Hospital, Kamakura, Japan

BACKGROUND

Immunoglobulin G4 (IgG4)-related diseases (RD) are systemic diseases that frequently show elevated serum IgG4 levels and tumor-like masses with infiltration of IgG4-bearing plasma cells. Although diagnostic criteria of IgG4-RD indicate an IgG4/IgG ratio >40%, it is often difficult to count IgG-positive cells because of the low IgG staining intensity. Because the use of an antibody cocktail containing mixed IgG1, IgG2, IgG3, and IgG4 might have similar results to IgG immunohistochemistry in IgG4-RD organs, we compared antibody cocktail reactivity with the expression of IgG in autoimmune pancreatitis (AIP), a representative IgG4-RD.

MATERIALS & METHODS

Five AIP cases were selected from medical records. To determine the usefulness of the antibody cocktail, immunohistochemistry was performed and compared with IgG alone. The coefficient of variation (CV) was used to analyze differences between antibody cocktail and IgG in AIP by 13 board-certified pathologists. They counted cells in the same areas of tissue stained by the antibody cocktail or IgG alone in triplicate for a representative AIP case. Statistical analyses were performed using the Mann-Whitney rank sum test.

RESULTS

The antibody cocktail or IgG stained many positive plasma cells by immunohistochemistry in 5 AIP cases. A few plasma cells with dot-formed positive material in the cytoplasm were observed by immunohistochemistry using the antibody cocktail. There was no difference in the cytoplasmic intensity of cells classified as positive between the antibody cocktail [3(2–3)] and IgG [3(2.5–3)] (p=0.8130). Although there was no difference in the mean number of IgG-positive plasma cells between the antibody cocktail [34.3(28.9-37.1)] and IgG [31.3(23.0-45.6)] (p=0.6066) in a representative AIP case, the CV value was lower in the antibody cocktail (32.6%) than in IgG (50.5%). There was no difference in CV values of IgG-positive plasma cells between the antibody cocktail [14.5(8.2-26.4)] and IgG [11.5 (7.3-22.4)] (p=0.5000) in a representative AIP case.

Figure 1

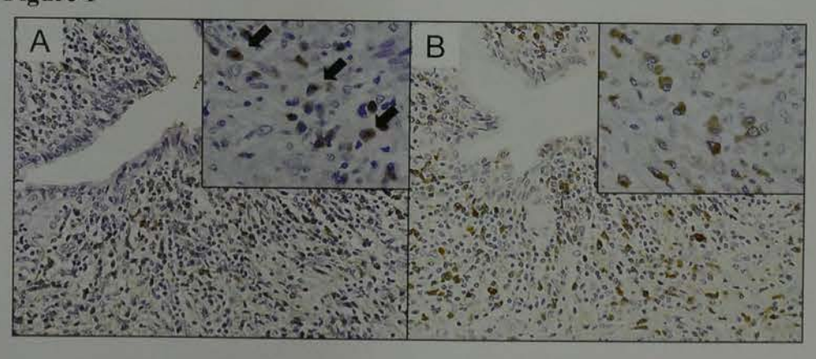

Immunohistochemical staining by antibody cocktail and IgG in a representative AIP case. A, Many positive plasma cells are detected with the antibody cocktail. The insert shows a few plasma cells with dot-formed positive material in the cytoplasm. B, Many positive plasma cells are detected with IgG. No plasma cells with dot-formed positive material in the cytoplasm are present in the insert. (A-B): Original magnification for all micrographs, ×400.

Table 1. Comparison of cytoplasmic intensity by antibody cocktail and IgG

	Antibody cocktail	IgG	p-value
Cytoplasm	3(2-3)	3(2.5-3.0)	p=0.8130

0; Negative, 1; Weak positive, 2; Positive, 3; Strongly positive.
Scores are expressed as minimum, 25th and 75th (percentiles), and maximum

Figure 2

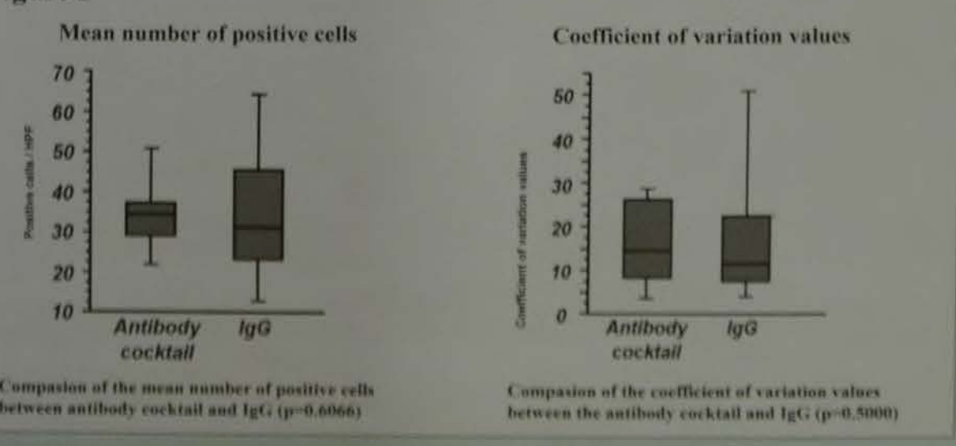

Compasion of the mean number of positive cells between antibody cocktail and IgG (p=0.6066)

Compasion of the coefficient of variation values between the antibody cocktail and IgG (p=0.5000)

CONCLUSIONS

The antibody cocktail might be used to count IgG-positive cells in place of IgG because of its lower CV value. The decrease in CV value observed between pathologists may contribute to a more precise diagnosis of IgG4-RD. A further study with a larger number of AIP cases is warranted to confirm these conclusions.

Pathology
PE-34

Using ultrasonic waves to promote delipidation and decalcification

Yamada Hiroshi, Yanagita Emmy, Endo Akikazu, Tsukamoto Ryuko, Ito Tomoo

The Department of Diagnostic Pathology of Kobe University Hospital

1. Introduction

Fixation → Cutting → Delipida-tion → Decalcifi-cation → Embed-ding → Slicing → Staining

- Many processes are required for creating pathological samples
- Delipidation is required for sections containing much adipose tissue such as mammary glands
- Decalcification is required for hard tissue; sometimes, decalcification at low temperature is indispensable
- Many days taken to sample completion
- Hours taken to pathological diagnosis

We have accordingly examined if using the delipidation/decalcification device, Histra-DC (manufactured by Jokoh Co., LTD.), which uses ultrasonic waves, can shorten the time.

2. About Histra-DC

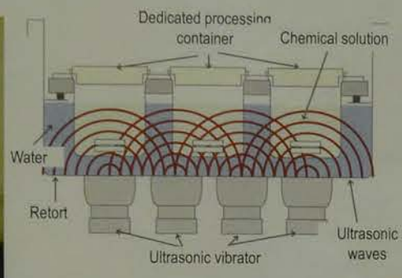

The vibration of minute bubbles caused by ultrasonic cavitation promotes filtration into cellular tissues. The increase in solution temperature resulting from ultrasonic waves can be restrained with a cooling system, which enables setting it at a low temperature.

3. What is cavitation?

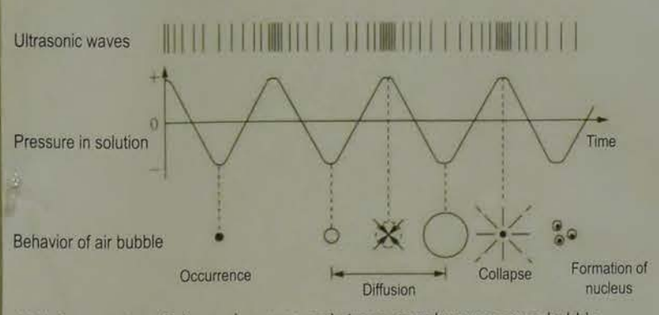

High frequencies of ultrasonic waves and strong sound waves cause bubble generation in solutions due to negative pressure. This phenomenon is called cavitation. Generated minute air bubbles collapse after repeated contraction and expansion. At that time, the temperature and pressure in air bubbles respectively reach thousands of degrees and thousands of units of atmospheric pressure . Vibrations of minute air bubbles stimulate cell membranes to enhance penetrability.

4. Method 1 : Delipidation

Immersion of adipose tissue in delipidation reagent

(1) Use Histra-DC.
Measure the time to complete delipidation.

(2) Stop the immersion on the way.
Remove the sample from the delipidation reagent after completing delipidation.

(3) Leave the sample at ambient temperature.
Measure the time to complete delipidation.

Materials to be used

Use 2x2x0.5 cm of lipomata and mammary glands

Consider using ethanol or ethanol/chloroform as a delipidation reagent

Comparison of times to complete delipidation

5. Delipidation results

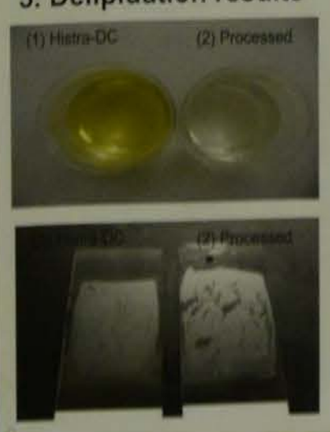

	(1) Histra-DC	(3) Normally processed
Ethanol/chloroform	1 hour and 30 minutes	6 hours
Ethanol	5 hours	16 hours

5. Delipidation results

Histra-DC / Normally processed

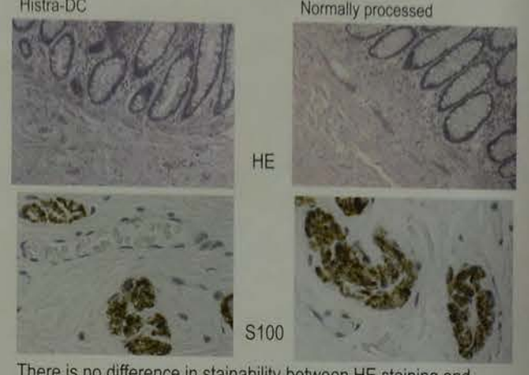

There is no difference in stainability between HE staining and immunostaining.

6. Method 2 : Decalcification

Immersion of hard tissue in decalcifying reagent

(1) Use Histra-DC.
Measure the time to complete decalcification.

(2) Stop the immersion on the way.
Remove the sample from the decalcifying reagent after completing decalcifying it.

(3) Leave the sample at ambient temperature.
Measure the time to complete decalcification.

Materials to be used

1) Use knee joint bone
2) Consider using 10% formic acid, Plank-Rychlo's solution or EDTA as a decalcifying reagent
3) The bone was cut to 2 grams for each sample given the Ca amount.

Comparison of times to complete decalcification and the results of each stain sample

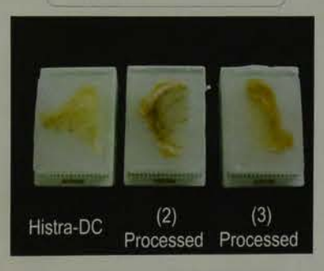

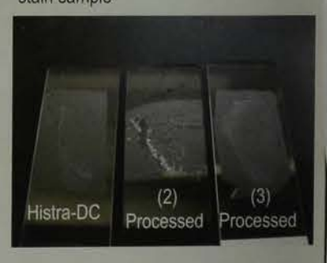

Results	Histra-DC	Concussion
Plank-Rychlo's solution	8 hours	23 hours
Formic acid	19 hours	59 hours
EDTA	10 days	19 days

(1) Histra-DC (3) Processed Hematoxylin single stain

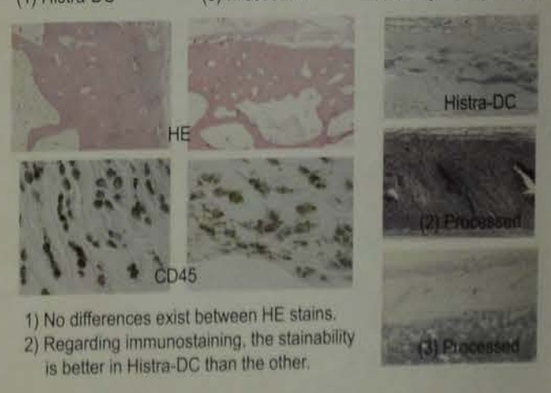

1) No differences exist between HE stains.
2) Regarding immunostaining, the stainability is better in Histra-DC than the other.

7. Conclusions

1) Time can be shortened in each process of fixation, delipidation and decalcification.
2) Using ultrasonic waves has no adverse effect on the stainability.
3) Immunostaining may reduce the influence of a decalcifying reagent.

Using Histra-DC enables operation and temperature control to be simplified and takes one-fifth the time in delipidation and about one-third in decalcification at the shortest to complete each process as compared with the concussion process conducted in this hospital. Therefore, using Histra-DC can contribute to reducing the time up to the diagnosis.

Pathology

PE-35

A Case Report : Myeloid sarcoma with chromosomal aberration
- Observation of tumor cells using the chromosome analysis -

PE-35

Masaru Nakamura, Yoshiya Goto, Masayo Shuto,
Koji Nagata, Masanori Yasuda, Takao Tashiro

Department of Pathology, Saitama medical University ,International Medical Center,Hidaka,Saitama,Japan
Faculty of Health and Medical Care, Saitama Medical University
Graduate School of Arts and Science, The Open University of Japan

【Introduction】
According to WHO classification, myeloid sarcoma MS is defined as a tumor mass consisting of myeloid blasts with or without maturation occurring at an anatomical site other than the bone marrow. It is important that distinguish a MS from a lymphoma /leukemia, and it is important for a well differentiated MS to taka eosinophilic myelocyte.

【Case】
The case 10 years old boy. Tumor in the anterior mediastinum on chest CT was observed and pericardial effusion was pointed out. Clinical diagnosis made from the peripheral blood laboratory test initially suggested T-lymphoblastic lymphoma / leukemia. Thus open chest biopsy and pericardial effusion examination was performed.

【Histological findings】
Atypical cells with high N / C ratio and irregular nuclei were monotonically growth. IHC staining were performed on paraffin sections. In the MPO staining few weakly positive cells were observed. A few Eosinophilic myelocyte were found.
【Result of immunohistochemycal study】
Positive:CD7
Weakly positive:CD99,CD117,TdT,CD34,CD56,MPO
Negative:CD3,CD4,CD8,CD20,CD68
【Differential diagnosis】
"T-LBL of myeloid marker-positive" vs. " myeloid sarcoma of TdT-positive" .
We have diagnosed with MS by focusing on the MPO-positive cells.
CD7 is the most sensitive but not specific T-cell marker, therefore the tumor cells of AML-cell and NK-cell leukemia show CD7-positive, frequently.
【Pathological diagnosis】
Myeloid sarcoma
【Findings of pericardial effusion cell block】
High N / C ratio of atypical cells were mainly seen. MPO-positive cells were observed. It was also observed scattered and partial leaves eosinophils, eosinophilic myelocyte in the background.

【Chromosome analysis】
Tumor tissue culture: 46, XY, inv (9) (p12q13), t (10; 11) (p13; q14)
Pericardial effusion culture
: 48, XY, inv (9) (p12q13), t (10; 11) (p13; q14), + 4, + 19

Evolution of the karyotype appeared in the cells of Pericardial effusion.

【Consideration】
In this case, monotonous image of blast cells was observed in the biopsy tissue.
But differentiation of the cells was observed in the pericardial effusion. We had added double staining method through virtual slide. Furthermore "+19 tumor cells" were observed in the triple staining method.

【Summary】
We have presented a case of MS with chromosomal abnormality.
"+19 tumor cells" appeared in the biopsy tissue and pericardial effusion.
"+19 tumor cells" appeared in cell block spesimen.
"+19 Tumor cells" was not associated with MPO positivity.
Triple staining method through virtual slide is useful technique that can detect the three elements morphology, immunohistochemycal traits and genetics with material.

【Reference】
1) S.A.Pileri, A.Oozi, et al. Myeloid sarcoma. WHO Classification of Tumors of Hematopoietic and Lymphoid Tissues. 4th edition. IARC , 2008. P140-143.
2) Hidekazu Kayano, Michio Shimizu, eosinophilic myelocyte in granulocytic sarcoma (myeloid sarcoma), Pathol. and Clinicol Med 2003 ; 21:540-541.

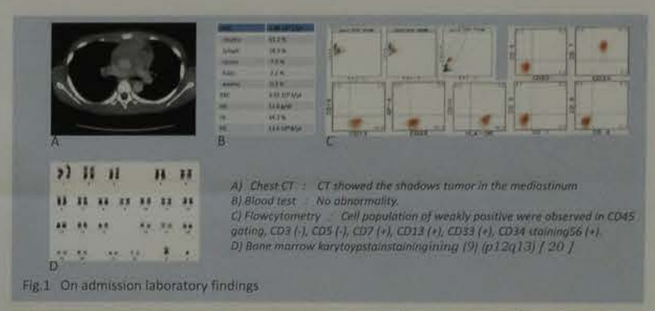

A) Chest CT : CT showed the shadows tumor in the mediastinum
B) Blood test : No abnormality.
C) Flowcytometry : Cell population of weakly positive were observed in CD45 gating, CD3 (-), CD5 (-), CD7 (+), CD13 (+), CD33 (+), CD34 staining56 (+).
D) Bone marrow karyotypstainstaininginingining (9) (p12q13) [20]
Fig.1 On admission laboratory findings

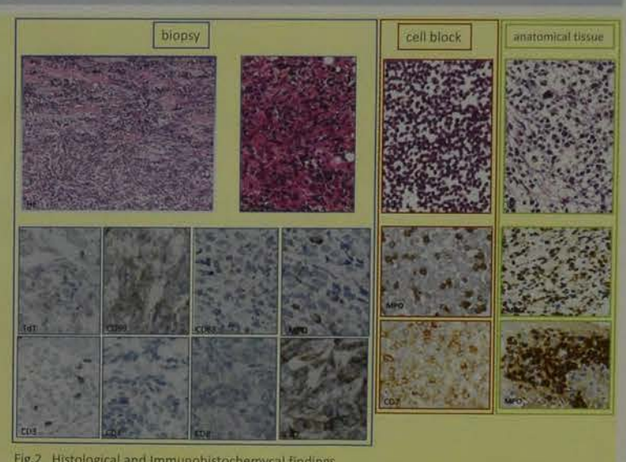

Fig.2 Histological and Immunohistochemycal findings

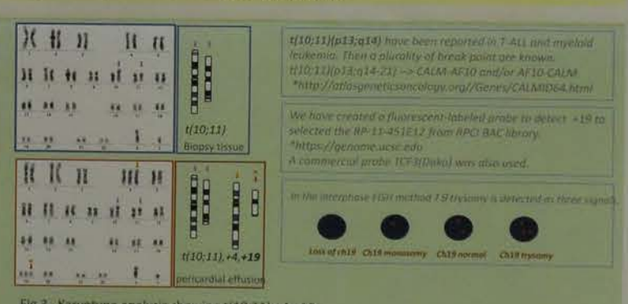

Fig.3 Karyotype analysis showing t(10;11),+4,+19

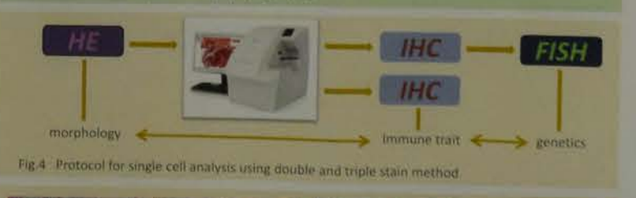

Fig.4 Protocol for single cell analysis using double and triple stain method

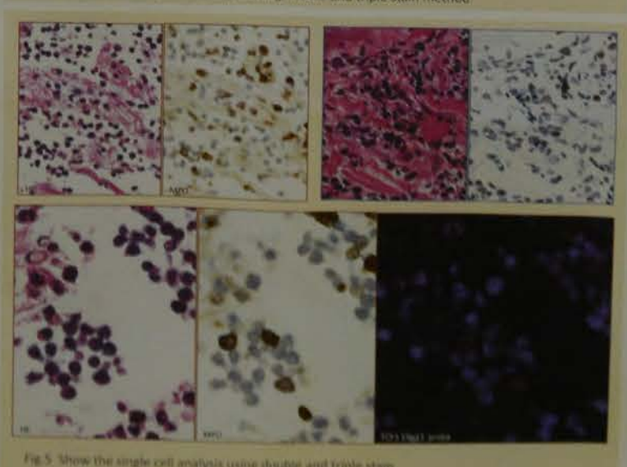

Fig.5 Show the single cell analysis using double and triple stain

Pathology

PE-36

To make multiplex immunohistochemistry more efficient and quiker in Electric Field Non-Contact Techniques.

●Emmy Yanagita (CT), Akikazu Endo (CT),
Hiroshi Yamada (CT), Tomoo Itoh (MD)
Department of Diagnostic Pathology
Kobe University Graduate School of Medicine

Background

■Immunohistochemical (IHC) examination plays an important role in differentiating various tumors.

Although multiplex immunohistochemistry only requires a single slide glass in detecting antigens, it is time-consuming, especially in the staining process.

■We have recently developed a new IHC (called R-IHC) method in which alternating current electric field is applied to mix microdroplets on the slide and thus to facilitate the antigen-antibody reaction. In this method, it only takes 30 minutes for immunostaining.

Objective

To seek a quicker procedure in multiplex immunohistochemistry through R-IHC.

(Rapid-IHC)

Histo-Tek R-IHC

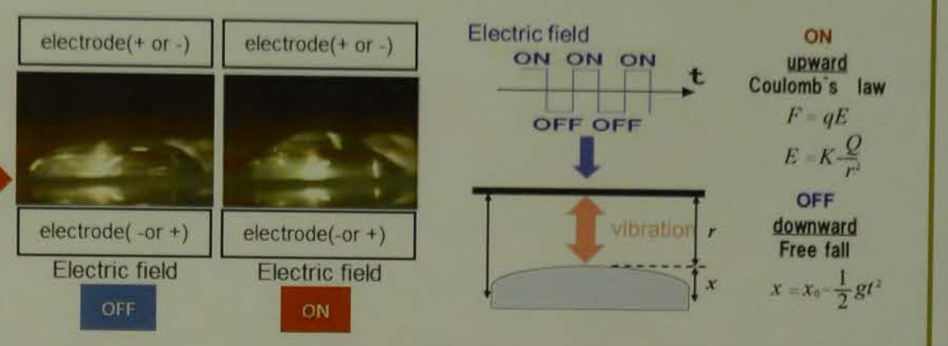

■In this method, an alternating-current(AC) electric field is used to promote the antigen antibody reaction within the microdroplet.

Method

1) 4-$\mu\ell$-thick sections of tissue biopsied from normal pancreas and pituitary gland were fixed in 10% buffered neutral formalin and embedded in paraffin.

2) The slides were categorized into three subgroups in terms of the number of staining procedures to undergo (i.e. (I) single-staining, (II) double-staining, and (III) triple-staining).
The antibodies used for each sub-group are as follows:

I. *anti-somatostatin* for pancreas, and *anti-human growth hormone (hGH)* for pituitary gland.
II. *anti-somatostatin* and *anti-glucagon* for pancreas, and *anti-hGH* and *anti-adrenocorticotropin (anti-ACTH)* for pituitary gland.
III. *anti-somatostatin, anti-glucagon* and *anti-insulin* for pancreas, and *anti-hGH, anti-ACTH*, and *anti-prolactin* for pituitary gland.

3) The staining process is 5 minutes for each section. The sections in the double-staining and triple-staining sub-groups were re-stained once and twice, respectively, with the respective antibodies mentioned above.

Protocol

Single

1. Deparaffinization
2. Blocking with 3% hydrogen peroxide for 5minutes
3. Washing
4. Primary antibody reaction for 5minutes
6. Washing with TBS
7. Secondary antibody reaction for 5minutes
8. Washing with TBS
9. DAB
10. Washing
11. Primary antibody reaction for 5minutes
12. Washing with TBS
13. Secondary antibody reaction for 5minutes
14. Washing with TBS
15. PermaRed/AP
16. Denaturing Solution for 5minutes
17. Washing
18. Primary antibody reaction for 5minutes
19. Washing with TBS
20. Secondary antibody reaction for 5minutes
21. Washing with TBS
22. PermaBlue/AP
23. Drying
24. Mounting with Malinol

Double

Triple

pancreas

Somatostatin:Brown, insulin:Red, glucagon:Blue

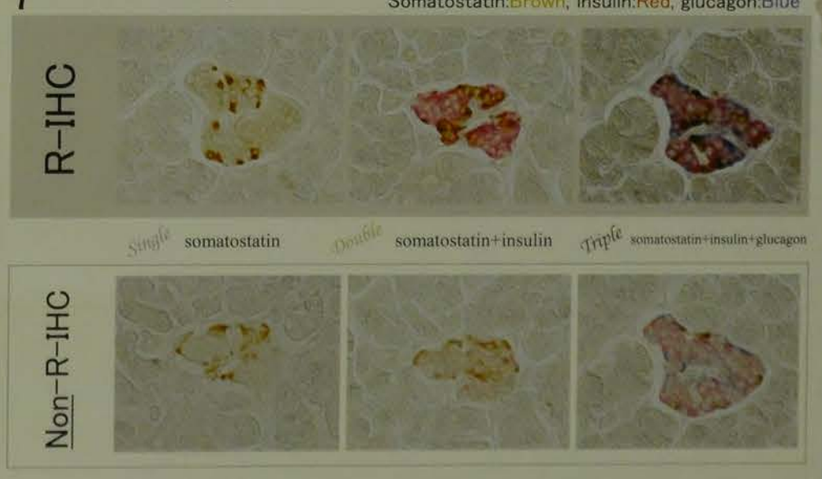

pituitary

hGH:Brown, ACTH:Red, prolactin:Blue

Results

Original		R-IHC
Single: 100min	1/3	30min
Double: 230min	1/4	60min
Triple: 340min	1/4	80min

The results showed the effectiveness of the proposed method.

This results show the shortened duration of time in the R-IHC method; 60minutes for double staining and 80minutes for triple staining.

Pathology

PE-37

Developing techniques for differentiating between clear cell carcinoma and serous adenocarcinoma.

●Emmy Yanagita (CT), Akikazu Endo (CT), Naoko Imagawa (CT), Hiroshi Yamada (CT), Ryuko Tsukamoto (CT), Tomoo Itoh (MD)
Department of Diagnostic Pathology
Kobe University Graduate School of Medicine

Background 1

■ Immunohistochemical (IHC) examination plays an important role in differentiating various tumors. Although multiplex immunohistochemistry only requires a single slide glass in detecting antigens, it is time-consuming, especially in the staining process.

Background 2

■ We have recently developed a new IHC (called R-IHC) method in which alternating current electric field is applied to mix microdroproplets on the slide and thus to facilitate the antigen-antibody reaction.

↓

In this method, it only takes 30 minutes for immunostaining.

antibody & protocol

Clear cell adenocarcinoma	HNF-1β (SIGMA #HPA002083) Rabbit Monoclonal	cocktail
Serous adenocarcinoma	WT1 (Leica #NCL-L-WT-562) Mouse Monoclonal :WT49	

Clear cell adenocarcinoma.

Serous adenocarcinoma.

Secondary antibody
Mach 2 Double Stain #2

Anti-Rabbit IgG + ALP ↙PermaBlue/AP
Anti-Mouse IgG + HRP ← DAB

1. Deparaffinization
2. Heat-induced antigen retrieval with pH8.0 EDTA for 3minutes
3. Blocking with 3% hydrogen peroxide in methanol for 10minutes
4. Washing with TBS
5. Primary antibody reaction (HNF-1β+WT1) for 50minutes
6. Washing with TBS
7. Secondary antibody reaction for 30minutes
8. Washing with TBS
9. DAB
10. Washing
11. PermaBlue for 15minutes
12. Washing
13. Drying
14. Mounting with Malinol

One Step

Total : 130minutes

R-IHC **combination** Cocktail antibody

Histo-Tek R-IHC

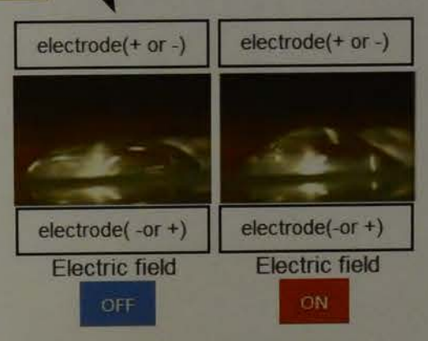

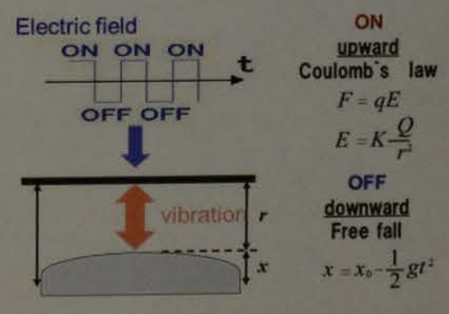

■ In this method, an alternating-current(AC) electric field is used to promote the antigen antibody reaction within the microdroplet.

Cocktail antibody and R-IHC to study differentiating between clear cell adenocarcinoma and serous adenocarcinoma in ovary.

Results

1. Deparaffinization
2. Heat-induced antigen retrieval with pH8.0 EDTA for 3minutes
3. Blocking with 3% hydrogen peroxide in methanol for 3minutes
4. Washing with TBS
5. Primary antibody reaction (HNF-1β+WT1) for 7minutes
6. Washing with TBS
7. Secondary antibody reaction for 7minutes
8. Washing with TBS
9. DAB
10. Washing
11. PermaBlue/AP
12. Washing

Total : 30minutes

	Nucleus
Clear cell Adenocarcinoma	blue
Serous adenocarcinoma	brown

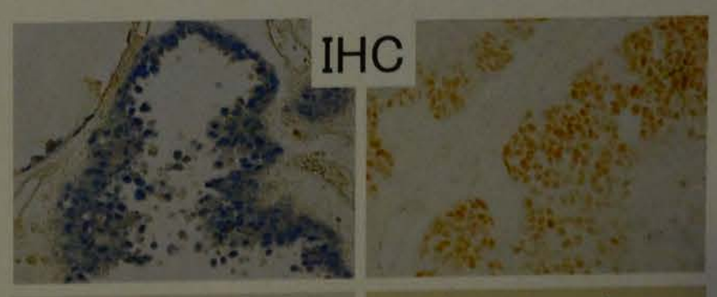

The results showed the effectiveness of the proposed method.

Pathology

PE-39

Improved efficiency for an auto slide preparation system

Miho YOSHIDA-TANAKA [1],
Kazuya KURAOKA [1,2], Arisa KAN [1], Hiroki FUJISAWA [1], Naoko YASUMURA [1],
Hiroshi OHNISHI [1], Hideki NAKANO [3], Daiki TANIYAMA [1], Junichi ZAITSU [1],
Akihisa SAITO [1], Takashi ONOE [2,3], Kiyomi TANIYAMA [4]

Department of 1) Diagnostic Pathology, 2) Institute for Clinical Research, 3) Clinical Laboratory, and 4) President, National Hospital Organization, **Kure Medical Center and Cancer Center**, Kure, Japan

Conclusions We investigated use of an auto slide preparation system, procedures, and various matrics for HE stained slides (4μm). The efficiency of tissue sections by the automatic slice apparatus improved dramatically.

Background An auto slide preparation system (AS-400M; DAINIPPON SEIKI CO., LTD., Kyoto, Japan) was introduced to our center in September 2013. The AS-400M had a good specimen manufacture rate of 68.5% from introduction until April 2014.

AS-400M

Objects 21,323 paraffin blocks made from surgically resected tissues between May and December 2014, and May 2015 and March 2016.

Methods

We investigated causes of poor specimens in regards to automatic slice conditions, and reviewed preliminary procedures. Rough cutting of all specimens were performed manually. Poor specimens posed a problem for pathological diagnosis and they were confirmed by pathologists. Excessive calcification and very small specimens were handled manually.

【Study-1】 The main causes for poor specimens were calcification tissue and surgical lint. (Figure 1a,b)

(Figure 1a)

(Figure 1b)

Adjusting slice speed and steam humidification time can be done for four types of automatical tissue setting of the slice condition as: A, B, C, D (Table 1).

(Table1) Slide settings of the slice condition

Items	A*	B*	C*	D*
Cutting speed (mm/s)	40	35	50	40
Paste speed (mm/s)	40	35	50	40
Tape speed (%)	91	91	91	94
Steam humidification time (sec)	3	5	2	1
Extension time (sec)	30	25	25	25
0.1% solution of acetate (μl)	80	80	80	30
Materials	Breast Digestive tract Lymph node	Uterus Prostate gland	Placenta Liver Spleen	Cell line Biopsy

*A: alimentary canal tissue, B: hard tissue, C:considerable blood tissue, D: small tissue

【Study-2】 Additionally, to reduce defective slides due to a cracked specimen, the operators were coached in:

(1) Embedding in paraffin (Figure 2)

(2) Shavinge off paraffin around the block (Figure 3)

(3) Decalcifying the surface using KCX (1:1) for two to three hours (Figure 4)

(4) Determining cutting direction properly (Figure 5)

(5) Correct positioning of the calcified blocks at every 4th site (Figure 6)

(Figure 2)

(Figure 3)

(Figure 4)

(Figure 5)

(Figure 6)

Results

【Study-1】 The good specimen manufacture rate increased to 76.8%(7,423/9,667 blocks) at end of study-1(December 2014).
【Study-2】 The good specimen manufacture rate increased to 93.7% (10,922/11,656 blocks) at end of study-2(March 2016).

(Table2) The current of good specimen manufacture rate

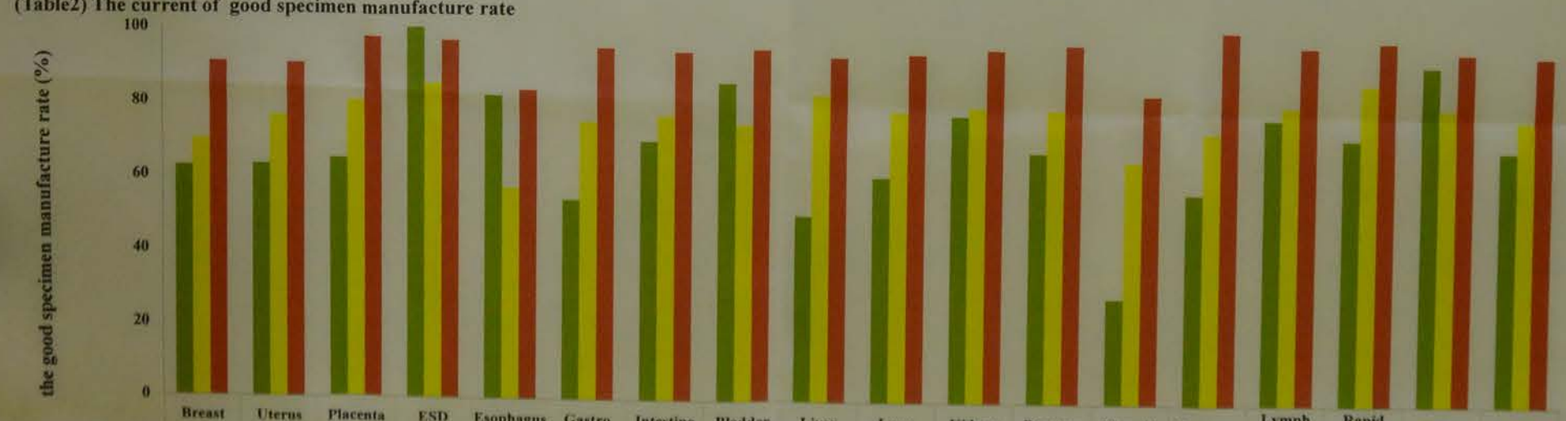

	Breast	Uterus	Placenta	ESD	Esophagus	Gastro	Intestine	Bladder	Liver	Lung	Kidney	Prostate	Thyroid	Pancreas	Lymph node	Rapid specimens	Other	Average
Introduction period	62.5	63.0	64.9	100.0	82.1	54.0	70.0	85.7	50.0	60.6	77.1	67.7	28.6	56.7	76.8	71.4	91.2	68.4
I	69.7	76.1	80.3	85.1	57.0	74.9	76.8	74.5	82.3	78.0	79.3	79.0	65.4	72.8	79.9	86.0	79.5	76.3
II	90.7	90.3	97.6	96.6	83.6	95.0	93.9	94.7	92.7	93.8	95.3	96.8	83.3	100.0	96.2	97.7	94.7	93.7

The good specimen manufacture rate with an average of 95.7% has been achieved after various kinds of invention from an average of 68.5% of introduction period. (Table 2)

The 32nd World Congress of Biomedical Laboratory Science
Disclosure of Conflict of Interest
Name of first author: Miho Yoshida-Tanaka
I have no COI with regard to our presentation.

National Hospital Organization Kure Medical Center and Chugoku Cancer Center

Pathology

PE-40

Pathologic features of desmoplastic malignant mesothelioma

Sadayuki Hiroi, Susumu Tominaga, Tatsuya Yamazaki, Tomoko Yokoo, Mari Takashima, Satoru Nakano, Tetsuro Seita and Ayumi Sasaki.
Department of Clinical Laboratory Sciences, Nitobebunka College, Nakano, Tokyo, Japan
Department of pathology and Laboratory Medicine, National Defense Medical College, Tokorozawa, Saitama, Japan
Department of Human Pathology, Graduate School of Medicine Gunma University
Maebasi, Gunma, japan

Background

- Desmoplastic malignant mesothelioma (DMM) is a rare neoplasm that is proposed as a subtype of malignant pleural mesothelioma.
- It is difficult to distinguish DMM from reactive pleural fibrosis.
- Histologically, DMM has abundant collagenous tissue, forming sarcomatous, storiform or "patternless" pattern.
- DMM is rarely associated with a pleural effusion, and if there is an effusion it exfoliates very few cells into the fluid.

Aim

We present a case of DMM with cytopathological, histopathological and immunohistochemical features.

Conclusion

- DMM usually shows cytologic atypia, but with a poor cellular component. So, it may not be difficult to diagnose 'malignancy', but in cases with a poor cellular component.
- Immunohistochemistry may be useful for diagnosis.

Case

78-years-old man admitted to a hospital for chest pain and dyspenia.
He had a 5-year history of occupational asbestoes exposure.
He had worked for a roof industrial company between his ages 35 and 40.
At laboratory data, tumor markers, all of them were within normal limits.

Laboratory examination
WBC: 5100 ul, RBC: 405 x10 ul, Hb: 11.8 g/dl, Hct 36.7%, Plt 32.2 x10 ul, TP 8.7 g/dl, ALB: 3.7 g/dl, LDH: 240 IU/L, GOT: 15 IU/L, GPT: 12 IU/L, ALP: 486 IU/L, BS: 187 mg/dl, BUN: 7.6 mg/dl, Crea: 0.57 mg/dl, CRP: 7.03 mg/dl, HbA_{1c}: 9.7%
Tumor markers
CEA: 0.8 ng/ml, CKA: 0.9 ng/ml, SCC: 1.0 ng/ml, CA19-9: 5.3 U/ml, SLX: 27.6 U/ml

Cytological Findings
(Pleural effusion at autopsy)

In pleural effusion cytology, papanicolau stain showed large tumor cells with high N/C ratio and ireggular nuclei, and showed some nucleoli.

Histological Findings

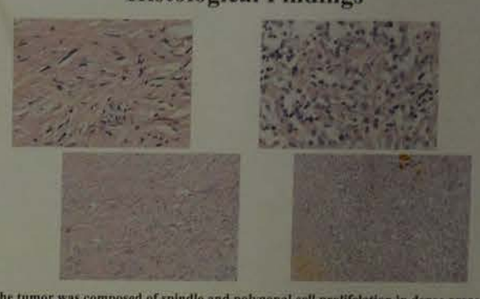

The tumor was composed of spindle and polygonal cell prolifelation in dense areas of collagenous tissue. And high density of the tumor cells at part of tumor tissues.

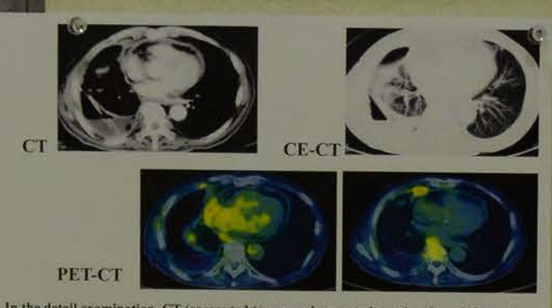

In the detail examination, CT (computed tomography scan) showed a pleural thickening, and a pleural effusion. In PET-CT, focally strong uptake was recognized. In addition to these findings, thoracoscopic lung biopsy was performed and was suggesting of DMM. The patient had chemotherapy, but unfortunately he died about 4 months after admission due to respiratory failure and cardiac depression by tumor invasion.

Imprint cytology

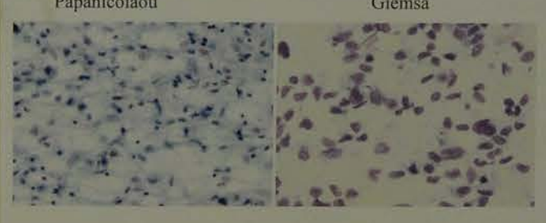

Left ; Papanicolau stain and Light ; giemsa stain showed Many spindle and polygonal tumor cells with abundant cytoplasm were found. The nuclei were atypical and with large nucleoli.

Immunohistochemistry

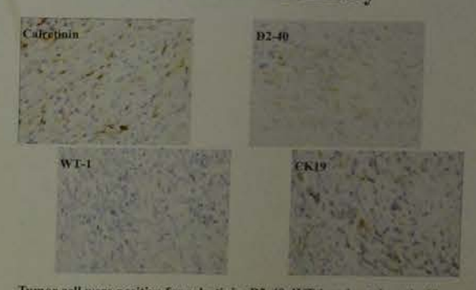

Tumor cell were positive for calretinin, D2-40, WT-1 and cytokeratin 19. These results were the same as cytology specimens.

Autopsy findings

Left slide, The tumor invaded the right thoracic cavity and diffuse fibrous thickening was found around the pericardium.
Light slide, The sternum, Tumor invaded the sternum.

Immunocytochemistry
(Pleural effusion)

Tumor cells showed positive reaction of calretinin, D2-40 and cytokeratin19. Calretinin positivity area was nucreus and cytoplasm, D2-40 and cytokeratin 19 were cytoplasm.

Immunocytochemistry (imprint)

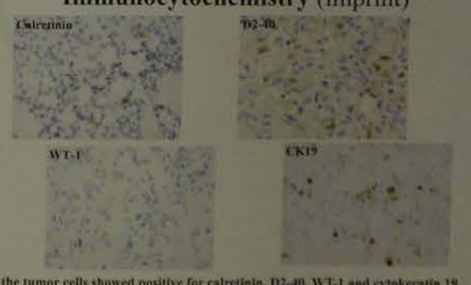

the tumor cells showed positive for calretinin, D2-40, WT-1 and cytokeratin 19. This result were the same as pleural effusion cytology.

Pathology

PE-41

96366

Tumor complexity index is significantly associated with metastasis in patients diagnosed with colon carcinoma

UPPSALA UNIVERSITET

Victoria Hahn-Strömberg PhD
Department of Medical Cell Biology, Uppsala University, SE 75105 Uppsala, Sweden

Background and Aim: Research has shown that the growth pattern of tumors has information about the metastatic ability of the tumor, where a more irregular shape of the tumor invasive front is correlated to a high metastatic potential. Growth pattern of the tumor has been studied for its association with survival in colorectal cancer. Among different growth pattern evaluating techniques, very little is known about prognostic significance of complexity index. Aim of this study was to develop a prognostic model, which could be used to predict survival as well as tumor metastasis in the patients diagnosed with colon carcinoma.

Figure 2: Human colon biopsies showing tumor growth patterns in colon carcinoma. Fig 2A shows expensive tumor growth with smooth invasive front (low complexity index), Fig 2B indicates the medium complexity index and 2C shows the infiltrative growth pattern with highly coarse invasive front with dispersed tumor cells with high complexity index. (Fig 2D, E and F) are the same images that are thresholded to get tumor area black with white background. (G, H and I) are indicating a tumor invasive front outline during image processing.

Material and methods: Formalin fixed paraffin embedded tissues samples from 316 patients diagnosed with colon carcinoma, were used to prepare immunohistochemical slides. Slides were stained for cytokeratin 8 and images were captured of the invasive front of the tumor. Images were then thresholded to get tumor area black and tumor outline as a single pixel line to analyze fractal dimension and number of tumor cells. These two features were then used to calculate the complexity index by performing tree diagram analysis. Complexity index was correlated with 5-years survival and other clinicopathological data of the patients.

Results: Five years survival of the patients was not influenced by complexity index ($P>0.05$) but clinicopathological parameters like tumor metastasis, localization, gender and differentiation were significantly associated with complexity index with p=0.000, p=0.002, p=0.024 and p=0.000 respectively. A positive trend was also observed between complexity index of tumor and age (p=0.051).

Table 3: Correlation between complexity index and clinicopathological parameters of the patients diagnosed with colon carcinoma.

Parameters		Complexity index low	medium	high	P value
Age	Age1	12(3.80%)	59(18.67%)	22(6.96%)	0.051
			108(34.18%		
	Age2	42(13.29%)	)	73(23.10%)	
Gender	Male	32(10.1%)	90(28.5%)	37(11.7%)	0.024
	Female	22(7.0%)	77(24.4%)	58(18.4%)	
	T1	1(0.4%)	3(1.2%)	0(0.0%)	0.857
T	T2	9(3.8%)	19(7.9%)	12(5.0%)	
	T3	29(12.1%)	86(35.8%)	53(22.1%)	
	T4	4(1.7%)	15(6.2%)	9(3.8%)	
N	N0	26(10.8%)	73(30.4%)	38(15.8%)	0.783
	N1	10(4.2%)	29(12.1%)	19(7.9%)	
	N2	7(2.9%)	21(8.8%)	16(6.7%)	
	N3	0(0.0%)	0(0.0%)	1(0.4%)	
M	MX	15(6.2%)	65(27.1%)	57(23.8%)	0.000
	M1	1(0.4%)	6(2.5%)	1(0.4%)	
	M2	27(11.2%)	52(21.7%)	16(6.7%)	
Differentiation	Low	4(1.3%)	16(5.3%)	34(11.3%)	0.000
	Medium	35(11.6%)	104(34.6%)	36(12.0%)	
	High	10(3.3%)	42(14.0%)	20(6.6%)	
Duke's Stages	A	8(3.0%)	18(6.8%)	8(3.0%)	0.647
	B	24(9.0%)	65(24.4%)	30(11.3%)	
	C	16(6.0%)	50(18.8%)	35(13.2%)	
	D	2(0.8%)	8(3.0%)	2(0.8%)	
Localization	Right colon	32(10.13%)	86(27.22%)	61(19.30%)	0.002
	Left colon	13(4.11%)	40(12.66%)	6(1.90%)	

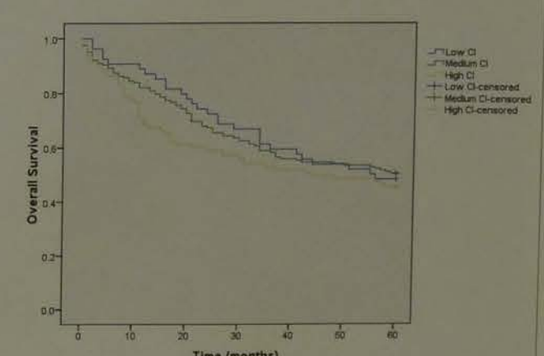

Figure 1: Survival curve presenting the different groups of complexity index (CI) and their association with survival of the patients diagnosed with colon carcinoma.

Conclusion: We conclude that complexity index is associated with systemic metastasis and differentiation of tumor but is not a predictive biomarker of survival in patients diagnosed with colon carcinoma. However, complexity index is a reliable technique to analyse tumor characteristics and further investigations with follow-up periods are required to reveal the potential targets for therapeutic intervention.

Pathology

PE-42

Cytotoxic activity of crude extract from selected Philippine seaweeds against human lung adenocarcinoma

Krisel Rosales-Sandoval, Oliver Shane R. Dumaoal, Anacleta P. Valdez

Graduate School, Lyceum of the Philippines University - Batangas; College of Allied Medical Professions, Lyceum of the Philippines University - Batangas

ABSTRACT

Cancer is one of the most dreaded diseases worldwide with limited treatment and management strategies often accompanied by serious side effects. Previous studies on marine products particularly seaweeds pose a significant avenue for alternative cancer treatment. This study determined the cytotoxic activity of selected Philippine seaweeds namely *Caulerpa lentillifera* (CLDE), *Eucheuma denticulatum* (EDDE), *Kappaphycus alvarezii* (KADE) and *Sargassum polycystum* (SPDE). Dichloromethane crude seaweed extracts were tested against A549 human lung adenocarcinoma cell line using 3-(4,5-dimethylethylthiazol-2-yl)-2,5-diphenyltetrazolium bromide (MTT) assay. Results indicate that SPDE exerts the highest cytotoxic activity against the cancer cell line with IC_{50} of 6.00 + 0.19 µg/mL as compared to other seaweeds tested (CLDE = 49.39 + 0.61 µg/mL; EDDE = >50 µg/mL; KADE = 45.44 + 4.51 µg/mL). Phytosterol is the common phytochemical among the seaweed extracts tested using standard phytochemical analysis and Fourier transform infrared spectroscopy (FTIR). SPDE shows potential for the treatment of lung adenocarcinoma and warrants further studies for the isolation of its bioactive compounds.

INTRODUCTION AND OBJECTIVES

According to the World Health Organization (WHO), cancer is a leading cause of death worldwide, accounting for 8.2 million deaths in 2012. In the Philippines, it is the third leading cause of mortality in 2010 as reported by the Department of Health. Although the advancement in chemotherapy and therapeutic medicines are undeniably present, the quest for safe and promising substances from natural products continues. Marine organisms are important and promising in cancer research. The marine environment, being rich in its biodiversity, makes marine organisms and their metabolites unique. The isolation and characterization of the biologically active components from marine organisms have gained attention from various research groups around the world (Kim & Taylor, 2011). Although several studies have been conducted for the biological activities of marine organisms, little are known about the biopharmaceutical potential of seaweeds, particularly those that thrive in the Philippines. Seaweeds, as part of the aquatic resources of the country, are produced in substantial quantity. This study aimed to evaluate the crude extract from selected seaweeds in the Philippines. Particularly, it determined the phytochemical content of *Eucheuma denticulatum*, *Kappaphycus alvarezii*, *Caulerpa lentillifera* and *Sargassum polycystum* and tested their potential cytotoxic activity against A549 human lung adenocarcinoma cell line.

Table 2

Mean IC50 values (µg/mL) of extracts

Seaweed	IC_{50} (µg/mL)
CLDE	49.39 + 0.61
EDDE	>50.00
KADE	45.44 + 4.51
SPDE	6.00 + 0.19

*Results were expressed as the minimum concentration able to destroy 50% population ± standard error of mean.

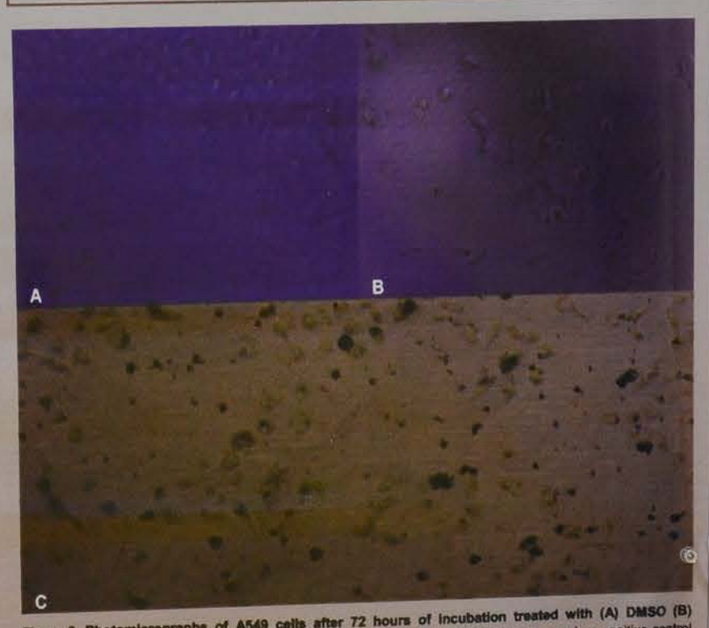

Figure 2. **Photomicrographs of A549 cells after 72 hours of incubation treated with (A) DMSO (B) Doxorubicin and (C) 6.25 µg/mL SPDE at 100x magnification.** Doxorubicin was used as positive control while DMSO was used as negative control.

METHODS

Plant preparation

Phytochemical screening

- Standard phytochemical procedures
- Fourier Transform Infrared Spectroscopy

Evaluation of cytotoxic activity

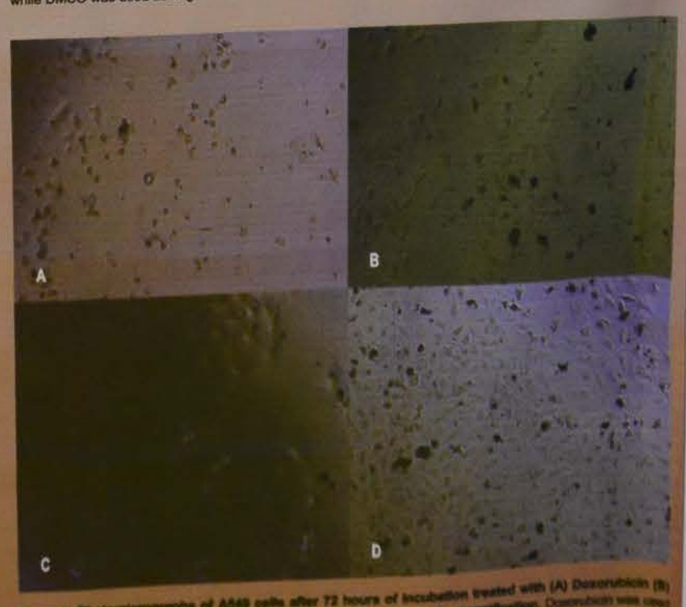

Figure 3. **Photomicrographs of A549 cells after 72 hours of incubation treated with (A) Doxorubicin (B) 50 µg/mL CLDE (C) 50 µg/mL EDDE and (D) 50 µg/mL KADE at 100x magnification.** Doxorubicin was used as positive control while DMSO was used as negative control.

RESULTS

Table 1

Resulting spectra of each extract from FTIR spectroscopy

	CLDE		EDDE		KADE		SPDE	
	A	B	A	B	A	B	A	B
Alkaloid	+	+	+	+	+	+	-	+
Carbohydrate	-	+	-	+	-	+	-	+
Phytosterol	+	+	+	+	+	+	+	+
Phenol	+	+	-	+	+	+	-	+
Tannin	-	+	+	+	+	+	-	+
Flavonoid	+/-	+	+	+	+/-	+	-	+
Protein	+	+	+	+	-	+	-	+
Diterpene	-	+	+	+	+	+	+	+

*Results of phytochemical analysis by (A) standard phytochemical screening and (B) FTIR spectroscopy. Presence of the constituents is represented by (+); absence is represented by (-); +/- means trace.

Figure 1

Mean IC50 values of seaweed extracts against A549 human lung adenocarcinoma

CONCLUSIONS

Results indicate that SPDE exerts the highest cytotoxic activity against the cancer cell line with IC_{50} of 6.00 + 0.19 µg/mL as compared to other seaweeds tested (CLDE = 49.39 + 0.61 µg/mL; EDDE = >50 µg/mL; KADE = 45.44 + 4.51 µg/mL). Phytosterol is the common phytochemical among the seaweed extracts tested using standard phytochemical analysis and Fourier transform infrared spectroscopy. SPDE shows potential for the treatment of lung adenocarcinoma.

RECOMMENDATIONS

It is suggested that the extracts of *C. lentillifera*, *E. denticulatum* and *K. alvarezii* be subjected to partition to determine whether the fractions will give higher cytotoxic activity. Further studies on *S. polycystum* can be conducted to ascertain the active compounds present in order to maximize its potential in the development of new chemotherapeutic drugs. Additional studies on the extracts' cytotoxic activities using other types of cancer cell lines as well as using the cell line on normal human lung cells are also recommended.